ISSN No. 0737-5352-27

Objectively Estimating Tropical Cyclone Intensity and Wind Structure Using the Advanced Microwave Sounding Unit

Julie Demuth
Thomas H. Vonder Haar

Funding for this research is supplied in part by an American Meteorological Society Graduate Student Fellowship, sponsored by GTE Government Systems, and also by the United States Weather Research Program, NOAA grant NA67RJ0152.

CIRA Cooperative Institute for Research in the Atmosphere

Colorado State University

OBJECTIVELY ESTIMATING TROPICAL CYCLONE INTENSITY AND WIND STRUCTURE USING THE ADVANCED MICROWAVE SOUNDING UNIT

Submitted by

Julie L. Demuth

Department of Atmospheric Science

In partial fulfillment of the requirements

For the Degree of Master of Science

Colorado State University

Fort Collins, Colorado

Fall 2001

ABSTRACT

OBJECTIVELY ESTIMATING TROPICAL CYCLONE INTENSITY AND WIND STRUCTURE USING THE ADVANCED MICROWAVE SOUNDING UNIT

Estimating tropical cyclone (TC) intensity and structure is becoming increasingly important in light of population expansion along coastal regions. The two most commonly used techniques for estimating TC intensity, the Dvorak Technique and the Objective Dvorak Technique (ODT), utilize visible and infrared satellite imagery. However, both have limitations, as do observing techniques of TC wind structure. Satellite-borne passive microwave radiometers provide an opportune alternative for near real-time assessments of TC maximum sustained winds and wind radii. The first Advanced Microwave Sounding Unit (AMSU), aboard the NOAA-15 polar orbiting satellite, is the first NOAA instrument with sufficient resolution to do so.

In this study, data derived from AMSU temperature, pressure, and wind retrievals are used to make objective intensity and wind radii estimates for tropical disturbances in the Atlantic and East Pacific basins. To approximate TC maximum sustained winds and azimuthally averaged wind radii of 34, 50, and 64 kt winds, algorithms are developed via correlations and multiple linear regressions from AMSU data from the 1999 tropical season; they then are tested independently on the 2000 tropical season data. Additionally, the AMSU-derived estimates of the azimuthally averaged wind radii are used with a modified Rankine vortex model to assess the wind radii asymmetrically, specifically in the northeast (NE), northwest (NW), southeast (SE), and southwest (SW) quadrants of the TC. Validation data are from the National Hurricane Center (NHC) best

track data for the intensity estimates, and from the NHC operational forecast advisories for the average and asymmetric wind radii estimates.

Results show the objective AMSU algorithm is comparable to the ODT for estimating TC intensity in the Atlantic, with a root mean square error (RMSE) of 13 kts. The RMSE increases slightly to 16 kts for both basins combined. In general, the AMSU algorithm has a tendency to over (under) approximate the intensity of weak (strong) TCs.

For the AMSU-estimated azimuthally averaged 34, 50, and 64 kt wind radii, the mean absolute errors (MAE) are 16, 17, and 8 nautical miles (nm), respectively. With respect to the average radii of each, these correspond to errors of 14.4 percent, 24.6 percent, and 17.8 percent. As with the intensity estimation algorithm, there is a tendency toward over (under) estimation of small (large) azimuthally averaged wind radii by the AMSU. Additionally, the wind radii estimates in the NE, SE, SW, and NW quadrants capture the asymmetric structure well, generally comparing favorably with the NHC operational advisory estimates. In some cases, the AMSU estimates may even be superior to NHC estimates, especially in the Eastern Pacific.

Finally, the 1999 and 2000 AMSU data are combined to refine the TC intensity and azimuthally averaged wind radii estimation algorithms. The two-year based algorithms currently are being tested on AMSU data received from the Atlantic and East Pacific basins during the 2001 tropical season.

Julie L. Demuth
Department of Atmospheric Science
Colorado State University
Fort Collins, Colorado 80523-1371
Fall 2001

Acknowledgements

Many thanks to my advisor, Dr. Thomas Vonder Haar, and committee members, Dr. Mark DeMaria, Dr. Wayne Schubert, and Dr. Ingrid Burke. Their suggestions have been extremely helpful and their time is greatly appreciated. Extra special thanks to Dr. Mark DeMaria for all his guidance and teachings, which were invaluable to me during my research. I also want to thank all of the Vonder Haar research group, especially Rich Moore, Brian McNoldy, and Rob Fleishauer, for their advice, assistance, and most importantly, their friendship.

Additional thanks are in order for many of the scientists at the Cooperative Institute for Research in the Atmosphere (CIRA) for their help, especially Stan Kidder, John Knaff, Jim Kossin, and Ray Zehr.

Thank you to many of my fellow classmates, with whom I worked countless hours on homeworks and studying for exams, including Andrea Williams, Crystal Pettet, Katie Walters, Sarah Tessendorf, Dan Lindsay, and Steve Brown.

I would like to thank my family and my closest friends, for their love and support, not just in the past two years, but always. Finally, extra special thanks to my fiancé, Sheldon Drobot; his unfailing love, support, and assistance has been invaluable to me the past 24 months, and I can truly say I would not be here without him.

Funding for this research is supplied in part by an American Meteorological Society Graduate Student Fellowship, sponsored by GTE Government Systems, and also by the United States Weather Research Program, NOAA grant NA67RJ0152.

Table of Contents

ABSTRACT ..... **III**

ACKNOWLEDGEMENTS ..... **V**

TABLE OF CONTENTS ..... **VI**

CHAPTER 1 - INTRODUCTION **1**

CHAPTER 2 - AMSU BACKGROUND **8**

2.1 PASSIVE MICROWAVE REMOTE SENSING 8
2.2 THE AMSU INSTRUMENT 11
2.3 THE AMSU TEMPERATURE RETRIEVAL 12
2.4 THE AMSU WIND RETRIEVAL 15

CHAPTER 3 - AMSU DATA ADJUSTMENTS **23**

3.1 HYDROMETEOR ATTENUATION CORRECTION 23
3.1.1 CLW Correction *24*
3.1.2 Ice Correction *25*
3.2 DATA SMOOTHING 27

CHAPTER 4 - OBJECTIVELY ESTIMATING TROPICAL CYCLONE INTENSITY **36**

4.1 INTENSITY ESTIMATION 36
4.1.1 Data *36*
4.1.2 Methods *40*
4.1.3 Results and Error Analysis *44*
4.1.4 1999 and 2000 Combined Data Set *48*

CHAPTER 5 - OBJECTIVELY ESTIMATING TROPICAL CYCLONE WIND RADII **68**

5.1 AXISYMMETRIC WIND RADII ESTIMATIONS 68
5.1.1 Data *69*
5.1.2 Methods *70*
5.1.3 Results and Error Analysis *71*
5.1.4 1999 and 2000 Combined Data Set *77*
5.2 ASYMMETRIC WIND RADII ESTIMATIONS 80
5.2.1 Data *80*
5.2.2 Methods *82*
5.2.3 Results and Error Analysis *88*

CHAPTER 6 - CONCLUSIONS AND FUTURE WORK **124**

6.1 CONCLUSIONS 124
6.2 FUTURE WORK 125

REFERENCES **128**

Chapter 1 - Introduction

In the past century, tropical cyclone (TC) forecasting and preparedness has improved dramatically, resulting in greater public awareness and substantially reduced loss of life. Nevertheless, Pielke and Landsea (1998) note that society has become more vulnerable to the effects of hurricanes; population and development along coastal areas are ever increasing, tourism is heightened along the United States coastal regions during hurricane season, and ocean vessels continue to be economically important, highlighting that a significant potential for large loss of life and property remains. Furthermore, Gray *et al.* (2000) and Goldenberg *et al.* (2001) (hereafter G00/G01) note that TC occurrence has been on the increase in the Atlantic basin since the mid-1990s; despite the less active El Niño year of 1997, the last six tropical seasons (1995-2000) combined are the most active consecutive years on record. G00/G01 suggest the increased activity is associated with changing sea surface temperatures (SSTs) due to a shift towards a stronger thermohaline circulation. The broad periodicity of this shift could mean decades of increased hurricane activity in the Atlantic. Of greatest concern is G00/G01's documented increase of intense hurricanes (IH) and intense hurricane days (IHD), compared to the 25 years prior (1970-1994). The ratio of the 1995-2000 to the 1970-1994 data reveals a 250% increase for IH and 373% for IHD. These threats of death and destruction drive the continual study for improving TC intensity and wind structure observations.

The United States Weather Research Program (USWRP) Hurricane Landfall research group recognizes that "...a gap exists between research accomplishments and operational implementation." (Elsberry, 2001). The USWRP indicates its goals are to assist the National Hurricane Center (NHC) by advancing scientific understanding and guidance products. Consequently, a major investment of USWRP FY01 funding is dedicated to accomplishing transitions to operational products for the NHC. Among their objectives is the desire to aid the NHC in (1) reducing intensity forecast errors by 20 percent, and (2) making skillful forecasts of gale and hurricane force radii.

The best method of estimating tropical cyclone intensity and wind structure is with *in situ* observations via aircraft reconnaissance. Unfortunately, because of the expense, reconnaissance operations are only available for the Atlantic basin, including the Atlantic Ocean, the Gulf of Mexico, and the Caribbean Sea (WMO, 1993). As a result, since the mid-1970s, operational estimates of TC intensity have relied upon a method developed by Dvorak (1975), which uses visible (VIS) satellite imagery to observe the central and banding features of TCs. A three-step analysis of the features is performed, including a comparison with previous imagery (if applicable), pattern recognition during which a T-number (a measure of TC intensity) is assigned (Table 1.1), and a quantified analysis of cloud features using a decision tree. Upon completion of the three steps, a final current intensity (CI) number is assigned to the TC, including a possible adjustment of up to one T-number for situations with rapidly changing environments. However, the reliance on VIS imagery limits TC intensity estimates to daytime. Dvorak (1984) later proposed an enhanced infrared (EIR) technique and then a simpler digital infrared (IR) technique to allow for TC intensity estimations 24 hours a day. Excluding the early stages of TC cyclogenesis, the IR techniques remove some of the subjectivity of the VIS technique. Dvorak's techniques currently are the worldwide

standard for TC intensity monitoring, especially when *in situ* data from aircraft reconnaissance are not available (WMO, 1993). Although Dvorak's methods are augmented by a set of empirical rules, analysts' interpretation of TC attributes nevertheless is subjective and can result in differences in intensity estimates of the same storm.

Velden *et al.* (1998) extended Dvorak's work on the digital IR technique to create an Objective Dvorak Technique (ODT), which uses the Man-Computer Interactive Direct Access System (McIDAS) computer system, and for which the only subjectivity comes from the user's selection of the storm center location. Once the center location is chosen, the ODT finds the warmest pixel within 40 km and considers that the eye temperature. It then analyzes a set of concentric rings outward from the eye to determine the surrounding temperature. This method is based on the theory that stronger eyewall convection is associated with colder cloud-top temperatures, and that eyewall convection is a proxy indicator of TC intensity. Based on the difference between the warm eye temperature and the coldest surrounding temperature, a T-number (Table 1.1.) is assigned to represent the intensity. Despite its desirable objective nature, the ODT is not applicable to tropical depressions (TD) or weak tropical storms (TS). Velden *et al.* (1998) recognize several other limitations as well, including when (1) a central dense overcast (CDO) is present, (2) strong vertical wind shear exists, and (3) the TC intensity is fluctuating rapidly.

Estimates of TC structure via the extent of 34, 50, and 64 kt winds also are challenging. Hawkins and Black (1983) used data from the Seasat Scatterometer to suggest that hurricane forecast centers consistently overestimate the radius of gale-force (34 kt) winds. Wind radii observations can be obtained from aircraft reconnaissance data, ship reports, buoy data, or scatterometer data. However, all these

observing techniques are lacking spatially; reconnaissance, ship, and buoy data occur opportunistically; and scatterometers are not useful when the ocean is foamy due to very high winds.

Due to the shortcomings of estimating TC intensity and wind structure, an alternate method is desired that is entirely objective and can be applied to tropical cyclones of all strengths, including tropical depressions, tropical storms, and hurricanes. Because anything other than sporadic *in situ* observations from aircraft reconnaissance is unfeasible, satellite remote sensing is a more viable option for data gathering. Visible and infrared imagery have desirable temporal resolution, but information cannot be obtained below the cloud top layer, and VIS imagery is only useful during the day when there is solar light to reflect. Alternatively, passive microwave remote sensing is opportune for TC studies. Microwaves penetrate clouds beyond the top layer, a quality most notably beneficial when a CDO exists, and they are unaffected by hydrometeor contamination except in heavily precipitating regions. Moreover, microwave sensing is not limited to a certain time of day. Accordingly, the Advanced Microwave Sounding Unit (AMSU) is utilized in the quest for effective, objective TC intensity and structure estimates.

Although previous TC studies have been done with older, poorer resolution microwave instruments (Kidder *et al*, 1980; Velden, 1989; and Velden *et al.*, 1991), the AMSU is the first microwave instrument on a NOAA satellite with adequate spatial and vertical resolution to estimate TC intensity and winds objectively; although the spatial resolution is not good enough to resolve the important inner core structure of a TC for direct use, the detail is sufficient to derive several parameters for analysis. In their implementation plan, the USWRP acknowledges the potential of the AMSU to provide tropical cyclone maximum wind and wind structure estimates (Elsberry, 2001). Spencer

and Braswell (2001) used limb-adjusted brightness temperatures to statistically relate six AMSU-derived parameters, four with temperature information and two for correction hydrometeor contamination, to the maximum sustained winds of a TC. While their results are good for cases with corresponding *in situ* data, the results degrade measurably for non-*in situ* cases. In another study, Brueske and Velden (2001) first corrected for scan geometry and then used both AMSU-A and AMSU-B to estimate TC intensity via the minimum sea level pressure. Their reported results are comparable with the Dvorak technique. However, both studies are limited to estimating TC intensity in the Atlantic basin only.

This study investigates an alternative method of using AMSU data to estimate TC intensity objectively via the maximum wind speed. Additionally, unlike the work Spencer and Braswell (2001) or Brueske and Velden (2001), this study also uses AMSU data to approximate the wind structure of TCs via the azimuthally averaged radii of 34, 50, and 64 kt winds. AMSU retrieved temperature data from the Atlantic and East Pacific basins from the 1999 tropical season are used to derive various parameters at 23 pressure levels over a TC. The parameters are used statistically to develop the intensity and azimuthally averaged wind algorithms, which then are tested on the 1999 data and cross-validated on data from the 2000 tropical season. Estimations of the azimuthally averaged wind radii subsequently are used in association with a Rankine vortex model to provide asymmetric radii profiles of the three wind speeds. Finally, using the 1999 and 2000 data sets combined, the estimative intensity and azimuthally averaged wind algorithms are refined and will be tested independently during the 2001 tropical season.

Chapter Two provides a background of using passive microwave theory in remote sensing as well as specific attributes and data retrieval processes of the AMSU. A correction for the aforementioned hydrometeor attenuation, which occurs in the

strongly convective areas of a TC, is discussed in Chapter Three. The data, methods, and results of the TC intensity estimations are presented in Chapter Four as well as the refined estimators from the 1999/2000 combined data. This same layout is used in the following chapter for the wind radii estimations, with the exception of the latter section for the asymmetric radii. The discussion is concluded with a brief summary of the major findings followed by suggestions for future work.

Table 1.1. Empirically derived relationship between the Dvorak current intensity (CI) number, the maximum wind speed (MWS) at the surface, and the minimum sea level pressure (MSLP) for Atlantic tropical cyclones.

CI / T – Number	MWS (kts)	MSLP (hPa)
1	25	N/A
1.5	25	N/A
2	30	1009
2.5	35	1005
3	45	1000
3.5	55	994
4	65	987
4.5	77	979
5	90	970
5.5	102	960
6	115	948
6.5	127	935
7	140	921
7.5	155	906
8	170	890

Chapter 2 - AMSU Background

2.1 Passive Microwave Remote Sensing

Two fundamental properties governing satellite remote sensing are that (1) all matter above absolute zero emits radiation that can be measured by means of the electromagnetic spectrum, and (2) electromagnetic radiation transports energy which interacts with the atmosphere before being detected by satellites. Radiation is characterized by wavelength, the distance between successive crests or troughs of the wave, or by frequency, the number of waves that pass a point per unit time. Wavelength is measured in length with a base unit of meters (m), but it typically is expressed in millimeters (mm), centimeters (cm), or micrometers (μm). Frequency is expressed in hertz (Hz) or gigahertz (GHz). Frequency (ν) and wavelength (λ) are related by the speed of light in a vacuum, c = 2.997 x 10^8 meters per second, by the following equation:

$$\nu = \frac{c}{\lambda} \qquad [2.1]$$

Radiation is a function of temperature and wavelength such that two identical objects at the same temperature will emit different amounts of radiation at different wavelengths, or two identical objects at the same wavelength will emit different radiation amounts at different temperatures. From this observation came the idea of a blackbody (BB), an object that absorbs the maximum amount of possible radiation at each wavelength, so that none is reflected, and then perfectly emits all radiation as well.

Upon his discovery of quanta, Max Planck derived an equation showing the relationship among the radiance emitted by a blackbody, temperature, and wavelength,

$$B_\lambda(T) = \frac{c_1 \lambda^{-5}}{\exp\left(\frac{c_2}{\lambda T}\right) - 1} \qquad [2.2]$$

where c_1 and c_2 are the first and second radiation constants, and T is temperature (Figures 2.1a,b). However, no object is a true BB, thus most materials are less than perfect emitters. In the microwave (MW) frequency range, an approximation to Planck's function is applicable. For temperatures existing on Earth and in its atmosphere, the relatively long millimeter and centimeter wavelengths of microwaves cause the exponent factor in [2.2] to be much less than unity. Accordingly, the approximation can be made that,

$$\exp\left(\frac{c_2}{\lambda T}\right) \cong 1 + \frac{c_2}{\lambda T} \qquad [2.3]$$

Making this substitution into [2.2] reduces it to,

$$B_\lambda(T) = \frac{c_1}{c_2} \lambda^{-4} T \qquad [2.4]$$

Equation 2.4 is known as the Rayleigh-Jeans approximation, and it illustrates that there is a linear relationship between temperature and radiance in the microwave portion of the spectrum (Figure 2.1b). It is common to divide [2.4] by $(c_1/c_2)\lambda^{-4}$, the result of which is called the brightness temperature (T_b), which typically is defined as,

$$T_b = eT \qquad [2.5]$$

where e is the emissivity and T is the physical temperature of the observed volume. In nature, emissivities are less than unity and T_bs are less than the physical temperature (Ulaby *et al*, 1986).

The MW portion of the electromagnetic spectrum ranges from approximately 0.1 cm (300 GHz) to 3.0 cm (10 GHz) (Figure 2.2). In this spectral region, all natural entities emit MW radiation, albeit weakly. The acquired T_b is therefore a function of emission from within Earth, Earth's surface, and the atmosphere. Over short horizontal distances (e.g. tropical cyclones) variations in T_b primarily are due to fluctuations in emissivity as opposed to physical temperature (Ulaby *et al*, 1986).

The transmittance of the Earth's atmosphere in the MW spectrum (Figure 2.2) shows three window (high transmittance) regions, one at the lower frequencies, another centered at about 90 GHz, and a final one centered around 150 GHz. On the contrary, there are four absorptive regions, two each for water vapor and oxygen. The water vapor regions exist at roughly 25 and 180 GHz, the oxygen regions at 60 and 120 GHz. As will be discussed in Section 2.3, it is the numerous AMSU channels around the 60 GHz region of the spectrum that allow for the valuable vertical temperature profile.

In addition to emissivity variations, the T_bs for TCs are particularly influenced by hydrometeor scattering and absorption. As mentioned previously, the advantage of MW over VIS or IR imagery is that MWs penetrate clouds, obtaining information below the cloud top layer. Physically, this is attributed to Rayleigh scattering; the sizes of cloud droplets are so much smaller than MW wavelengths that they only weakly interact with MW radiation. Kidder and Vonder Haar (1995) specifically note that the transmittance of MW radiation through a typical non-raining cloud is greater than 90 percent. However, Mie scattering explains that, because their larger particle sizes are on the order of the radiation wavelength, raindrops and ice particles do interact with microwaves. Raindrops are dominated by absorption, ice particles by scattering. As will be discussed in Section 3.1, these particles attenuate the MW signal, reducing the amount of radiation

reaching the sensor. The result is lower T_bs and consequently, colder retrieved temperatures. Thus, a hydrometeor correction is needed.

2.2 The AMSU Instrument

The first AMSU instrument was launched 13 May 1998 aboard the NOAA-15 polar orbiting satellite. A considerable improvement over its predecessor, the Microwave Sounding Unit (MSU), the horizontal resolution of the AMSU is more than doubled with a nadir resolution of 48 km (Figure 2.3). There are 20 total channels from which the AMSU senses MW radiation, 12 of which have frequencies on the low-frequency side of the oxygen absorption band between 50 and 60 GHz. This tripled number of channels over the MSU improves the vertical resolution considerably and provides a superior temperature sounding between the surface and 1 hPa. A complete listing of all AMSU channels and frequencies are given in Table 2.1.

The AMSU is comprised of three different instruments. AMSU-A1 (Channels 3-15) includes all channels in the oxygen band for temperature sounding as well as a window channel at 89.0 GHz to monitor surface features. AMSU-A2 (Channels 1 and 2) includes the 23.8 GHz channel for obtaining total precipitable water (TPW) over oceans and another window channel at 31.4 GHz. The primary objective of these two instruments, collectively referred to as AMSU-A, is to provide temperature soundings. However, it also is useful in deriving other tropical cyclone parameters of interest, including cloud liquid water (CLW) and rain rate (Kidder *et al.*, 2001) (hereafter K00). The third instrument, AMSU-B, has three of its channels centered around the water vapor absorption band at 180 GHz while the other two channels, 89.0 and 150.0 GHz are window channels. Its primary task is to provide moisture soundings; no data from it are used in this study, but Brueske and Velden (2001) use AMSU-B data to estimate TC eye size in their work. Finally, the AMSU-A is a cross-track scanning instrument with 30

footprints combining to create a swath width of 2179 km. For a detailed comparison between the AMSU channels and those of other microwave instruments flown on polar orbiting satellites, see K00.

While the AMSU provides many advantages for studying tropical cyclones, including its ability to monitor storm location and movement and measure thermal anomalies, wind speeds, cloud liquid water, and rain rate, there are disadvantages, too. In general, a polar orbiting satellite will pass over each position on Earth twice daily. With the launch of a second AMSU on 21 September 2000 aboard NOAA-16, the current temporal resolution of the tropics is four times daily. This study uses only data from the first AMSU, although both instruments are receiving data for the current 2001 tropical season. Even with the additional instrument, however, significant changes in a tropical cyclone can occur between AMSU passes. Furthermore, because the AMSU is aboard a polar-orbiting satellite, coverage at and near the equator is not contiguous (Figure 2.4). Consequently, tropical disturbances can fall between passes and not be observed. Finally, although the horizontal resolution of the AMSU is much improved compared to that of the MSU, it nevertheless is too coarse to be used directly to observe tropical cyclones. According to Landsea (2001), the eye size of a tropical cyclone can range from 8 km to over 200 km, but most range from 30 to 60 km. Even the best AMSU horizontal resolution of 48 km is not sufficient to resolve the important inner core structure of TCs.

2.3 The AMSU Temperature Retrieval

While the AMSU-A system was developed with the original motivation to monitor temperature trends for climate applications (Goldberg, 1999), the temperature retrieval has been exploited for short range and nowcasting applications such as tropical cyclone analysis. As mentioned, the additional AMSU-A channels on the wings of the 60 GHz

oxygen absorption band represent a major improvement of AMSU over MSU, allowing for the retrieval of atmospheric temperature with greatly improved vertical resolution.

Prior to the retrieval, two corrections to the data are made for scan position and viewing angles. Using an algorithm by Mo (1999), the raw antennae measurements are converted to brightness temperatures by removing contributions from the antennae sidelobes, which can point at the spacecraft itself, space, or other parts of Earth. Next, a limb correction is made to adjust the T_bs to appear as nadir observations, accounting for the different view angles from the 30 different footprints (Wark 1993). K00 notes that, without the limb adjustment, the T_bs could vary by as much as 15 K along a scan line due to vertical variations in atmospheric temperature. Goldberg (1999) used 30 days of data to calculate mean T_bs from which regression coefficients were computed to make the limb adjustment.

Upon completion of the two corrections, atmospheric temperature is retrieved at 40 pressure levels between 1000 and 0.1 hPa by means of another regression analysis by Goldberg (1999). However, only 23 pressure levels between 920 and 50 hPa are used in this study (i.e. 50, 60, 70, 85, 100 115, 135, 150, 200, 250, 300, 350, 400, 430, 475, 500, 570, 620, 670, 700, 780, 850, and 920 hPa); the former constraint is due to the 1000-hPa level generally being below the surface for low pressure systems such as TCs, and the latter condition of 50 hPa prevents noise from lower pressure levels from influencing the retrieved surface pressure. For his retrieval, Goldberg (1999) used AMSU-A limb adjusted T_bs, collocated with four months of radiosonde temperature profiles to calculate regression coefficients to estimate temperature up to 10 hPa. Above that level, rocketsonde profiles compensated for the lack of radiosonde data.

The AMSU-A weighting functions, which show the fit of the retrievals to the limb-adjusted brightness temperatures, represent the height from which the strongest

microwave signal is acquired (Figure 2.5). Goldberg (1999) used different channel combinations for the retrievals at different levels. No channel lower than eight was used for retrievals above 100 hPa to protect against contamination from high terrain or intense precipitation. Additionally, Channels 3 through 5 were not utilized for the retrieval between 700 and 115 hPa to reduce errors due to hydrometeor attenuation. Finally, different coefficients were generated for ocean and non-ocean surfaces for the 780-hPa level and below, but the same coefficients were used for 700 hPa and above. Further information on the temperature retrieval methods and its error statistics can be found in Goldberg (1999).

An advantage of the statistical retrieval technique is the independence from operational data assimilation and model physics for an initial condition first guess. Rather, in order to compute an accurate temperature profile, only a climatological first guess is needed which is simplified by the previously discussed Rayleigh-Jeans approximation that MW radiance is linear with temperature. As a result, the temperature retrievals are particularly useful in data sparse regions and in regions where a model first guess is not particularly good, such as near TCs.

The most important application of the temperature retrieval to tropical cyclones is the ability of the AMSU to detect warm upper-tropospheric anomalies. Figure 2.6 is a radial-height cross-section of temperature anomalies through Hurricane Gert when it was a Category 4 storm with winds of 115 kts; the warm core of the TC at approximately 12 km is clearly evident. Knaff *et al.* (2000) demonstrated the utility of this capability by using the AMSU to differentiate between two cyclone systems, one warm core, the other cold core, existing simultaneously in the South Pacific Ocean.

2.4 The AMSU Wind Retrieval

There are several assumptions underlying the retrieval of the horizontal wind field from AMSU temperature data, including those of hydrostatic and gradient balance. The temperature retrievals described in the previous section provide temperature (T) as a function of pressure (p) at each of 23 pressure levels between 920 and 50 hPa. These data are interpolated to a radial grid, with the TC center located at the origin, so that T is a function of pressure and radius, r, which extends from 0 to 600 km. Details on the interpolation method can be found in K00. No surface temperature or pressure information can be derived from the AMSU; rather the surface pressure (p_s) at the boundaries (r = 600 km) and the surface temperatures (T_s) over the entire domain are obtained from the National Center for Environmental Prediction (NCEP) analyses closest in time to the AMSU swath.

The next step is deriving the geopotential height (Z) field as a function of pressure using hydrostatic integration. In doing so, additional assumptions are made that (1) temperature varies linearly with height between two pressure levels, (2) variations in gravity with height are neglected so that height and geopotential height are equivalent, and (3) virtual temperature effects are neglected. As K00 note, errors associated with the latter approximation of disregarding moisture effects should be small compared to errors in the mass field due to the coarse resolution of the AMSU.

Hydrostatic integration begins at the surface at the outer radius of the domain. The equation is integrated upward to give the height of the first AMSU pressure level (920 hPa) at r = 600 km, then upward again to acquire the height of the next pressure level, and so forth up to 50 hPa. A final assumption then is made that the 50 hPa level is above all perturbations associated with the TC so that the height of this level is constant at all radii. Hence, the hydrostatic equation can be integrated downward from 50 hPa at

all radii to give the height of each pressure level in the interior of the domain down to 920 hPa. With the height and temperature of the 920-hPa level as well as the surface temperature from NCEP, the hydrostatic equation is then integrated to get the surface pressure at all points inside the outer boundary. Upon calculation of the surface pressure, the surface density is calculated using the ideal gas law.

To reiterate, at this point the heights and temperatures are known as a function of radius for the 23 pressure levels between 920 and 50 hPa, as are the surface temperatures, pressures, and densities. Recalling the assumption of a linear variation in temperature with height, the temperature and pressure at any height can be calculated.

Again, the assumption of gradient balance is the basis for the wind retrieval. In height coordinates, the gradient wind equation is given by,

$$\frac{V^2}{r} + fV = \frac{1}{\rho}\frac{\partial p}{\partial r} \qquad [2.6]$$

where the terms, from left to right, represent the centrifugal force, the Coriolis force, and the pressure gradient force. For simplicity, the latter term will be written as P_g. Since the variable desired to be known is the tangential wind, [2.6] is solved for V via the quadratic equation.

$$V = \frac{-rf}{2} \pm \sqrt{\left(\frac{rf}{2}\right)^2 + rP_g} \qquad [2.7]$$

Since the tangential wind must be real, not all roots correspond to physically possible solutions. In the Northern Hemisphere, the Coriolis parameter, f, is always positive, and for a low pressure system (e.g. a tropical cyclone), pressure increases outward with radius so P_g is positive as well. Thus, for a low pressure system, the radicand in [2.7] will always be real, and V will be positive. On the contrary, for a high pressure system, pressure decreases with radius causing P_g to be negative so that the radicand in [2.7]

could be complex. To prevent this, the radicand is never allowed to be negative by stipulating that,

$$\left|P_g\right| \le r\left(\frac{f}{2}\right)^2 \qquad [2.8]$$

or by forcing,

$$P_g = -r\left(\frac{f}{2}\right)^2 \qquad [2.9]$$

when the magnitude of P_g is greater than the right hand side of [2.8]. The tangential wind calculations in pressure coordinates are the same as Equations 2.6 – 2.9, with the pressure gradient term expressed as follows.

$$P_g = g\frac{\partial Z}{\partial r} \qquad [2.10]$$

From [2.7], the tangential wind is found by first calculating the pressure gradient, P_g, of the tropical cyclone using centered derivatives for the radial derivative of pressure with a one-side difference at r = 600 km. With P_g, V is computed as a function of radius and height to get to horizontal wind field of the TC over the domain. DeMaria (2000a) explains the AMSU wind retrieval in great detail.

An example of the AMSU-derived gradient winds is shown in a radial-height cross-section of Hurricane Gert (Figure 2.7) corresponding to the time of the temperature anomaly plot in Figure 2.6. The hurricane had maximum sustained winds of 115 kts at this time, however, the coarse resolution of the AMSU and the smoothing of the AMSU data (to be discussed in the next chapter) leads to reported winds of only 45 kts. As will be explained in Chapter 4, this prevents direct usage of the AMSU in estimating TC intensity.

Table 2.1. Microwave frequencies (GHz) for AMSU A1, A2, and B channels.

Channel	Frequency	Instrument
1	23.8	A2
2	31.4	A2
3	50.3	A1
4	52.8	A1
5	53.6	A1
6	54.4	A1
7	54.9	A1
8	55.5	A1
9	57.2	A1
10	57.29 ± 0.217	A1
11	$57.29 \pm 0.322 \pm 0.048$	A1
12	$57.29 \pm 0.322 \pm 0.022$	A1
13	$57.29 \pm 0.322 \pm 0.010$	A1
14	$57.29 \pm 0.322 \pm 0.0045$	A1
15	89.0	A1
16	89.0	B
17	150.0	B
18	183.3 ± 1	B
19	183.3 ± 3	B
20	183.3 ± 7	B

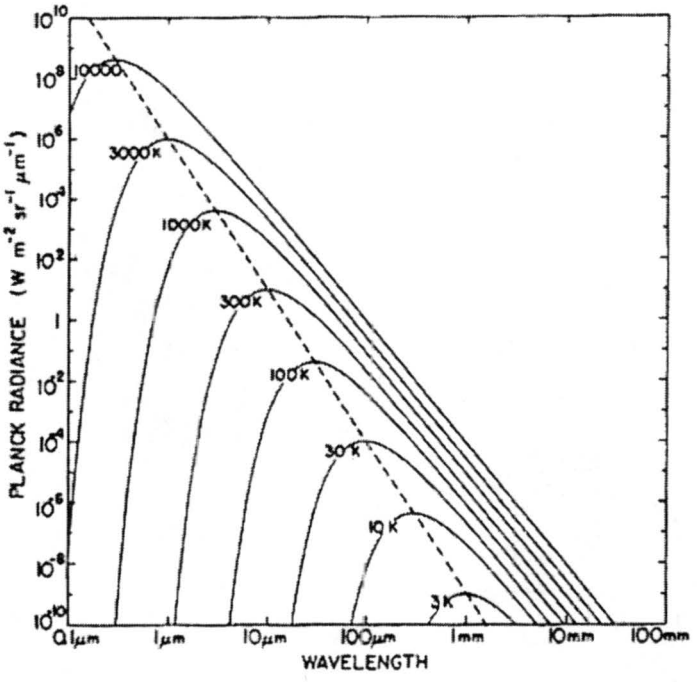

a)

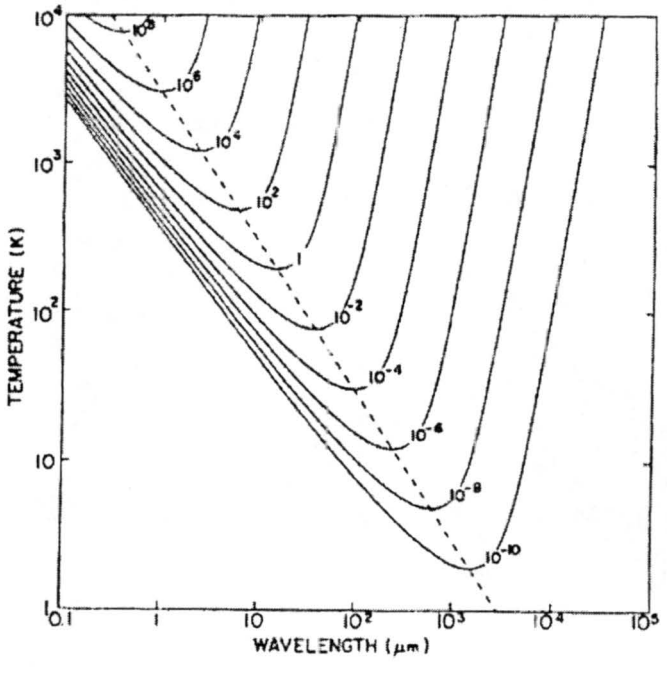

b)

Figure 2.1. The Planck function showing the relationship between blackbody radiance and wavelength for varying temperatures (a) and temperature and wavelength for varying radiances (b); from Kidder and Vonder Haar (1995).

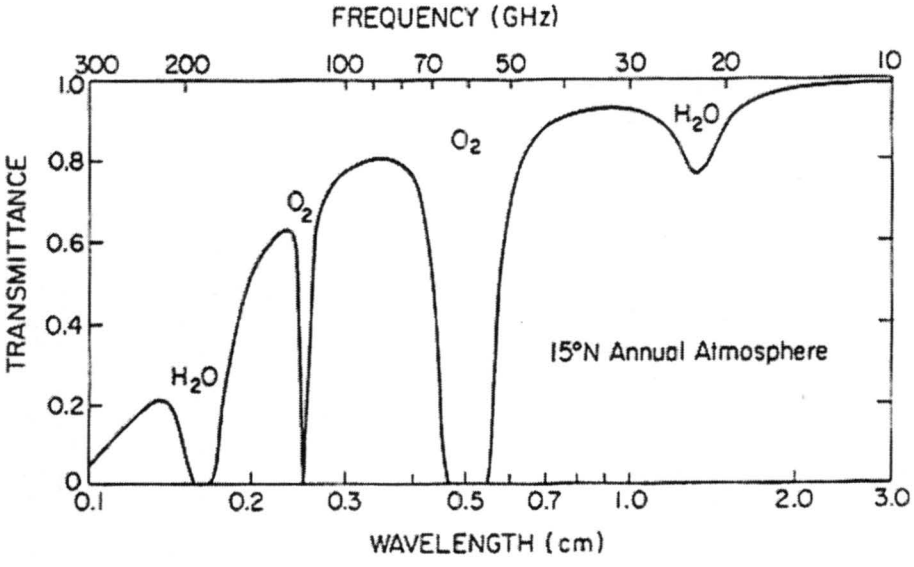

Figure 2.2. Transmittance in the microwave portion of the electromagnetic spectrum; from Kidder and Vonder Haar (1995).

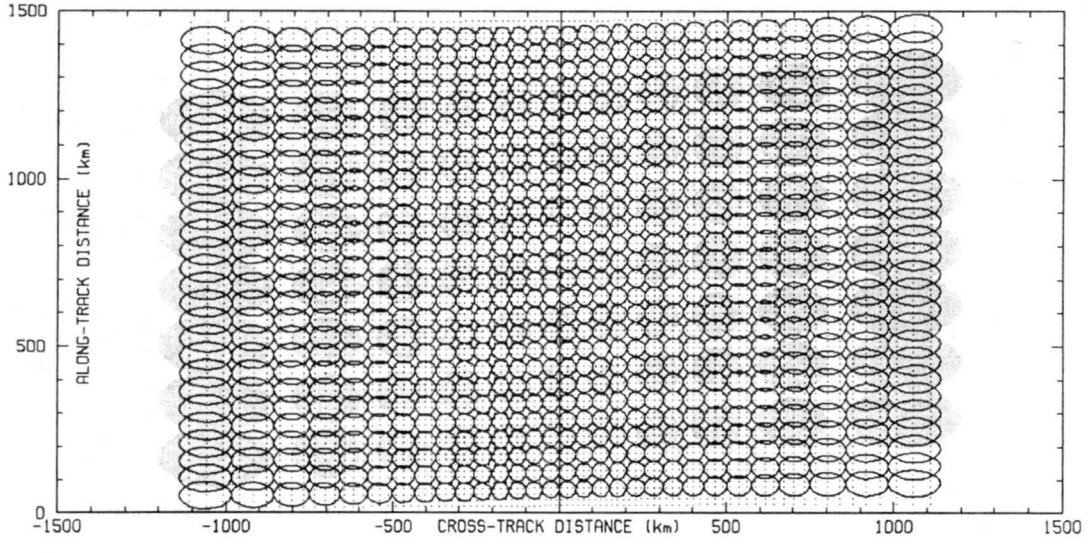

Figure 2.3. Comparison between the 110 km horizontal resolution of the Microwave Sounding Unit (gray shaded ellipses) and the 48 km horizontal resolution of the Advanced Microwave Sounding Unit-A unit (black outlined ellipses); from Kidder *et al.* (2000).

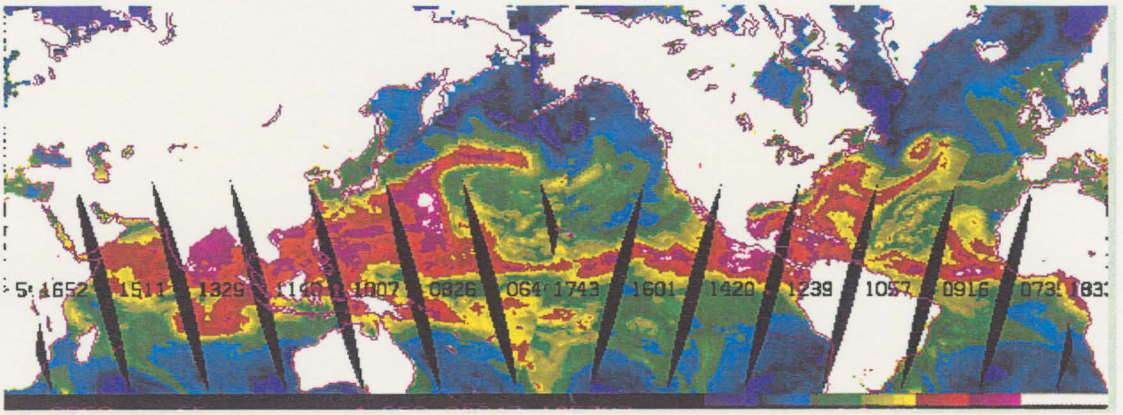

Figure 2.4. Swath data showing AMSU-derived total precipitable water, highlighting non-contiguous coverage at and near the Equator.

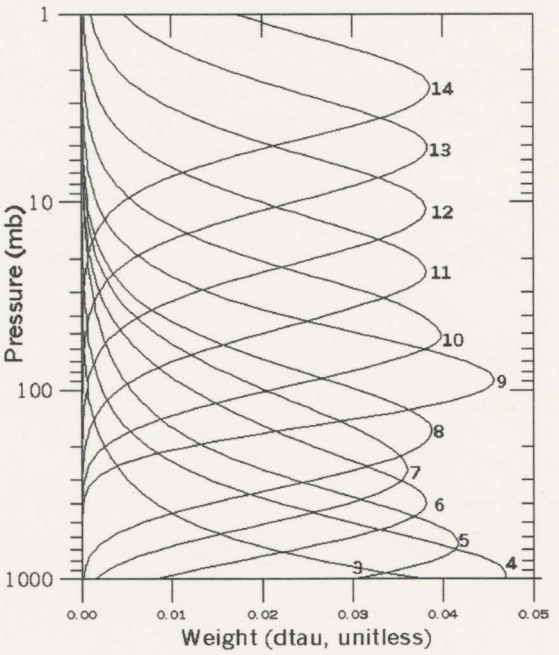

Figure 2.5. Weighting functions for AMSU-A temperature retrieval channels 3 – 14.

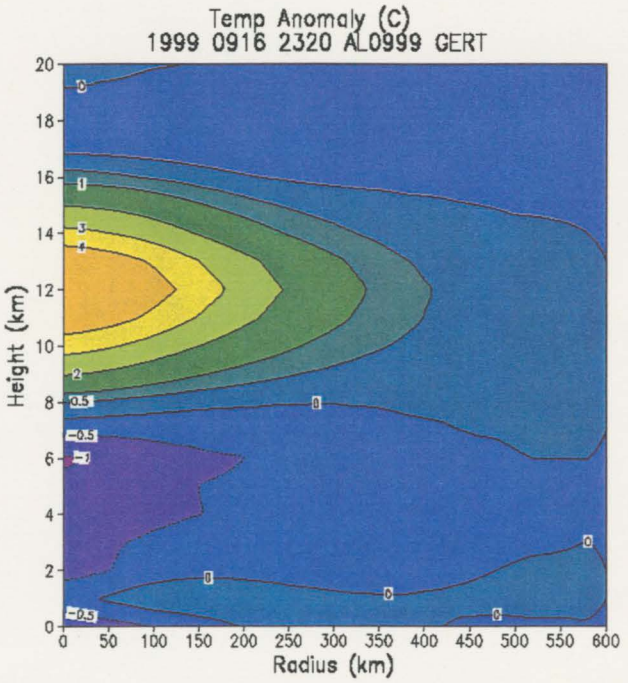

Figure 2.6. Radial-height cross-section of AMSU-derived temperature anomalies showing the warm core at a height of approximately 12 km for Hurricane Gert.

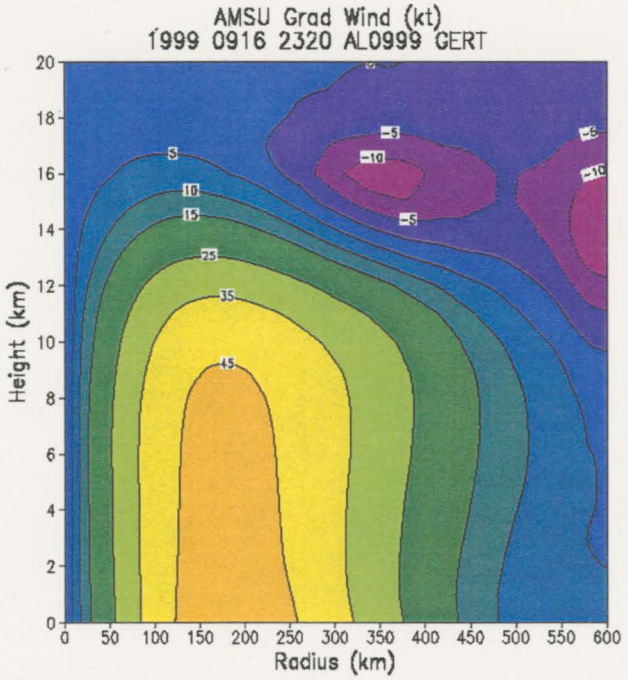

Figure 2.7. Radial-height cross-section of AMSU-derived gradient winds for Hurricane Gert.

Chapter 3 - AMSU Data Adjustments

3.1 Hydrometeor Attenuation Correction

As discussed previously, an advantage of microwave sounding is the ability for information to be relayed from many levels of the atmosphere, rather than from the cloud-top layer only as with VIS and IR imagery. However, utilizing MW in heavily precipitating regions presents a challenge. Because of their relatively large sizes, cloud liquid water (CLW) droplets and ice crystals absorb and scatter microwave radiation (Section 2.1). In strongly convective areas of tropical cyclones, CLW and ice crystals are abundant, reducing the amount of MW radiation reaching the AMSU sensor. The results are anomalously cold retrieved temperatures, which cause erroneously high pressures and, thus, reduced pressure gradients. As shown in Section 2.4, artificially weak pressure gradients mean unrealistically weaker winds. CLW contamination is especially problematic for the lower AMSU channels whose weighting functions peak in the lower troposphere (Figure 2.5) where copious amounts of CLW exist. On the other hand, ice crystals exist higher in the troposphere, thus corrections for their scattering affect are more important at low pressure levels.

In order to more accurately represent the TC temperature, pressure and wind fields, a correction for hydrometeor affects is necessary. DeMaria *et al.* (2000) discuss a preliminary correction for CLW effects, and Linstid (2000) outlines a method for rectification of ice crystal scattering. Modification of both works is done in this study to

provide two separate corrections, one for CLW attenuation and a subsequent one for ice scattering, as described below.

Both are corrected at 12 pressure levels between 350 and 920 hPa (i.e. 350, 400, 430, 475, 500, 570, 620, 670, 700, 780, 850, and 920 hPa) at which AMSU temperatures are retrieved. The data used in developing the correction come from 64 AMSU passes over Atlantic and East Pacific storms from the 1999 tropical season. Despite the 154 total passes over tropical disturbances that year, only those completely over ocean are used in order to provide homogeneity in the sample.

3.1.1 CLW Correction

The basis of the CLW correction is to remove the artificial relationship between lower temperatures and large amounts of CLW. The temperature data utilized in the correction consist of all AMSU swath points (footprints) within a 12° by 12° storm-centered grid. This number varies depending on where in the AMSU swath a TC falls. Recalling from Figure 2.3, more points are included when the TC falls near nadir as opposed to further out in the swath.

Each footprint has an associated temperature and CLW value. Initially, at each pressure level, the mean temperature of all the swath points is calculated for each storm and subsequently used to find the temperature deviation,

$$T_{dev}(i) = T_{mean} - T(i) \qquad [3.1]$$

at each footprint. From [3.1], a positive (negative) temperature deviation is representative of colder (warmer) temperatures compared to the mean. A linear regression then is performed 12 times, once at each pressure level, using the data points from all 64 AMSU passes with the temperature deviations as the dependent variable and the associated CLW values as the independent variable.

Next, the slopes of the 12 regression lines are plotted against the corresponding pressure level, and a quadratic curve then is fit to the data (Figure 3.1). At 350 hPa, the slope is nearly zero, indicating CLW does not affect temperature due to less CLW at this level. In contrast, the magnitude of the slope is largest at 920 hPa; this reveals temperature decreases when CLW increases, as expected, resulting in larger values of T_{dev}.

In order to correct for the artificially low temperatures, the quadratically fit value of the slope, m, at each pressure level (Figure 3.1) is the factor by which the temperatures are increased based on the following equation:

$$T_{corrected}(i) = T_{original}(i) + m * CLW(i) \qquad [3.2]$$

3.1.2 Ice Correction

Succeeding the CLW correction, the temperature data are corrected further for scattering by ice crystals via the method described by Linstid (2000) with minor modifications. Prior to the ice correction, a distance-weighted averaging method (Barnes 1964) is used to interpolate the unevenly spaced swath data to an evenly spaced 12° by 12° grid with 0.2° grid spacing. It would be preferable to do the ice correction on the swath data, as with the CLW correction, because Barnes's interpolation smoothes the data, as will be explained in Section 3.2. However, the Laplacian method utilized by Linstid (2000), described as follows, requires that the data be evenly spaced.

At each of the 12 aforesaid pressure levels, the mean temperature of the data unaffected by ice is calculated only using points where the associated CLW value is less than 0.2 mm. This constraint is based on the assumption that cloud ice does not occur where there is little or no CLW. Then, if the temperature at a given grid point is less than

the mean temperature minus 0.5 °C, the data point is considered too cold due to ice attenuation, and it is flagged to be corrected.

Once all the points affected by ice are flagged at each pressure level, Laplace's equation [3.3] is used to fix the corrupted data because it provides a smooth temperature field using uncorrupted data points (Linstid, 2000).

$$\nabla^2 T = 0 \qquad [3.3]$$

Equation 3.3 is solved by iteratively replacing each flagged data point with the average of its nearest neighbors, of which there are four if the point is in the center of the domain, three if it is on the side, and two if it is in the corner. This correction procedure is continued until the temperatures of all the flagged data points converge such that the difference in the temperatures between the previous and current iteration are less than 0.005 °C.

Figures 3.2 – 3.4 show the uncorrected versus the hydrometeor corrected plots of the radial-height cross-sections of temperature anomaly (°C) and azimuthally averaged gradient wind (kts) as well as the radial profiles of surface pressure (hPa); an example is shown for a tropical depression, a tropical storm, and a hurricane.

While the features of Tropical Depression are not well-defined, the improvement from the correction is evident (Figure 3.2). The anomalously cold temperatures in the lower troposphere are increased slightly, and the dual high pressure areas are removed. Nonetheless, because of the unorganized pressure field, the wind field is rather chaotic.

The improvements are more apparent in the plots of Tropical Storm Jose (Figure 3.3). The temperature anomalies are largely improved, warming a few degrees, and the high pressure area is removed. The resulting wind field is more realistic, having removed the anticyclonic feature near the storm center.

As expected, the effects of the CLW and ice corrections are most obvious for the stronger TCs for which hydrometeors are more abundant. Hurricane Gert was a Category 4 storm with maximum sustained winds of 115 kts at this time (Figure 3.4). Again, the correction removed the large area of cold temperatures and the large high pressure area. The adjusted wind profile is much more accurate than the uncorrected version, with the anticyclonic area at the storm's edge removed.

3.2 Data Smoothing

As mentioned above, part of the AMSU data retrieval includes interpolation from the swath to a grid which smoothes the data, the degree of which is important. Noise from errors or fine scale features causes perturbations in the cloud liquid water, temperature, pressure, and wind fields. On the other hand, the data can be smoothed too much, such that useful information is lost. This affects the AMSU-derived parameters (as discussed in Section 4.1), which, in turn, affects the estimates of intensity and wind structure.

As alluded to during the ice correction discussion, the smoothing process occurs via the interpolation of data from the swath to the grid as described by Barnes (1964). The smoothing process employs a technique in which the influence of each swath data point is weighted according to its distance from the grid point. In other words, the closer a swath point is to the grid point in question, the greater influence it exerts, thus it is weighted more. Such smoothing schemes tend to smooth all variations in a field, whether they are actual disturbances or data errors, but Barnes employed a technique for regaining lost details. He developed a weight factor based on the principle that a two-dimensional distribution of some atmospheric variable can be represented by a summation of an infinite number of independent harmonic waves (i.e. a Fourier integral

representation). DeMaria (2000b) discusses the application of Barnes's work to the AMSU retrievals, the highlights of which are included below.

For simplicity, only a single harmonic wave in one dimension is discussed, keeping in mind that the following is applicable to all component waves in greater dimensions. In this simple version, the value of some variable T (temperature in this case) at the analysis grid point x, where the summation is from i = 1 to N number of data points, is given as:

$$T(x) = \frac{\Sigma w_i T_i}{\Sigma w_i} \qquad [3.4]$$

T_i represents the observed temperature values, and w_k is the weight factor, given as:

$$w_i = e^{-(d/r_e)^2} \qquad [3.5]$$

where r_e is the e-folding radius in km, and d is the distance between the swath and grid points in km; the latter must be smaller than some pre-defined influence radius, r_i. Typically, r_i is set as 2 to 10 times the value of r_e to ensure at least a few data points are included in the summation in [3.4] for each analysis grid point, x. In summary, the interpolated value of a variable on the grid is simply the sum of the weighted values of the surrounding data on the swath within the influence radius.

From [3.5], the parameters influencing the smoothing are the e-folding and influence radii, the latter of which is set as five times the e-folding radius for this study. Regarding the importance of r_e, DeMaria (2000b) describes how a single sine wave [3.6] integrated over all points reduces to [3.7]:

$$T(x) = A\sin(kx) \qquad [3.6]$$

$$\overline{T(x_o)} = A\sin(kx_o) * e^{-(k^2 r_e^2/4)} \qquad [3.7]$$

where A is the amplitude and k is the wavenumber. The analysis of $T(x)$ (Equation 3.7) is a sine wave with no phase shift, but with an amplitude reduced by a factor $e^{\wedge}(kr_e/2)^2$. In other words, the Barnes analysis can be interpreted as a low-pass filter with a response function denoted as,

$$R(k, r_e) = e^{-(kr_e/2)^2} \qquad [3.8]$$

The wavenumber is a function of wavelength, λ, which in turn is a function of spatial scale, Δx. This can be represented as follows:

$$k = \frac{2\pi}{\lambda} \qquad [3.9]$$

$$\lambda = 2\Delta x \qquad [3.10]$$

$$k = \frac{\pi}{\Delta x} \qquad [3.11]$$

Substituting [3.11] into the response function [3.8] yields,

$$R(\Delta x, r_e) = e^{-(\pi r_e/2\Delta x)^2} \qquad [3.12]$$

Response function values range from 0 to 1, the former meaning the features are smoothed out entirely, and the latter meaning the features are not smoothed at all.

A plot of response functions over varying spatial scales shows how $R(\Delta x, r_e)$ changes with larger e-folding radii (Figure 3.5). At the smallest e-folding radius of 50 km, over 90 percent of the detail at a spatial scale of 50 km is smoothed out, but less than 50 percent is diminished for scales of 100 km and larger. The lack of smoothing for the larger scales retains too much noise in the data. On the other hand, the largest e-folding radius of 200 km over-smoothes the data. Features at scales of 50 to 150 km are eliminated almost entirely, and at larger scales up to 350 km, less than half of the original data is retained.

Obviously an e-folding radius amid the two extremes is desirable; the AMSU data should neither be under nor over smoothed. It is preferable that features at the smallest scales are highly smoothed while as much data as possible is retained at scales greater than 250 km. The exponential decline of the response function at the two smallest spatial scales as opposed to the more gradual decline at the larger scales makes these requirements feasible. An e-folding radius of 100 km accommodates both requirements. With r_e = 100 km, over 90 percent of all data is smoothed at scales of 100 km and smaller. Conversely, less than 20 percent is smoothed at spatial scales greater than 350 km, less than 25 percent is smoothed at 300 km, and only one-third is smoothed at 250 km. A comparison between r_e set at 80 and 100 km is shown for a surface pressure plot of Hurricane Gert (Figure 3.6a,b). The greater noise in the first figure, with the e-folding radius of 80 km, is clearly evident by the less smooth contours. Thus, 100 km is chosen as the smoothing parameter for the Barnes analysis for the AMSU data.

To recap, the hydrometeor corrections for CLW and ice contamination result in more realistic tropical cyclone fields and parameters. The subsequently smoothed data fields result in improved derived parameters, which further enhance the estimative intensity and wind radii algorithms as discussed in Chapters Four and Five.

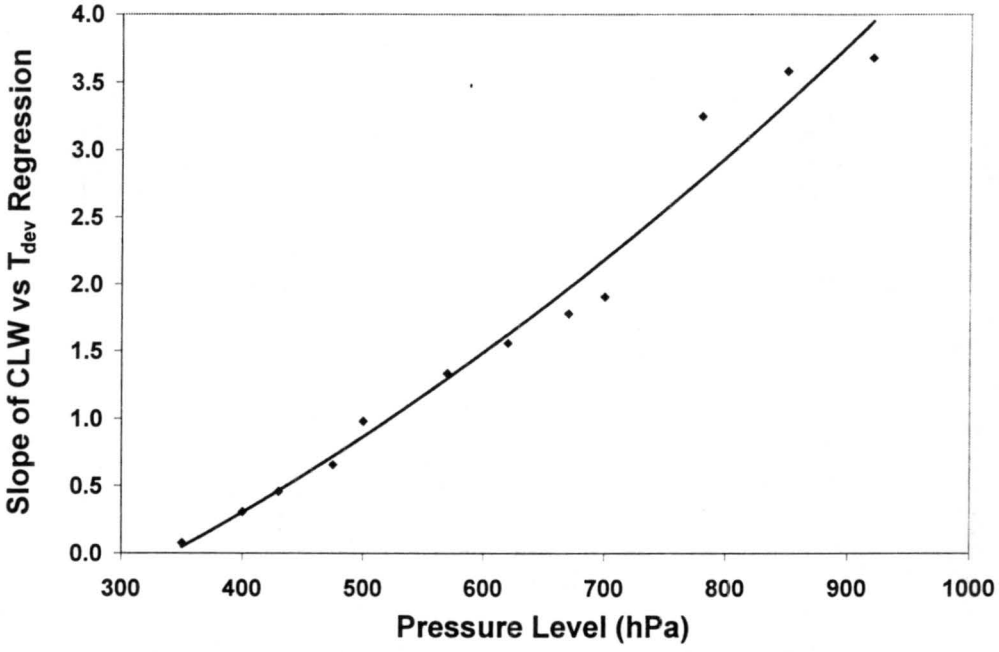

Figure 3.1. The slope of the cloud liquid water versus temperature deviation regression versus the corresponding pressure level, fit with a quadratic curve.

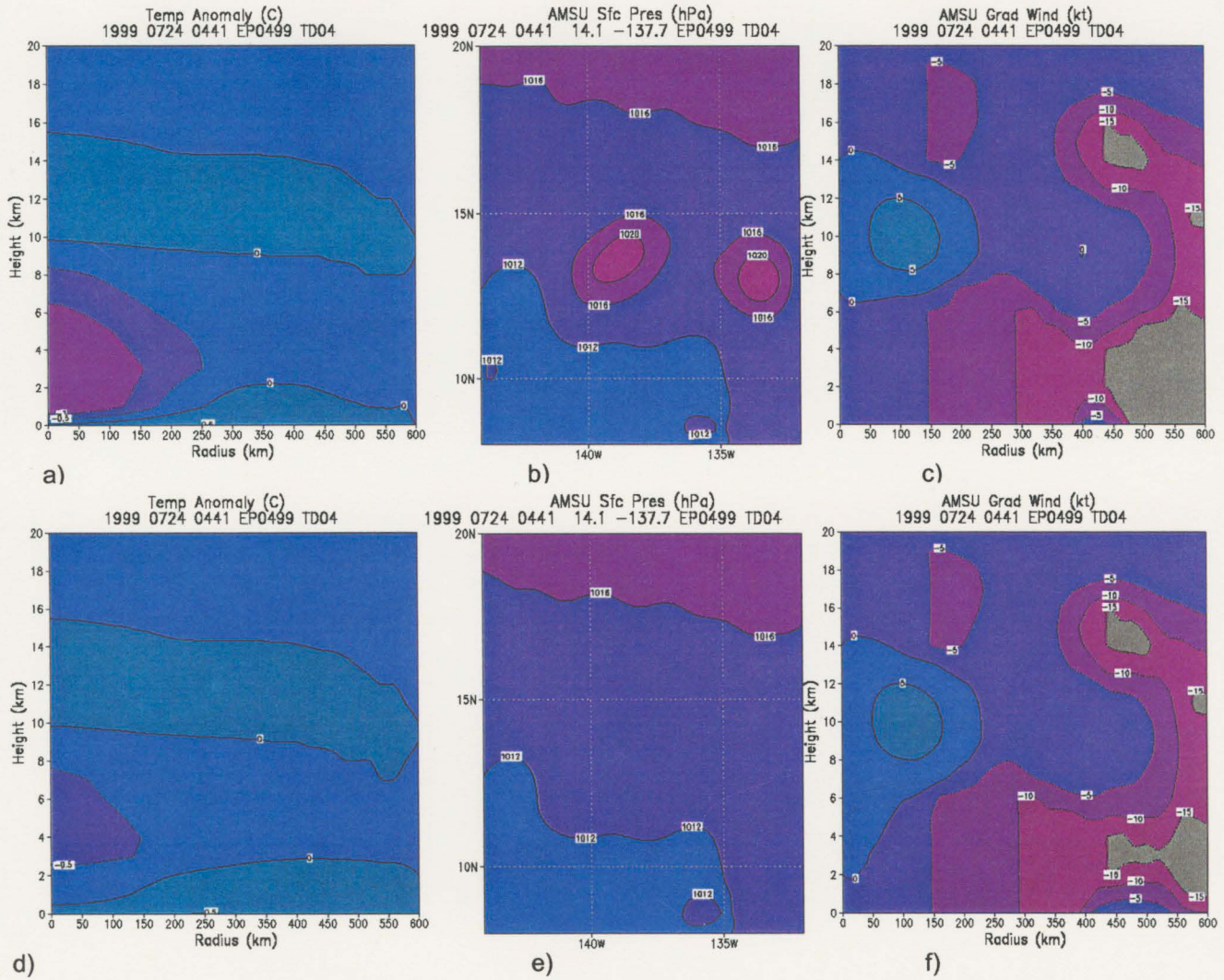

Figure 3.2. Non-hydrometeor corrected (a-c) and hydrometeor corrected (d-f) plots for Tropical Depression EP04 (30 kts) from 24 July 1999 at 0441 UTC showing: a,d) radial-height cross-section of temperature anomalies (ºC), b,e) lat-lon profile of surface pressure (hPa), c,f) radial-height profile of azimuthally-averaged gradient wind (kts).

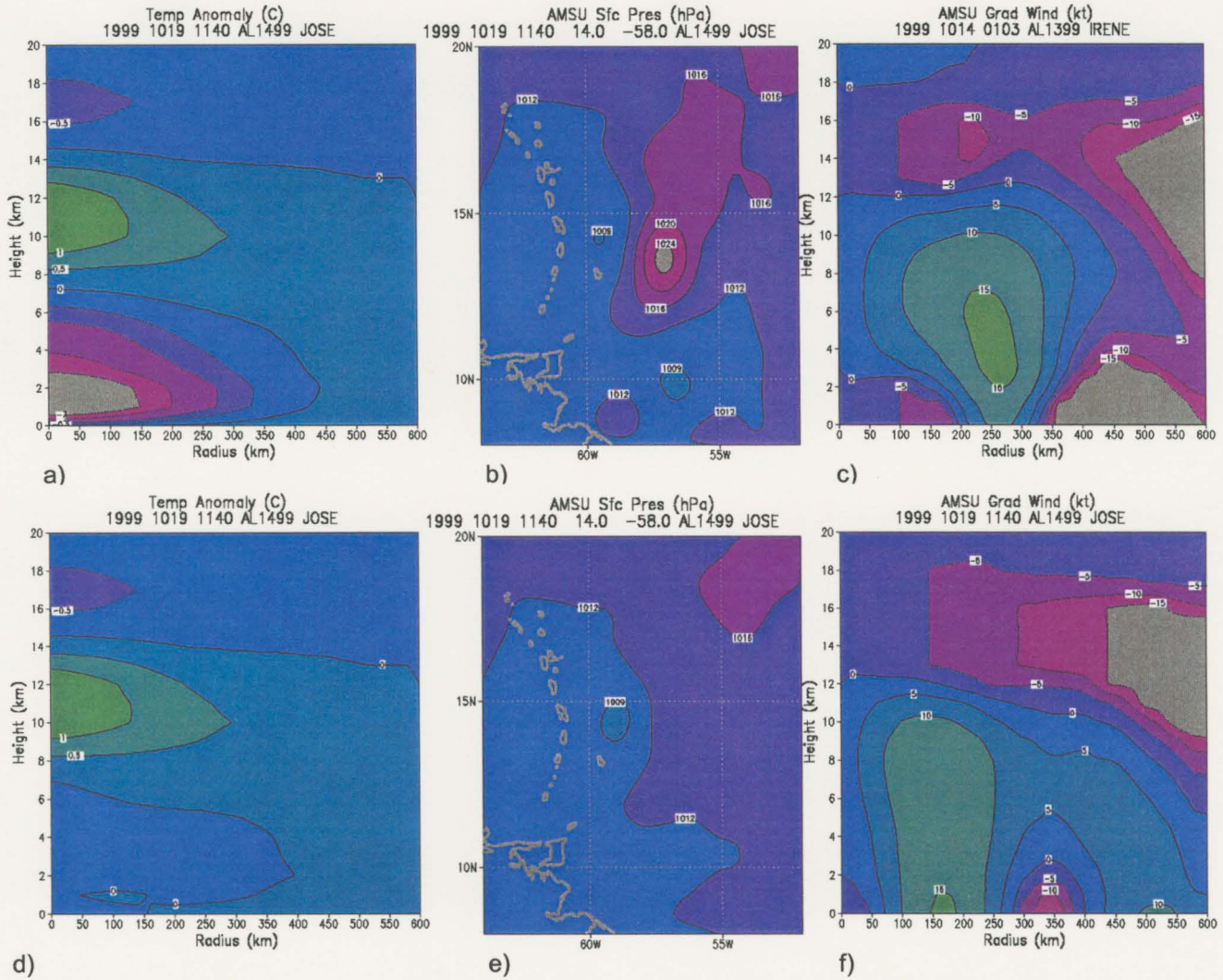

Figure 3.3. Non-hydrometeor corrected (a-c) and hydrometeor corrected (d-f) plots for Tropical Storm Jose (60 kts) from 19 October 1999 at 1140 UTC showing: a,d) radial-height cross-section of temperature anomalies (°C), b,e) lat-lon profile of surface pressure (hPa), c,f) radial-height profile of azimuthally-averaged gradient wind (kts).

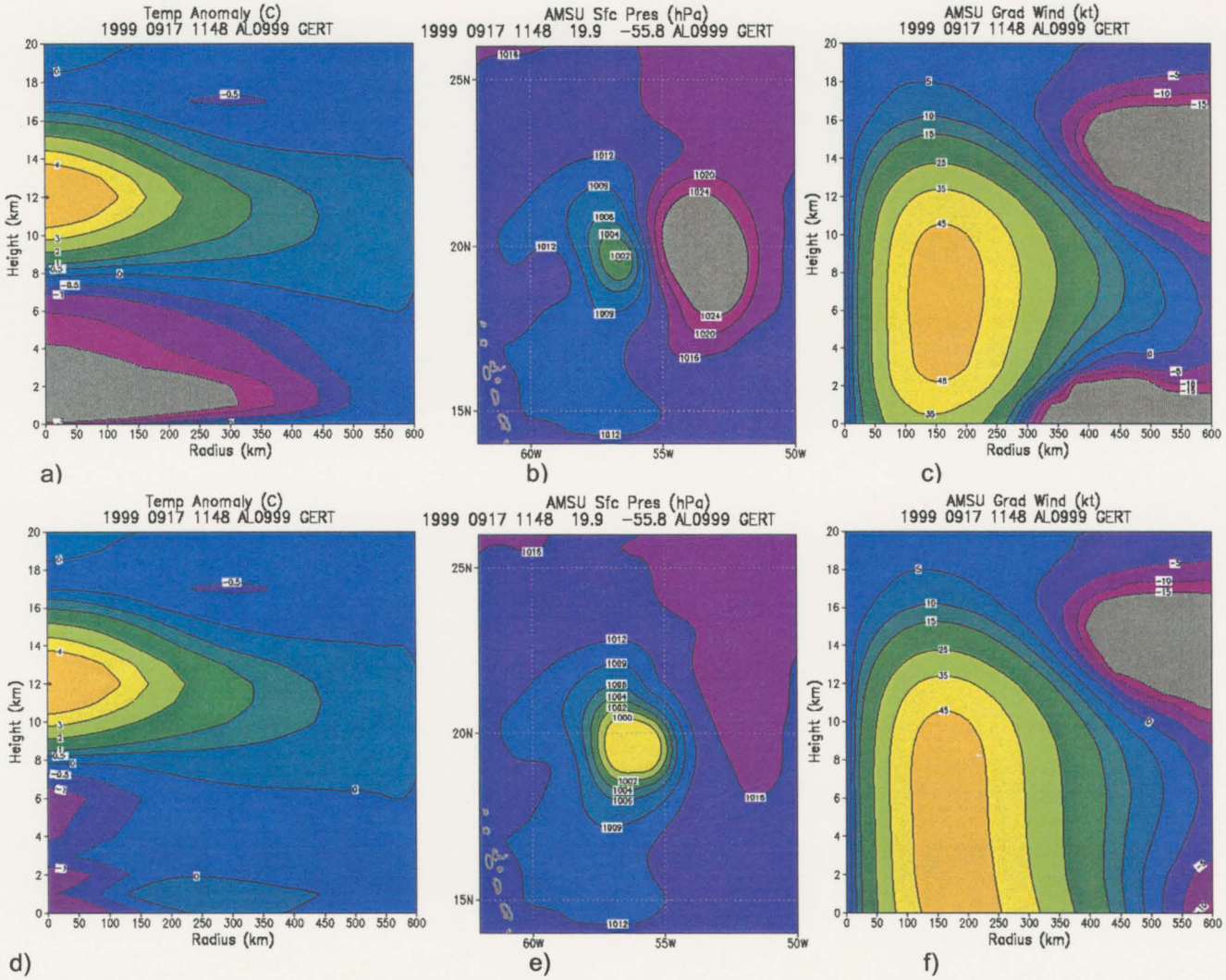

Figure 3.4. Non-hydrometeor corrected (a-c) and hydrometeor corrected (d-f) plots for Hurricane Gert (115kts) from 17 September 1999 at 1148 UTC showing: a,d) radial-height cross-section of temperature anomalies (°C), b,e) lat-lon profile of surface pressure (hPa), c,f) radial-height profile of azimuthally-averaged gradient wind (kts).

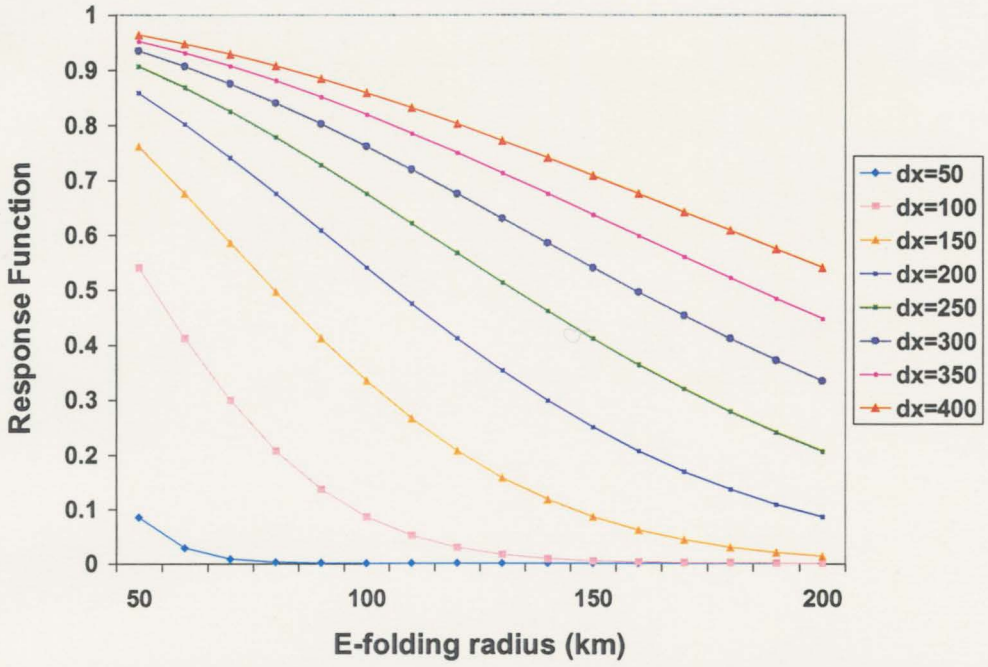

Figure 3.5. Response function as a function of e-folding radii for various spatial scales (dx).

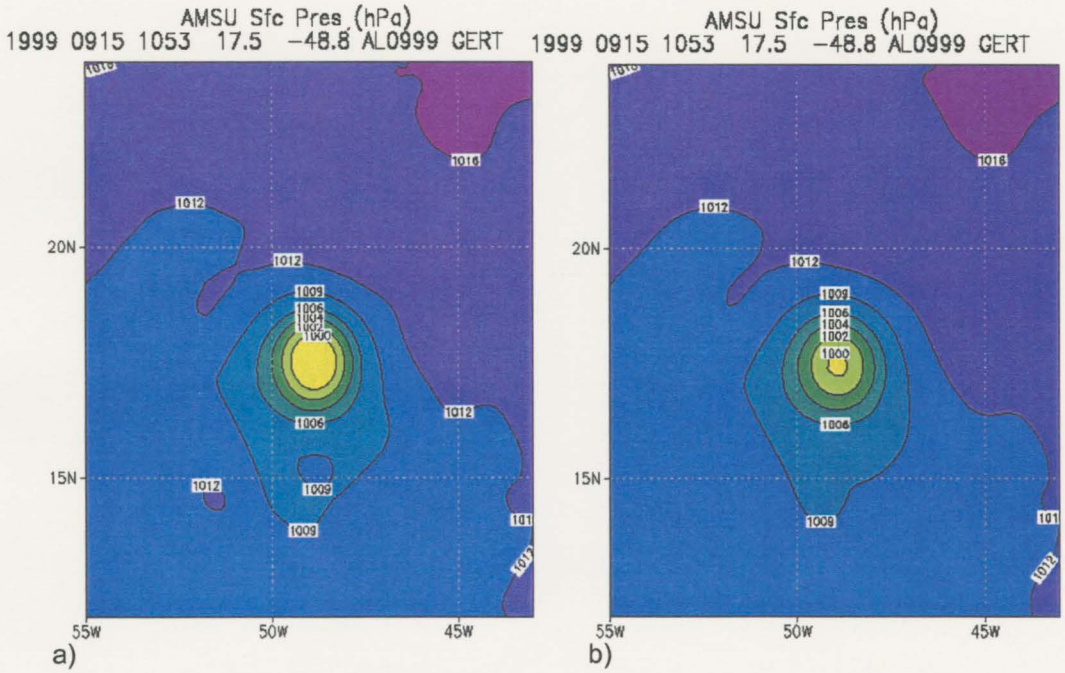

Figure 3.6. Comparison of the latitude-longitude profile of surface pressure (hPa) for Hurricane Gert with the e-folding radius set to a) 80 km and b) 100 km.

Chapter 4 - Objectively Estimating Tropical Cyclone Intensity

4.1 Intensity Estimation

Even with its aforementioned increased horizontal resolution, the AMSU cannot adequately resolve the inner core of tropical cyclones, especially the more intense ones with tighter pressure gradients. Thus, the AMSU cannot be used to directly estimate maximum winds. However, several parameters can be derived and used from the AMSU temperature, pressure and wind retrievals, in addition to other parameters available in real time. This study shows that an algorithm can be developed statistically with the AMSU data to give objective estimations of the maximum wind speed. In this chapter, the development of such an algorithm to objectively estimate the maximum wind speed of tropical cyclones of all intensities (i.e. tropical depressions, tropical storms, and hurricanes) is explained followed by an examination of the algorithm performance.

4.1.1 Data

Eleven parameters derived from AMSU serve as possible estimators of tropical cyclone intensity. Two additional, non-AMSU-derived parameters available in real time also are utilized. The combined 13 variables make up the independent data set (estimators) used in estimating TC intensity; they are listed below with their

corresponding descriptions in which the radius, r, at 0 km is taken to be at the storm center and the maximum radius is set at 600 km for all TCs. Furthermore, excepting SS, TMAX, and ZMAX, all AMSU-derived parameters are azimuthally averaged. Recall that, although the AMSU-derived maximum wind speed at the surface (VMX0) is a parameter, the coarse resolution of the AMSU prevents usage of it alone. The AMSU-derived parameters include:

1) CLW – cloud liquid water content (mm) from r = 0 to 100 km
2) DP – pressure drop (hPa) from r = 600 to 0 km
3) R015 – radius (km) of 15kt winds at the surface
4) R315 – radius (km) of 15kt winds at 3 km
5) RMX0 – radius (km) of maximum winds at the surface
6) RMX3 – radius (km) of maximum winds at 3 km
7) SS – resolution (km) of AMSU footprint at storm center
8) TMAX – maximum temperature perturbation (°C) calculated as T(r=0 km) minus T(r=600 km)
9) ZMAX – height (km) of the maximum temperature perturbation (TMAX)
10) VMX0 – maximum wind speed (kts) at the surface
11) VMX3 – maximum wind speed (kts) at z = 3 km

The two additional, non-AMSU-derived parameters available in real time are:

12) STORMLAT – latitude of the storm center at the time of the AMSU swath
13) STRMSP – storm translational speed, $\sqrt{c_x^{\,2} + c_y^{\,2}}$, where c_x and c_y are the speeds of the tropical cyclone in the x and y direction, respectively

The dependent (validation) data for the TC intensity estimations come from the 1999 NHC best track (BT) files. The BT data (denoted as VMX) are produced at the end of each tropical season via a subjective assessment of all available data, including air reconnaissance data, Dvorak estimates, ship data, and buoy data. The files include six-hourly reports of storm latitude, longitude, and maximum winds (kts). Reports closest in time to the AMSU swath are used as validation for intensity estimations with no report differing by more than three hours. It is noted that data in the best track files are not "ground truth", in that, excepting air reconnaissance observations, they are not *in situ* measurements. While a validation data set consisting entirely of *in situ* air reconnaissance data is preferable, AMSU and reconnaissance data were coincident within three hours only 24 times during 1999; this is too few cases from which to develop a statistical algorithm with multiple predictors, hence the regularly occurring best track data is used.

The intensity estimation parameters are developed from 1999 tropical cyclone data from the Atlantic and East Pacific basins. An AMSU analysis is performed if a satellite pass occurs within three hours of an NHC tropical cyclone position estimate, and if the center of the TC is within 600 km of nadir. The latter constraint is due to the worsening footprint resolution along the AMSU swath with distance from nadir; at a distance of 600 km from nadir, the footprint resolution is approximately 80 km.

There were 89 AMSU passes over Atlantic storms and 65 passes over East Pacific storms, for a total of 154 cases. Fourteen of these are not used because there is no corresponding best track report (validation data) within three hours. Fifteen more cases, for which the estimated storm center is within 100 km of land, are discarded also. The latter condition arises from the preference for at least two AMSU data points to be over open water for accurate pressure estimates near the storm center. Since the storm

center location can be in error by as much as 20 km, and the worst possible footprint resolution at storm center is approximately 80 km, a margin of 100 km is established.

Of the final 125-case data set, 31 cases are tropical depressions (sustained winds from 20 – 34 kts), 42 are tropical storms (35 – 64 kts), and 52 are hurricanes (65+ kts). Twenty cases are intense hurricanes (Category 3, 4, and 5), with wind speeds greater than 95 kts. The statistical procedure described in the following section is run on all 125 cases for the intensity estimation.

The 1999 tropical season consisted of four TDs, four TSs, and eight hurricanes in the Atlantic, combined with five TDs, three TSs, and six hurricanes in the East Pacific. Five of the hurricanes in the Atlantic basin were intense as were two in the East Pacific basin. The 1944 – 1996 climatological record for the Atlantic basin reveals that 1999 was a year for strong storms in the Atlantic (Figure 4.1) (National Hurricane Center, 2001). While the number of tropical storms was average, there were more hurricanes than usual, and the number of intense hurricanes was double the mean. On the contrary, the East Pacific climatological record, established from 1966 – 1996, suggests the numbers in that basin were well below average and the storms were weaker. With only nine named storms that year, compared to the usual 16.4, less than half of the mean of tropical storms occurred, as did less than two-thirds the usual number of hurricanes, and half the average number of intense hurricanes (Figure 4.1).

The intensity estimators developed from the 1999 tropical season data are cross-validated on the 2000 tropical cyclone data from the Atlantic and East Pacific basins, from which there were 77 and 73 AMSU passes, respectively. Eliminating the 12 cases without concurrent best track data for validation leaves a data set of 138 cases. Tropical cyclones within 100 km of land are not deleted for the cross-validation data set, as the intensity of these storms will be estimated operationally. Of the 138 cases, 35 are

tropical depressions, 54 are tropical storms, and 49 are hurricanes; only ten of the latter cases are intense hurricanes. During 2000, the Atlantic basin had less intense hurricane activity compared to the previous year, yet the number of tropical storms and hurricanes were slightly above average by climatological standards (Figure 4.1). The season consisted of four TDs, six TSs, and eight hurricanes, three of which were intense. In the East Pacific basin, overall activity nearly doubled from 1999 to 2000 to near climatological values. There were two TDs, 11 TSs, and six hurricanes, two of which were intense hurricanes.

4.1.2 Methods

Theoretically, every parameter discussed in the previous section is physically relevant to the maximum sustained winds of a tropical cyclone, but the specific significance of any particular variable is unclear. Hence, the relationship between the predictors and the predictand is analyzed using a multiple linear regression. Conventionally, y is the symbol for the dependent variable, or predictand, and x_i is the symbol for the independent variables, or predictors, where i = 1, 2, ..., K. For a given data set with K potential predictors, the predictive equation is of the form,

$$y = b_o + b_1 x_1 + b_2 x_2 + ... + b_K x_K \qquad [4.1]$$

where b_o is the regression constant, and b_1, b_2, ..., b_K are the regression coefficients. The regression procedure chooses the constant and coefficients of the line such that there is minimal error in estimations of y given actual observations of x_i. Most commonly, this is measured by minimizing the sum of the squared error, hence, it is referred to as a least squares regression. The error, or residual, is the simply the difference between the observed and predicted data, defined as,

$$e_i = o_i - y(x_i) \qquad [4.2]$$

Generally, it is not prudent to include every possible predictor in the regression equation. Some may not be valuable in estimating the predictand, while other valuable predictors may be mutually correlated (i.e. changes in one tend to be associated with changes in another), thus providing redundant information. Consequently, the list of potential predictors initially is shortened by correlating each predictor against the predictand, and testing the probability (p-value) that the correlation is zero. If the correlation is not statistically significant ($\alpha = 0.05$), then that predictor is excluded.

Subsequently, a backward stepwise regression is used to select a good set of predictors from the remaining variables. The backward stepwise regression is employed with a specific stopping condition of five percent significance ($\alpha = 0.05$), meaning there is a five percent chance the predictors chosen by the regression are not useful in predicting TC intensity. For some set of K potential predictors, the backward stepwise regression works by simultaneously analyzing the relationship all K have to the predictand. The "poorest" predictor (i.e. the least significant one) is removed, and the remaining (K–1) predictors are re-evaluated. The next poorest predictor is removed, the remaining (K–2) are re-evaluated, and so forth. The regression stops when a set of independent variables are left that, together, provide a strong relationship with the dependent variable. It is important to note that at each step of the regression, the coefficients of the regression constant and the remaining independent variables change. This is because the correlations among the predictors vary as some are removed, and the information the remaining parameters possess about the predictand is re-allotted.

As mentioned in Section 4.1.1, the data to be predicted comes from the NHC best track data. This data can be used in three ways to develop the AMSU intensity estimations. The most straightforward method is to predict the BT maximum sustained winds (VMX) using all 13 potential predictors. In this case, any contributions to the

maximum wind by storm motion are accounted for in the BT estimate. Alternatively, the predictand could be the BT maximum sustained winds minus the storm speed (VMX – STRMSP) as Spencer and Braswell (2001) did in their work. In this case, the AMSU parameters and STORMLAT can be used to predict the difference, and then the STRMSP can be added back on to give the VMX estimation. A final possibility is to use an empirically-derived relationship between storm speed and maximum sustained winds, which shows that tropical cyclone speed is not linearly added to give the maximum sustained winds of a tropical cyclone (Schwerdt et al., 1979). Rather, as storm speed increases, there is a decreasing influence on the added asymmetric wind speeds (Figure 4.2). The asymmetric equation showing this relationship is,

$$A = yc^x \cos\beta \qquad [4.3]$$

where y and x are empirical constants, c is the forward speed of the tropical cyclone, and β is the angle between the track direction and the surface wind direction, measured counterclockwise in degrees. Since the interest of this study lies in estimating the contribution of the storm speed to the maximum wind speed, it is assumed that β=0, reducing [4.3] to [4.4].

$$A = yc^x \qquad [4.4]$$

When c is expressed in knots, the empirical constants are y = 1.5 and x = 0.63. Rather than linearly subtracting the storm speed from the maximum sustained winds, the asymmetry parameter, A, is calculated from the storm speed and (VMX – A) is used as the predictand. Similar to the second possible method for developing intensity estimations, the AMSU parameters and STORMLAT are used in the regression, and then A is added back on to give the VMX estimation.

To determine which of the three dependent variables has the best statistical relationship with the BT maximum sustained wind, four goodness-of-fit measures (Wilks, 1995) are employed. The first measure, the mean-squared error (MSE) is the average of the squared differences between the predicted and observed values.

$$MSE = \frac{1}{n}\sum_{k=1}^{n}(y_k - o_k)^2 \qquad [4.5]$$

It is an indication of the variability of the quantity being forecast around the forecast regression line, thus the smaller the MSE, the better the fit. However, since the MSE is computed by squaring estimation errors, it is especially sensitive to cases with large errors. Secondly, the coefficient of determination, R^2, denotes the proportion of the variation of the predictand that is described by the regression. It is represented as a percentage with higher R^2 values indicating a better fit. The F-ratio is the third goodness-of-fit measure. It is the ratio of the mean-square of the regression (MSR) to the MSE. The MSR is the regression sum of squares divided by the degrees of freedom. Thus, given an equal number of predictors, larger F-ratios are desirable as they indicate a smaller MSE. The final measure is the mean absolute error (MAE), which is the average of the absolute values of the differences between the predicted and observed values.

$$MAE = \frac{1}{n}\sum_{k=1}^{n}|y_k - o_k| \qquad [4.6]$$

Wilks (1995) notes the MAE is a typical measure for predicted errors in a given verification data set.

The primary error analysis uses two measures of estimation accuracy, including the MAE and the root-mean-squared error (RMSE), which is simply the square root of the MSE. Physically, it is easier to comprehend the MAE rather than the RMSE as the

former simply indicates how far errors are spread from the regression line. Due to the squaring procedures, the latter is less easy to visualize, and thus it will not be stressed as much as the MAE in this study.

4.1.3 Results and Error Analysis

The results of all the goodness-of-fit measures for the three predictands are shown in Table 4.1. For both statistical approaches, the F-ratio of using VMX alone as the predictand is lower than the F-ratios of (VMX-SP) and (VMX-A) despite its lower MSE. This is because using VMX alone as the predictand keeps more variables as predictors; the additional degrees of freedom lowers the MSR, and consequently the value of the F-ratio. Nonetheless, using VMX alone yields the lowest MSE, the highest R^2, and the lowest mean absolute error for both statistical approaches. Thus, VMX is used as the predictand for intensity estimations.

Of the entire set of 13 potential predictors, eight have p-values less than 0.05 and thus are considered significantly correlated with the best track data (VMX). They are CLW, DP, R015, R315, TMAX, ZMAX, VMX0, and VMX3 (Table 4.2). Of these eight, the backward stepwise regression retained only five to explain 68.9 percent of the variation in the 1999 best track observations (Figure 4.3). Included in Table 4.3 are the corresponding predictive variables, the regression coefficients, and the normalized coefficients. The latter clarifies the relative weight of each predictor in explaining the predictand; it is calculated by multiplying the predictor coefficient by its standard deviation and subsequently dividing by the standard deviation of the dependent variable.

An individual analysis of the independent variables is complicated by their interactions. Nonetheless, the normalized coefficients suggest the AMSU-derived intensities at the surface (VMX0) and at a height of 3 km (VMX3) explain the largest amount of the variation in best track intensity. The zero p-values of these two variables

confirms their usefulness. Using the data in Table 4.3 combined with Equation 4.1, tropical cyclone intensity, in terms of maximum sustained winds, can be estimated via the AMSU by the following equation:

$$VMX = 23.301 + (-2.122*DP) + (-2.325*VMX0) + (3.685*VMX3) + (5.760*TMAX) + (15.200*CLW) \quad [4.7]$$

In their evaluation of the Objective Dvorak Technique performance on Atlantic storms, Velden *et al.* (1998) report a root-mean-squared error of 8.34 hPa. In comparison, for the AMSU-derived intensity estimates, the MAE of the 1999 Atlantic cases is 10.3 kts, and the RMSE is 13.4 kts (Table 4.4). From Dvorak (1975), the maximum wind speed to which a given pressure corresponds differs with the intensity of a tropical cyclone (Table 1.1). A RMSE of 8 hPa can equate to a wind speed of approximately seven to 16 kts. Thus, in comparing the Atlantic basins, the objective AMSU technique appears to provide a viable alternative to estimating intensity, with the advantage of being able to produce intensity estimations for tropical depressions and tropical storms.

When the predictive relationship in Equation 4.7 is tested on both the Atlantic and East Pacific basins, the errors increase slightly compared to the Atlantic basin only errors (Table 4.4). From the 1999 data, the MAE (RMSE) is 12.5 (16.2) kts. As will be discussed in further detail below, the higher error when including the East Pacific cases is dubious. With no aircraft reconnaissance data to provide *in situ* observations, it is feasible that the AMSU estimates of intensity are more accurate than comparison with the best track data suggests.

An examination of the residuals against the AMSU calculated intensity (Figure 4.4) is useful in verifying that the linear regression is not inappropriate for the data.

Again, a residual is the difference between the observed value of a variable (best track intensity) and the value predicted by the model (AMSU predicted intensity) (4.2). Since the residual plot illustrates relatively equal scatter about the zero line and no obvious trend, the predictive equation [4.7] derived with AMSU data is deemed valid.

Although the statistical model seems sound, from a practical standpoint, it is important to look at the residuals versus the observed best track data. Note that since the residual is defined as (BT - AMSU), negative (positive) residuals are over (under) estimations. As shown in Figure 4.5, there is an overall tendency for the AMSU technique to over predict the intensity of weak storms and under predict strong storms. In 1999, 27 (4) of the 31 TDs are over (under) predicted, as are 23 (19) of 42 TSs, and 15 (37) of 52 hurricanes; total, there are 65 (60) cases over (under) predicted. Overall, most cases are in absolute error by less than 15 kts (70.4 percent) with only five in error by 35 kts or more (Figure 4.6a). By looking at the Atlantic and East Pacific basins individually, (Figures 4.6b,c), it is obvious that intensity estimates are better in the former and that there is much greater variability in the latter. In fact, the five cases of largest error magnitude occur in the East Pacific. Two possible reasons for this are because the validation data in the Atlantic is better, and physically, conditions in the East Pacific basin are more variable (i.e. there is a stronger gradient of sea surface temperatures). Thus, it may be wise to develop separate algorithms for each basin when a large enough data set becomes available.

The large number of over predicted weak storms likely is due to their disorganized structure, which causes some independent variables to be well defined but not others. To further investigate this, the average values of DP, VMX0, VMX3, TMAX, and CLW are calculated according to TC intensity (Table 4.5). For all variables, the values steadily increase with increasing storm strength. In the case of Tropical

Depression Hilary, the VMX0 and VMX3 values are 17.20 and 17.10 kts, respectively, much higher than the average for a TC of that strength. All other variables associated with Hilary have approximately average magnitudes, however, causing the overall intensity estimate to be in error, according to the best track, by more than 30 kts. Hilary occurred in the East Pacific basin, however, and it is important to recall that no air reconnaissance data is available to verify the storm's intensity. It is possible the best track data underestimates the storm's maximum sustained winds while the AMSU is giving a more accurate estimate. Additionally, many of the weak TCs actually can have an increase in the azimuthally averaged pressure gradient from the edge of the storm to the center. This causes DP to be negative which, according to Equation 4.7, increases the estimate of VMX, leading to over estimations; future work will include constraining DP so that it cannot be negative.

The under estimation of the stronger tropical cyclones appears to be due, in part, to a lack of significant increase in the magnitude of the predictors for intense hurricanes (> 95 kts). There is a slightly increasing trend in the values of VMX3 (Figure 4.7a) and a more pronounced increase in CLW (Figure 4.7b) for storms with best track intensities greater than 90 kts. However, the maximum values of DP, VMX0, and TMAX are approximately the same for all hurricane intensities (Figures 4.7c-e). Furthermore, there is a very wide range in the predictors' values for hurricane strength storms, often reaching as low as typical TD and TS values, causing a large underestimate of the strength. These problems possibly are due to the coarse resolution of the AMSU combined with the azimuthally averaged technique used in deriving the predictors. The latter further smoothes TC features in deriving one representative value for the storm. Work is in progress to better highlight the features of a given predictor, which will be utilized in the intensity estimation. Also, it is likely that the magnitude of error will lessen

when a larger data sample is used to develop the predictors; more data points allow for a better fit with less weight being attributed to outliers. As discussed in the next section, the 1999 and 2000 data sets are combined to refine the predictors; these are currently being tested on TCs from the 2001 season.

For the 2000 cross-validation data set, the MAE is 12.6 kts and the RMSE is 15.3 kts for the Atlantic basin, and the errors from both basins combined are 13.8 and 17.5 kts, respectively (Table 4.4). A similar trend of over predicting weak TCs and under predicting strong ones appears when the predictors are tested on the 2000 data (Figure 4.8), likely for the same reasons as discussed relevant to the 1999 data. For the 2000 data set, most of the cases have intensities within 20 kts of the observed values (Figure 4.9a). The error distribution of this data is slightly skewed toward under estimation (positive residuals). The bias, defined as the difference between the mean of the predicted values and the mean of the observed values, is –1.89 kts, further confirming the tendency toward under estimation. (Note that the 1999 data set has no bias because it was used in the regression, thus its residuals must sum to zero.) As with the 1999 data, the number of cases with smaller magnitudes of error are higher in the Atlantic basin, whereas the distribution is wider for the East Pacific (Figures 4.9b,c). This further reiterates the need for basin-specific algorithms.

4.1.4 1999 and 2000 Combined Data Set

With the additional data from the 2000 tropical season, a data set combining AMSU data from 1999 and 2000 (hereafter referred to as 9900) is used to refine the TC intensity predictors, which will be tested independently on tropical cyclones from the 2001 season. Predictions for the 2001 tropical activity in the Atlantic basin by Dr. William Gray's hurricane research group and by the Tropical Storm Risk consortium, both made in August 2001, suggest another active season compared to climatological

means (Figure 4.1). Gray *et al.* (2001) and TSR (2001) both predict 12 named storms, seven of which will be hurricanes, and three of which will be intense hurricanes. Thus, the likely active tropical season of 2001 will be a consistent data set with which to validate the 9900 intensity estimative algorithm.

As discussed in Section 4.1.1, the 1999 data consist of the same 125 cases, and the 138-case data set from 2000 is modified by removing ten cases within 100 km of land. Of the resultant 253-case data set, 64 cases are TDs, 92 are TSs, 97 are hurricanes, and 27 are intense hurricanes. Again, an initial correlation following by a backward stepwise regression are used to predict best track intensity (VMX); significance levels of five percent are used for these.

The initial correlation of all 13 potential predictors with VMX shows the eight variables, CLW, DP, R015, R315, TMAX, ZMAX, VMX0, and VMX3, are statistically significant (Table 4.6). These are the same eight that are significant for the 1999 data alone. The backward stepwise regression kept neither R015 nor R315, but it retained the other six predictors to explain 62.4 percent of the variation in the 9900 best track data (Table 4.7) (Figure 4.10). These are the same predictors for the 1999-only data with the addition of ZMAX. Despite VMX0 and VMX3 having the two largest normalized coefficients, as with the 1999-only data set, the higher p-value of VMX0 suggests it may not be as useful in estimating VMX as DP, TMAX, or CLW. The data in Table 4.7 are used to write the predictive equation for estimating the maximum sustained winds of a TC via AMSU data.

$$VMX = 14.581 + (-1.859*DP) + (-1.002*VMX0) + (2.124*VMX3) + (5.668*TMAX) + (0.602*ZMAX) + (20.109*CLW) \quad [4.8]$$

When [4.8] is tested on the 9900 data set, the MAE and RMSE decrease slightly compared to the 1999-only errors for both basins combined and for the Atlantic-only basin (Table 4.4). This suggests the addition of the ZMAX as a predictor perhaps better refines the algorithm. As with the 1999-only data, a plot of the residuals (best track – AMSU calculated) versus the AMSU calculated intensity shows no trend (Figure 4.11), indicating [4.8] is a valid algorithm. However, again it is important physically to look at the residuals plotted against the best track intensity (Figure 4.12). As usual, a positive (negative) residual is indicative of under (over) estimation of TC intensity by the AMSU. Not surprisingly, the same pattern of over (under) predicting weaker (stronger) TCs is apparent with the 9900 as with the 1999-only data, likely for the same reasons as discussed prior.

For this combined data set, 60 (4) of the 64 TDs are over (under) predicted, as are 53 (39) of 92 TSs, and 24 (73) of 97 hurricanes. Overall, slightly more cases are over predicted (137) than under predicted (116) (Figure 4.13a). This equates to 54.2 percent of cases being over predicted, which is consistent with the 1999 data (52.0 percent) and the 2000 data (52.2 percent). The majority (70.1 percent) of over predicted cases are in error by 15 kts or less, and only one case is over predicted by more than 35 kts. On the other hand, only 66.4 percent of under predicted cases fall within 15 kts, and seven cases are in error by more than 35 kts. The histogram for the Atlantic basin is roughly bell-shaped, with most intensity estimations exhibiting little error and only a few cases having large error (Figure 4.13.b). As with the 1999-only data, the same cannot be said for the East Pacific basin. Rather, the data is skewed to the right, with the intensity estimation of five cases in error by more than 40 kts (Figure 4.13c). Once again, this suggests the need to develop separate AMSU algorithms for each of the

tropical basins. Further validation of Equation 4.8 will be done once the 2001 tropical season comes to an end and the corresponding best track data is released by the NHC.

Table 4.1. Goodness of fit measures for the three possible intensity predictands for 1999 data.

	VMX	VMX - SP	VMX - A
F – ratio	52.61	71.04	79.88
Mean Square Error (MSE)	274.61	312.49	285.19
R^2	68.9%	63.8%	66.4%
Mean Absolute Error (MAE) on 1999 Data (kts)	12.50	13.52	12.85

Table 4.2. Correlations and p-values (that the correlation is zero) of best track intensity (VMX) with the predictors for 1999 data.

Independent Variable	Correlation Coefficient	P-Value
CLW	0.722	0.000
DP	0.542	0.000
R015	0.382	0.000
R315	0.491	0.000
RMX0	-0.134	1.000
RMX3	-0.002	1.000
SS	0.052	1.000
TMAX	0.599	0.000
ZMAX	0.421	0.000
VMX0	0.573	0.000
VMX3	0.686	0.000
STORMLAT	0.190	0.433
STRMSP	0.135	1.000

Table 4.3. Regression variables chosen to predict 1999 best track intensity data (VMX) and their corresponding coefficients, normalized coefficients, and p-values.

Dependent Variable	Independent Variable	Coefficient	Normalized Coefficent	P-Value
VMX n = 125 (r^2 = 68.9%)	Constant	23.301	0.000	0.000
	DP	-2.122	-0.521	0.014
	VMX0	-2.325	-1.178	0.000
	VMX3	3.685	1.812	0.000
	TMAX	5.760	0.404	0.012
	CLW	15.200	0.221	0.011

Table 4.4. Mean absolute errors (MAE) and root-mean-squared errors (RMSE) for the AMSU-derived intensity estimation algorithm. Errors are specified for the combined Atlantic and East Pacific basins, and for the Atlantic basin only, the latter of which is used to compared to the Objective Dvorak Technique (ODT).

* The RMSE of the ODT is 8.34 hPa when tested on Atlantic TCs (Velden *et al.*, 1998).

	Atlantic and East Pacific Basins		Atlantic Basin Only*	
	MAE	RMSE	MAE	RMSE
1999	12.5	16.2	10.3	13.4
2000	13.8	17.5	12.6	15.3
9900	12.4	16.1	10.2	13.2

Table 4.5. Average values of the five intensity predictors for VMX, calculated as a function of tropical cyclone intensity.

Independent Variable	Tropical Depressions	Tropical Storms	Hurricanes	All Tropical Cyclones
DP	0.79	4.47	8.54	5.25
VMX0	12.33	19.72	29.02	21.75
VMX3	8.86	16.16	28.02	9.28
TMAX	1.33	2.20	3.77	2.64
CLW	0.47	0.64	1.14	0.81

Table 4.6. Correlations and p-values (that the correlation is zero) of best track intensity (VMX) with the predictors for the 1999 and 2000 combined data.

Independent Variable	Correlation Coefficient	P-Value
CLW	0.698	0.000
DP	0.514	0.000
R015	0.362	0.000
R315	0.435	0.000
RMX0	-0.121	0.720
RMX3	-0.029	1.000
SS	0.050	1.000
TMAX	0.578	0.000
ZMAX	0.369	0.000
VMX0	0.546	0.000
VMX3	0.642	0.000
STORMLAT	0.174	0.072
STRMSP	0.158	0.155

Table 4.7. Regression variables chosen to predict best track intensity data (VMX) from the 1999 and 2000 combined data set, and their corresponding coefficients, normalized coefficients, and p-values.

Dependent Variable	Independent Variable	Coefficient	Normalized Coefficent	P-Value
VMX n = 253 (r^2 = 62.4%)	Constant	14.581	0.000	0.001
	DP	-1.859	-0.434	0.002
	VMX0	-1.002	-0.491	0.032
	VMX3	2.124	1.022	0.000
	TMAX	5.668	0.365	0.001
	ZMAX	0.602	0.112	0.043
	CLW	20.109	0.296	0.000

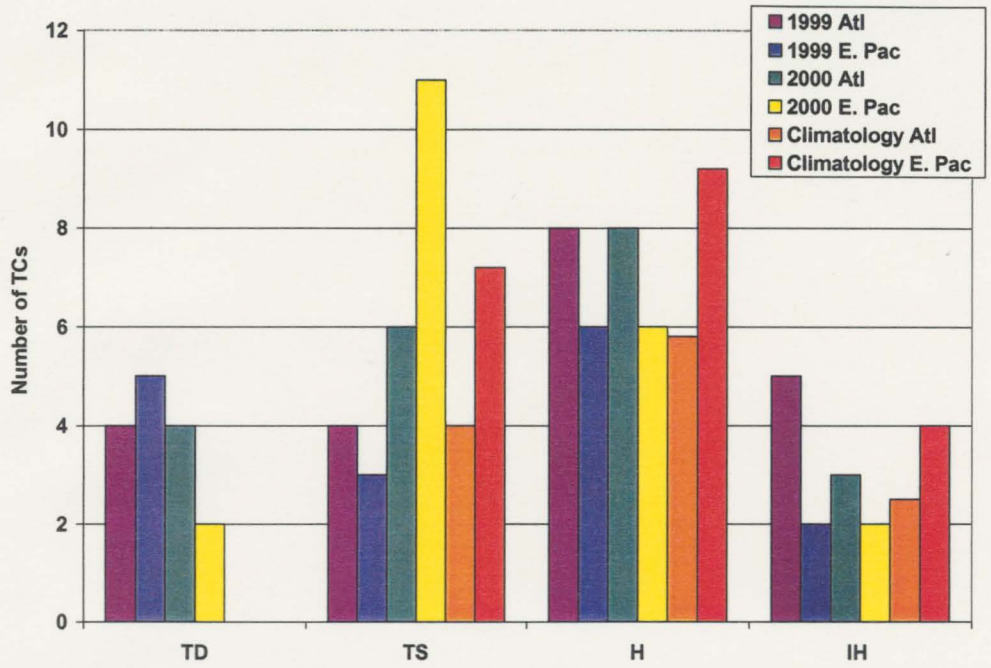

Figure 4.1. Bar chart showing # of tropical depressions (TD), tropical storms (TS), hurricanes (H), and intense hurricanes (IH) occurring in 1999 and 2000 compared to the climatological averages. Note, the climatological average for the Atlantic basin is based on data from 1944 – 1996; for the East Pacific basin, it is based on data from 1966 – 1996.

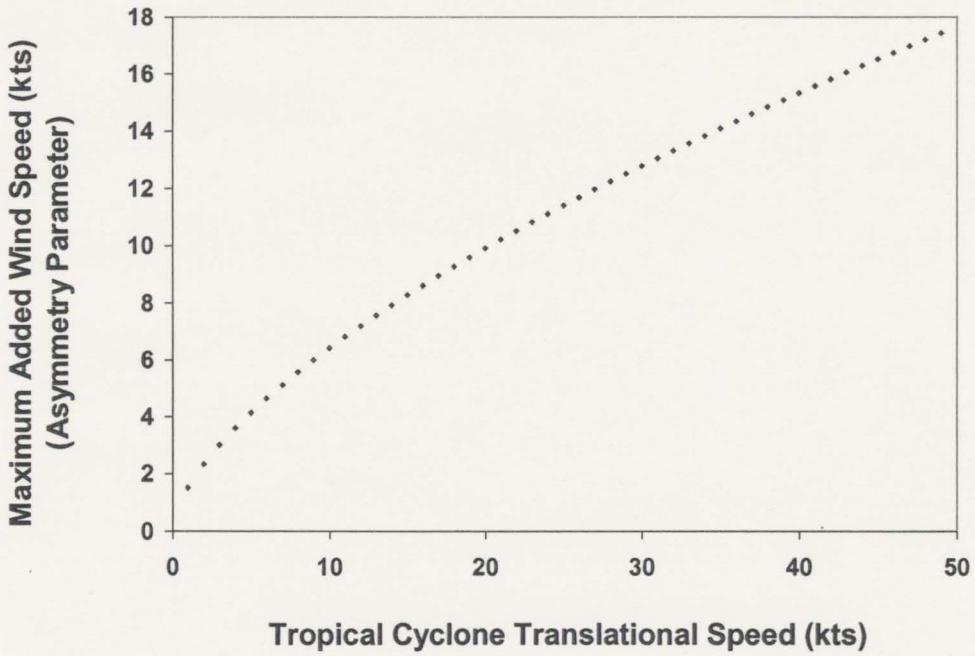

Figure 4.2. Asymmetry factor showing the maximum wind speeds added to a tropical cyclone as a function of its translational speed, based on equation [4.5].

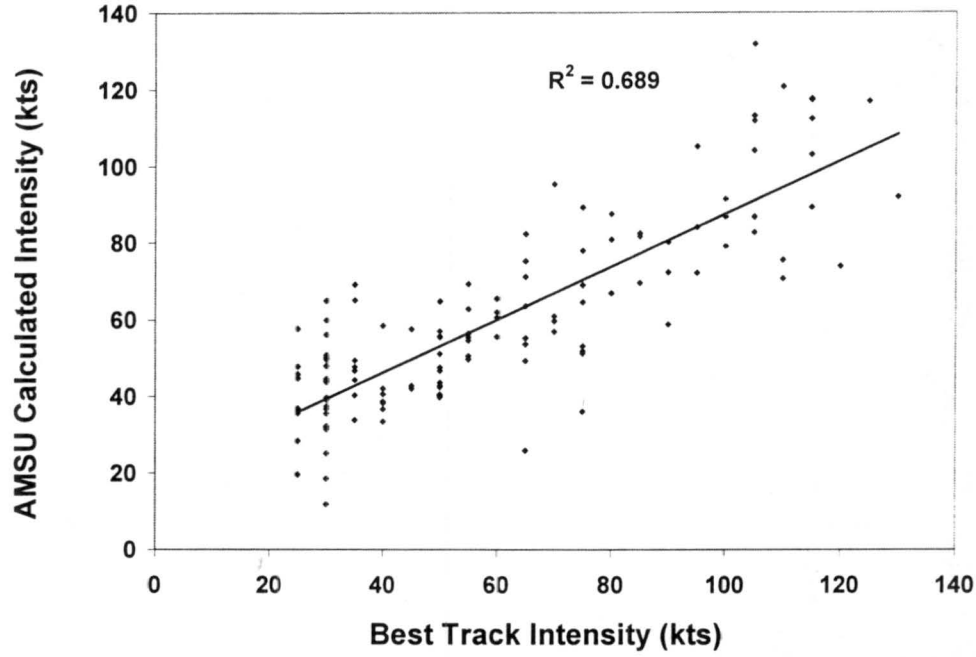

Figure 4.3. Relationship between the AMSU-derived and NHC best track reports of tropical cyclone intensity for 1999 data.

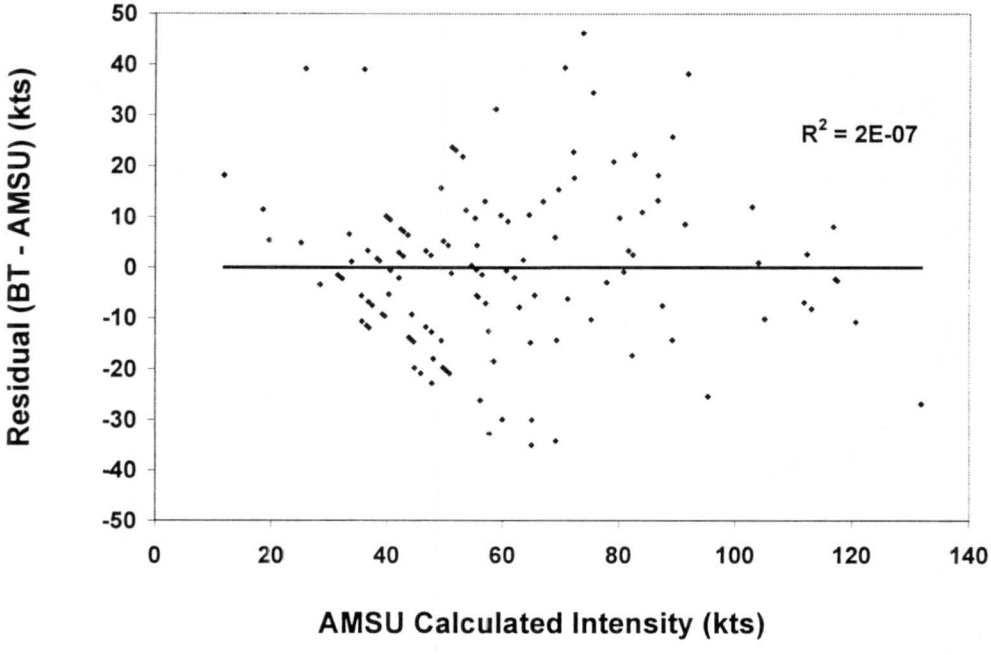

Figure 4.4. Residual (best track – AMSU calculated) plot versus AMSU calculated intensity for 1999.

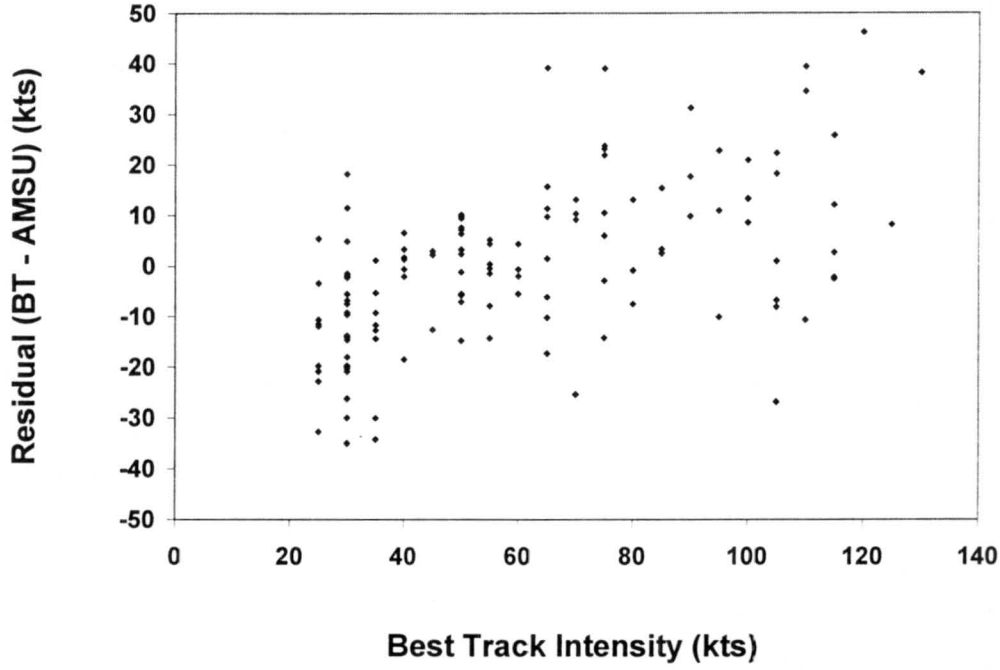

Figure 4.5. Residual (best track – AMSU calculated) plot versus best track intensity observations for 1999.

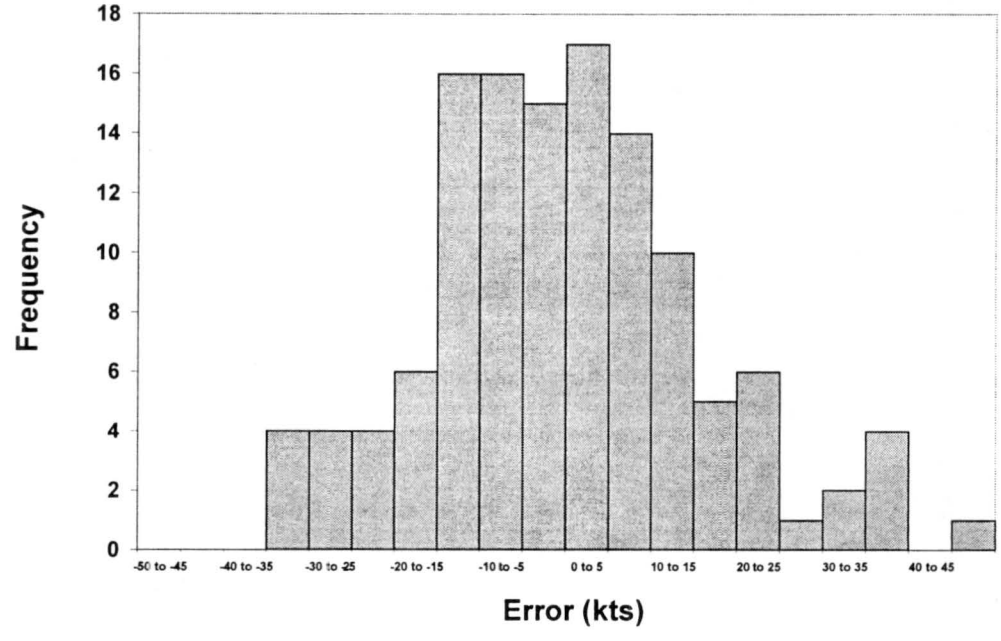

a)

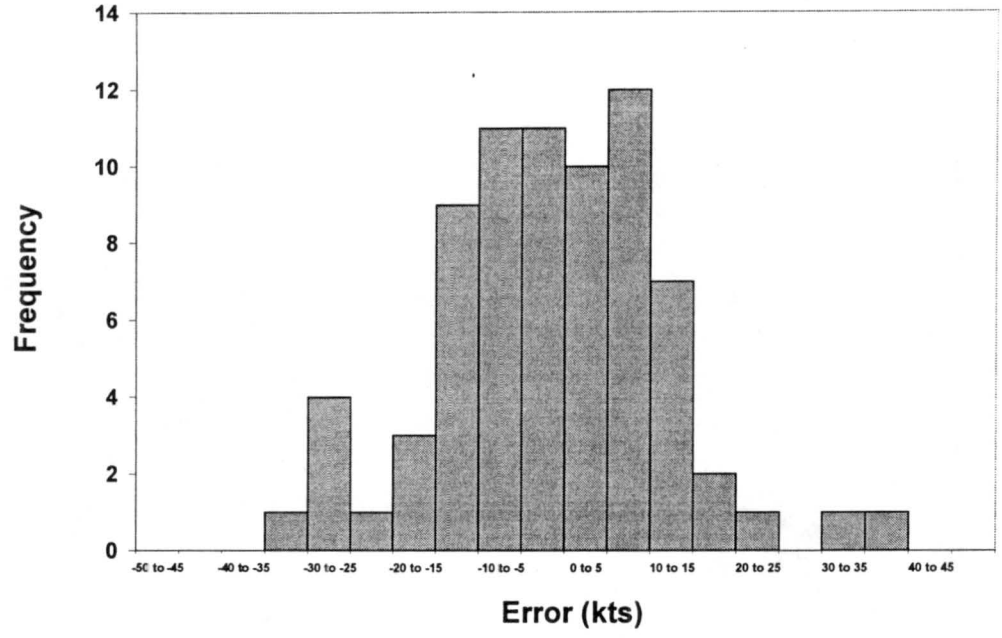

b)

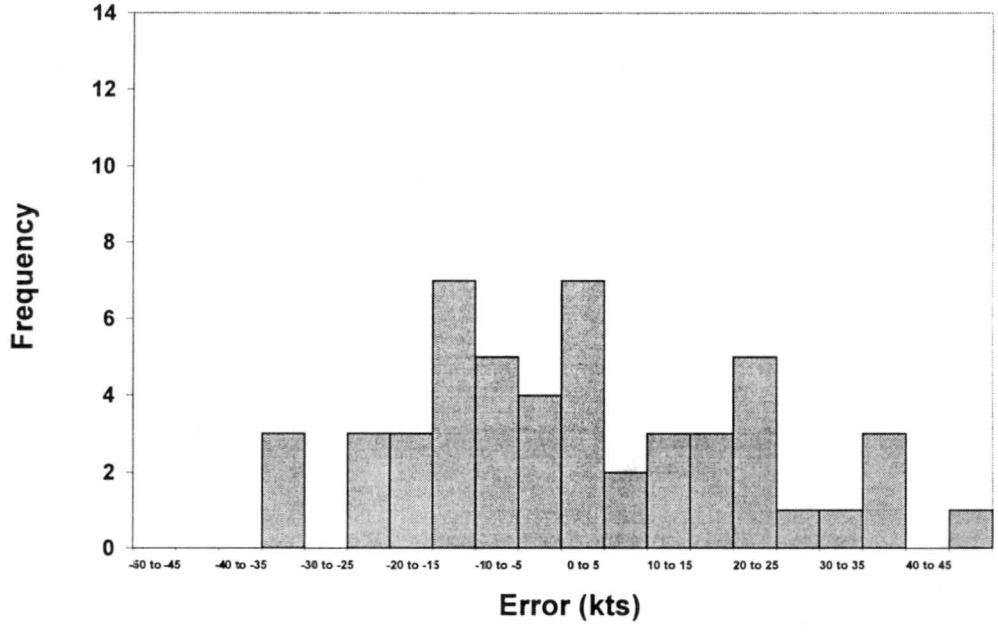

c)

Figure 4.6. Histogram of residuals (best track – AMSU predicted intensity) for 1999 data in a) both basins combined, b) Atlantic basin only, and c) East Pacific basin only.

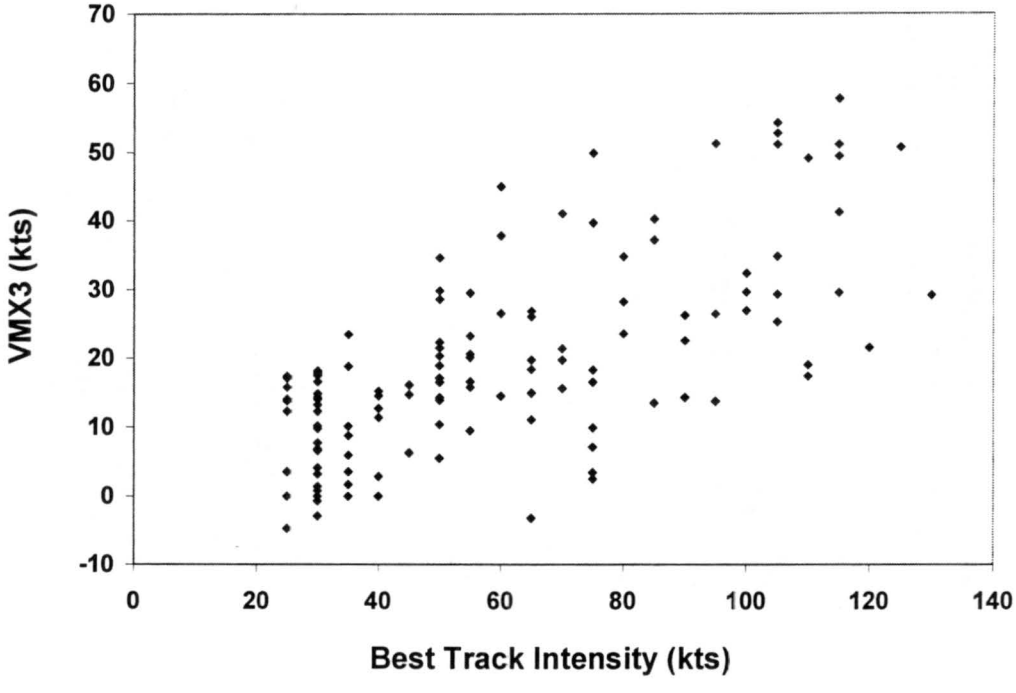
VMX3 (kts)
70
60
50
40
30
20
10
0
-10
0
20
40
60
80
100
120
140
Best Track Intensity (kts)

a)

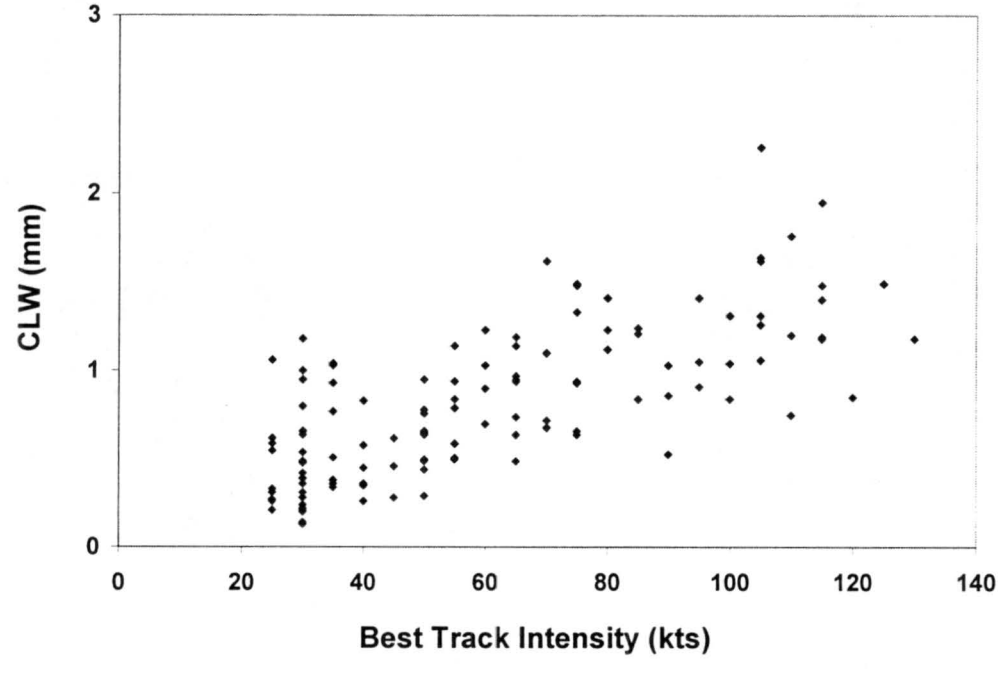
CLW (mm)
3
2
1
0
0
20
40
60
80
100
120
140
Best Track Intensity (kts)

b)

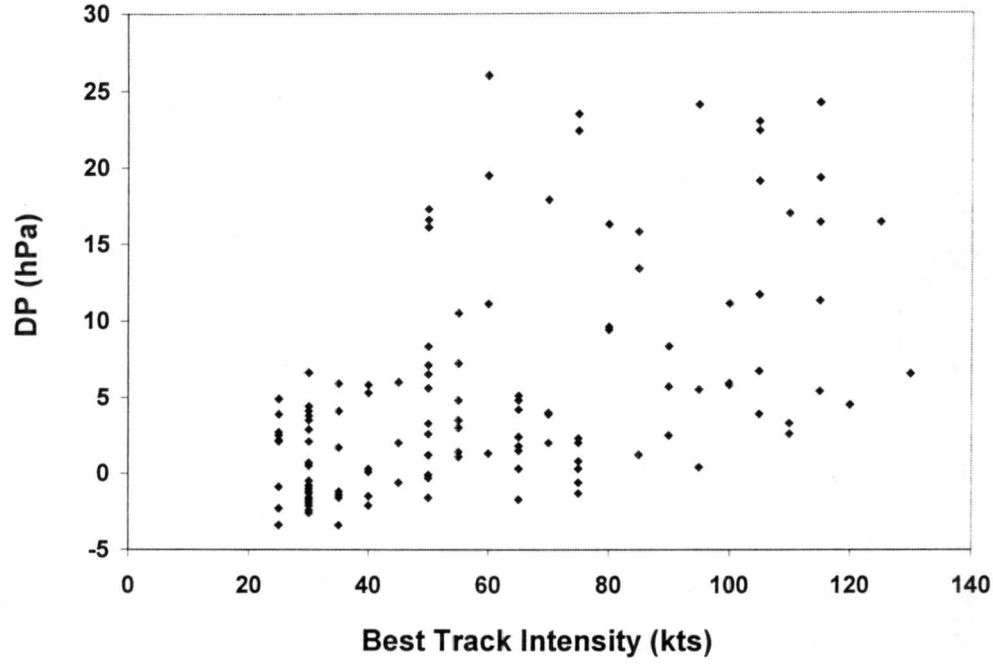
DP (hPa)
30
25
20
15
10
5
0
-5
0
20
40
60
80
100
120
140
Best Track Intensity (kts)

c)

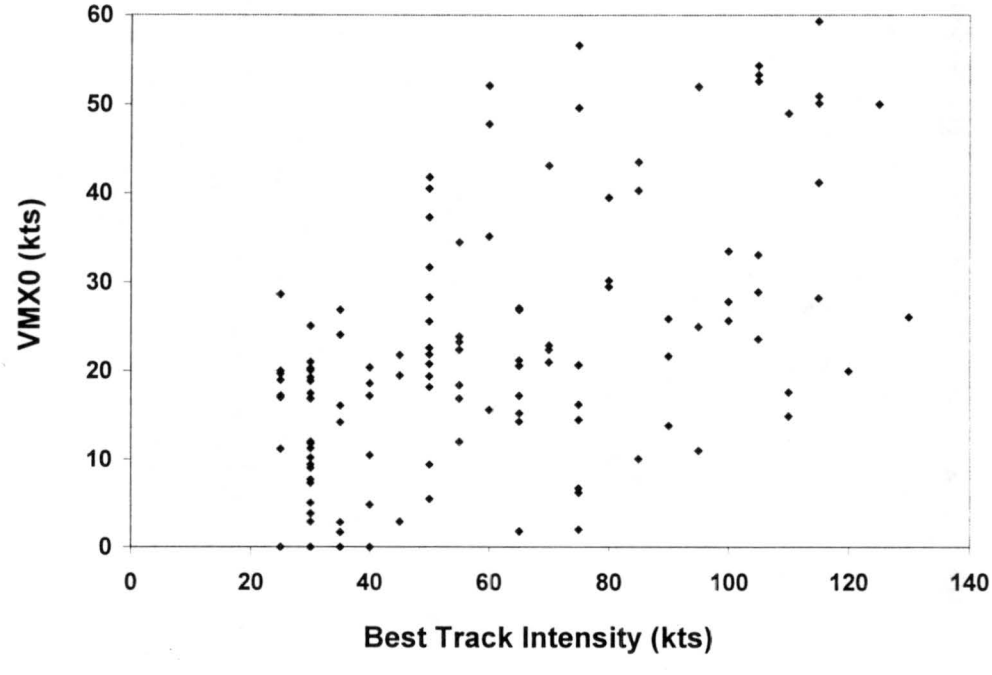
VMX0 (kts)
60
50
40
30
20
10
0
0
20
40
60
80
100
120
140
Best Track Intensity (kts)

d)

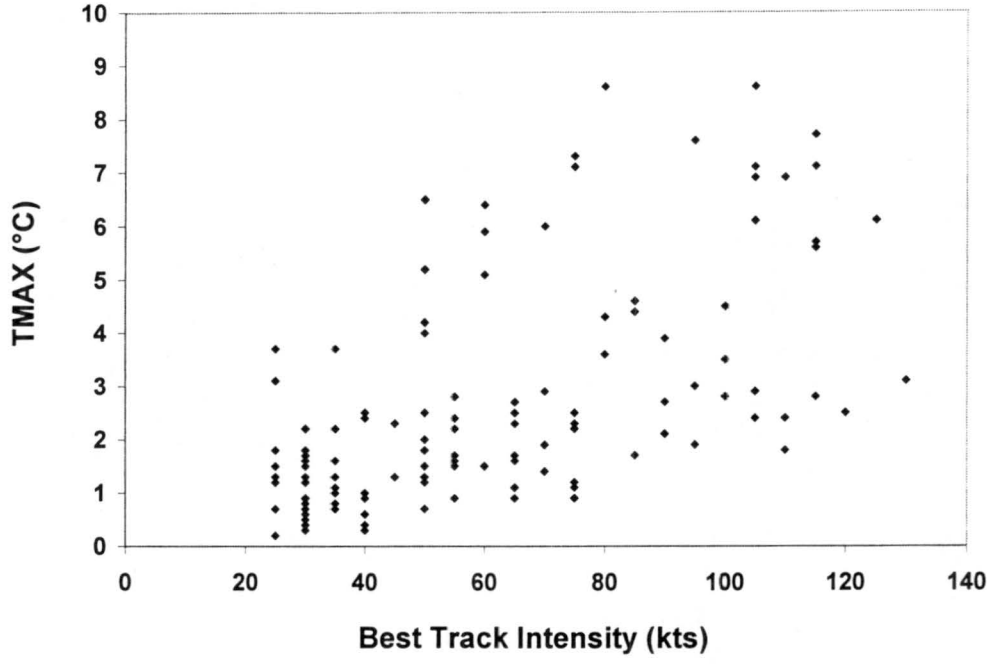

e)

Figure 4.7. Comparison of predictor values with best track intensity (VMX) for all 125 cases from 1999 data for a) VMX3, b) CLW, c) DP, d) VMX0, and e) TMAX.

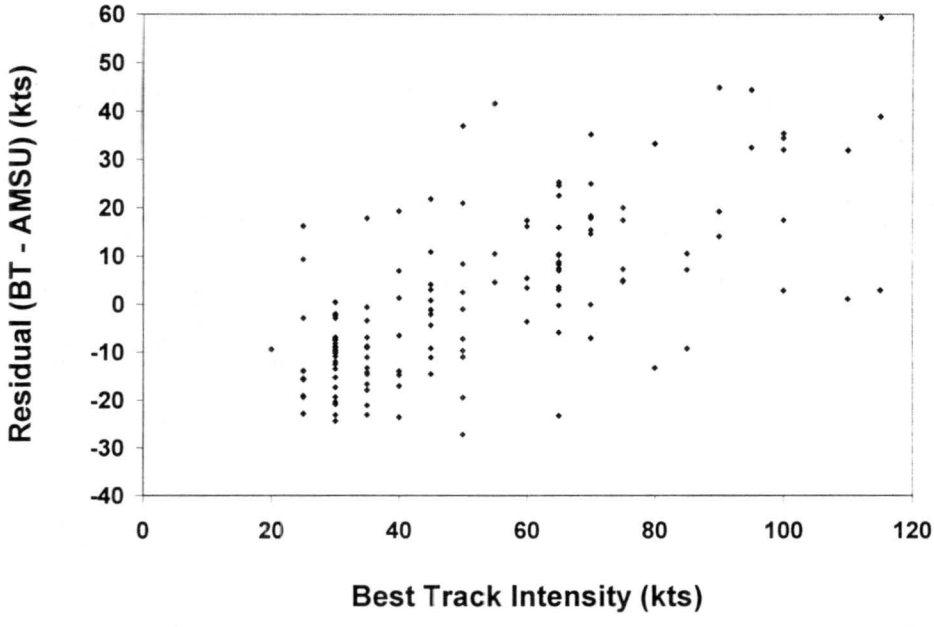

Figure 4.8. Residual (best track – AMSU calculated) plot versus best track intensity observations for 2000 cross-validation data.

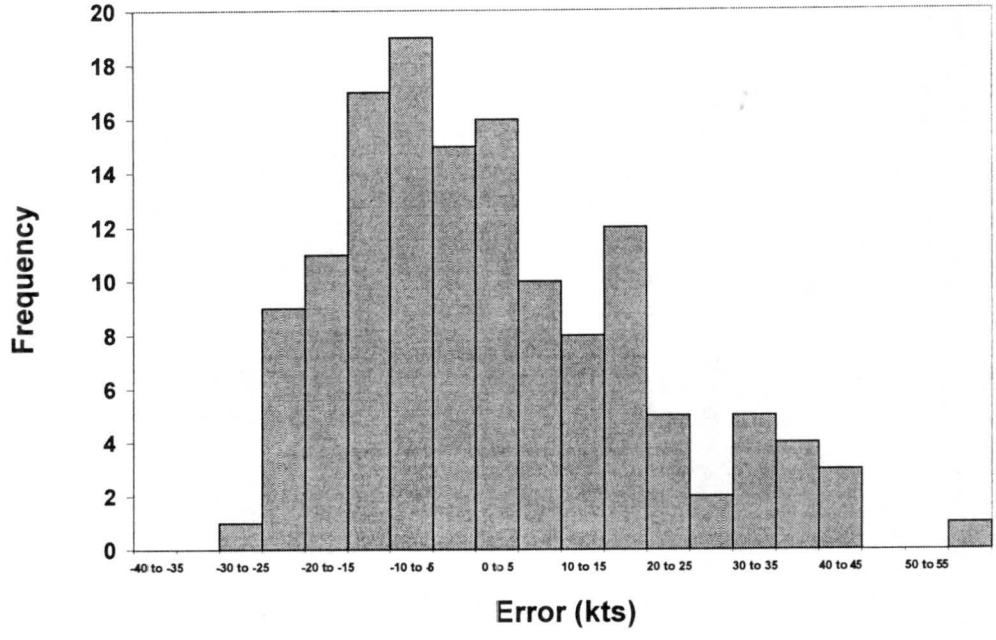
Frequency
20
18
16
14
12
10
8
6
4
2
0
-40 to -35
-30 to -25
-20 to -15
-10 to -6
0 to 5
10 to 15
20 to 25
30 to 35
40 to 45
50 to 55
Error (kts)

a)

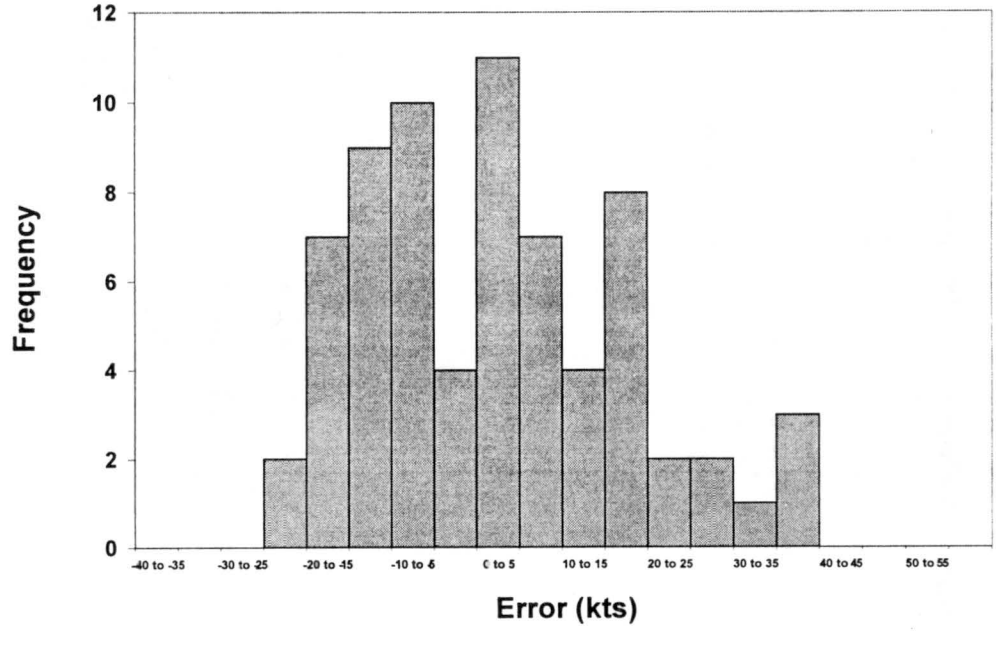
Frequency
12
10
8
6
4
2
0
-40 to -35
-30 to -25
-20 to -15
-10 to -6
0 to 5
10 to 15
20 to 25
30 to 35
40 to 45
50 to 55
Error (kts)

b)

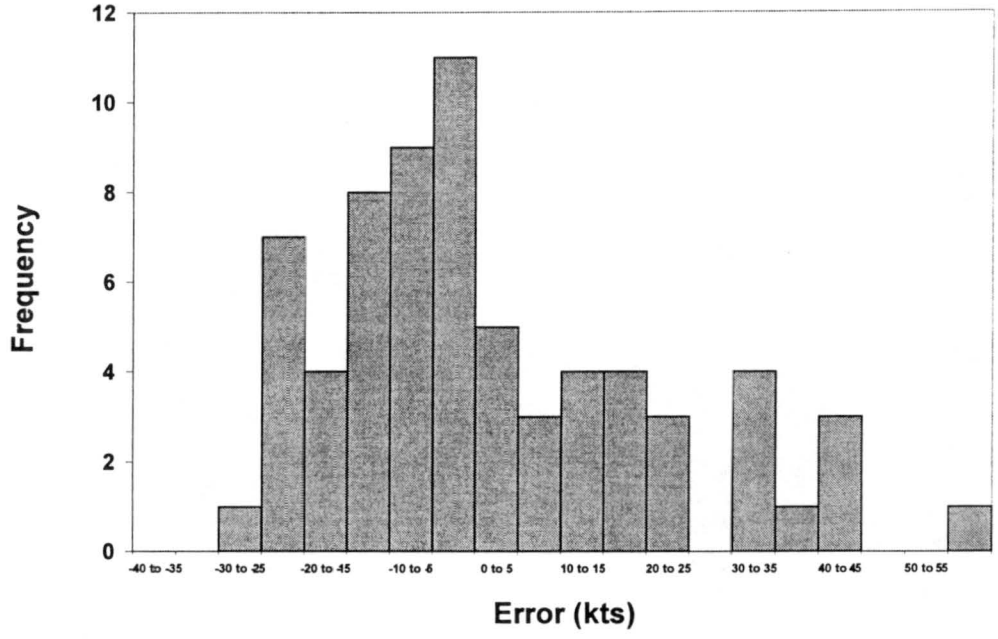

c)

Figure 4.9. Histogram of residuals (best track – AMSU predicted intensity) for 2000 cross-validation data in a) both basins combined, b) Atlantic basin only, and c) East Pacific basin only.

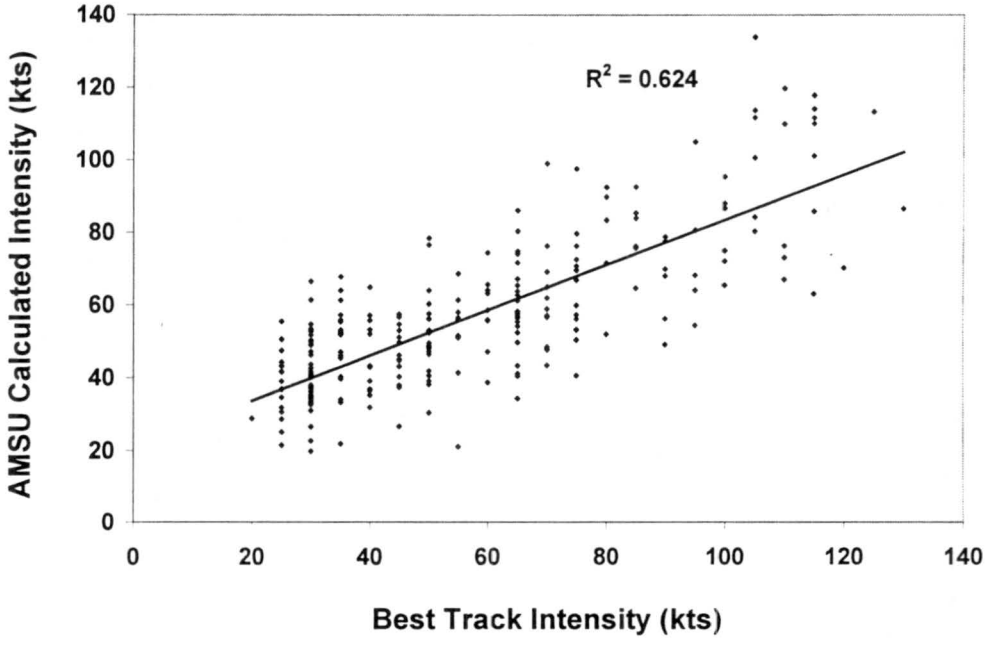

Figure 4.10. Relationship between the AMSU-derived and NHC best track reports of tropical cyclone intensity for 1999 and 2000 data combined.

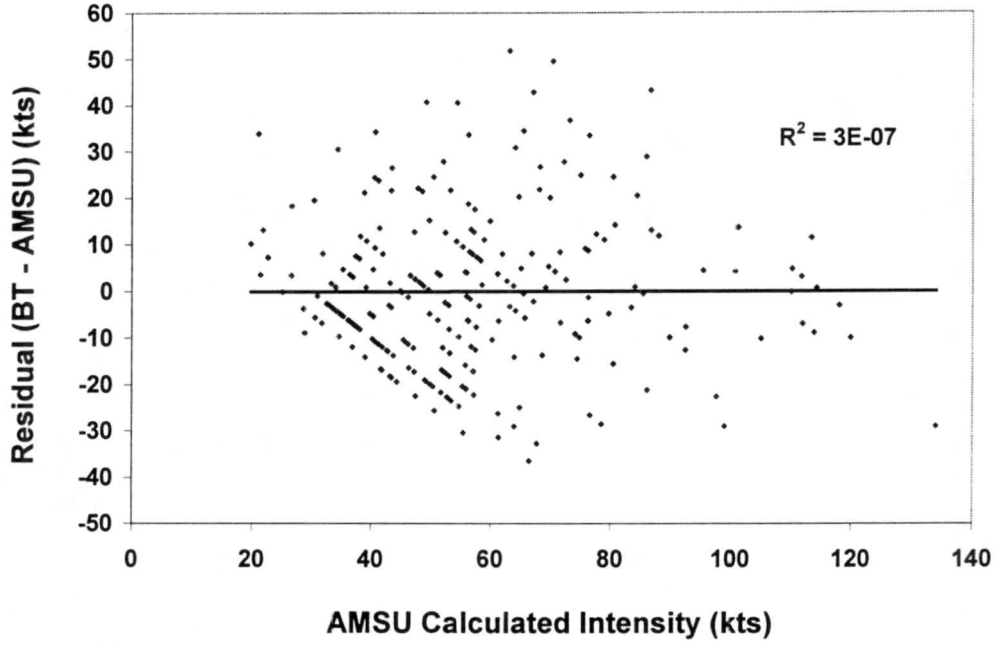

Figure 4.11. Residual (best track – AMSU calculated) plot versus AMSU calculated intensity for the combined 1999 and 2000 data set.

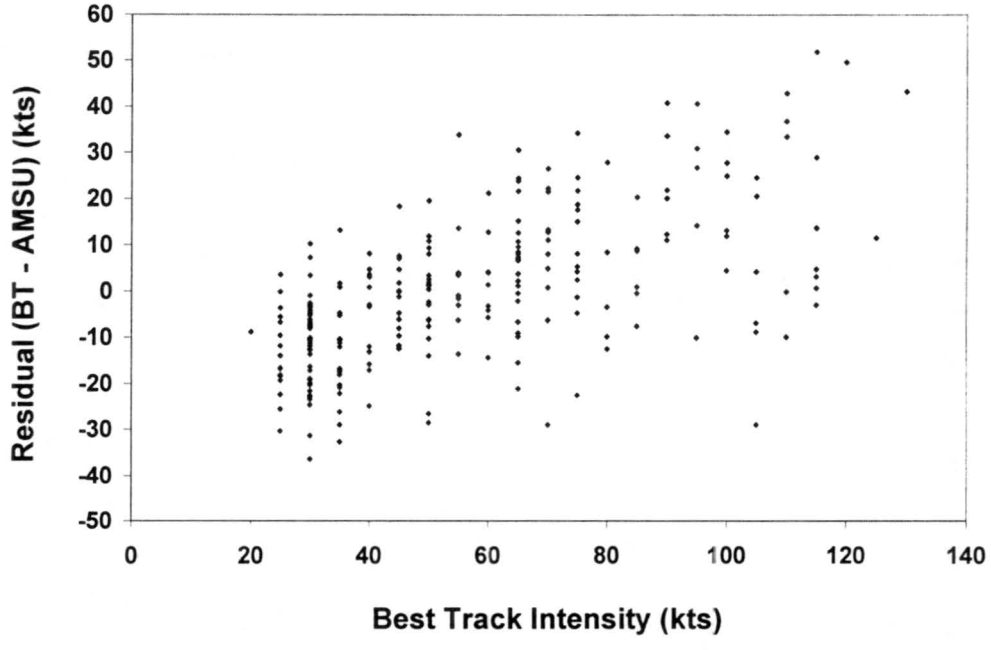

Figure 4.12. Residual (best track – AMSU calculated) plot versus best track intensity observations for 1999 and 2000 combined data.

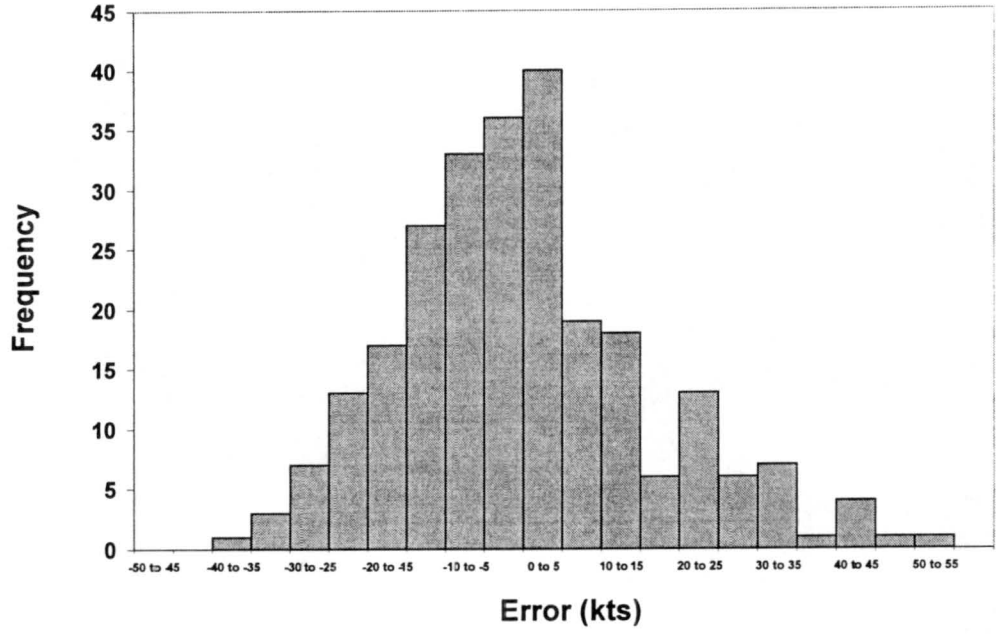
Frequency
45
40
35
30
25
20
15
10
5
0
-50 to -45
-40 to -35
-30 to -25
-20 to -15
-10 to -5
0 to 5
10 to 15
20 to 25
30 to 35
40 to 45
50 to 55
Error (kts)

a)

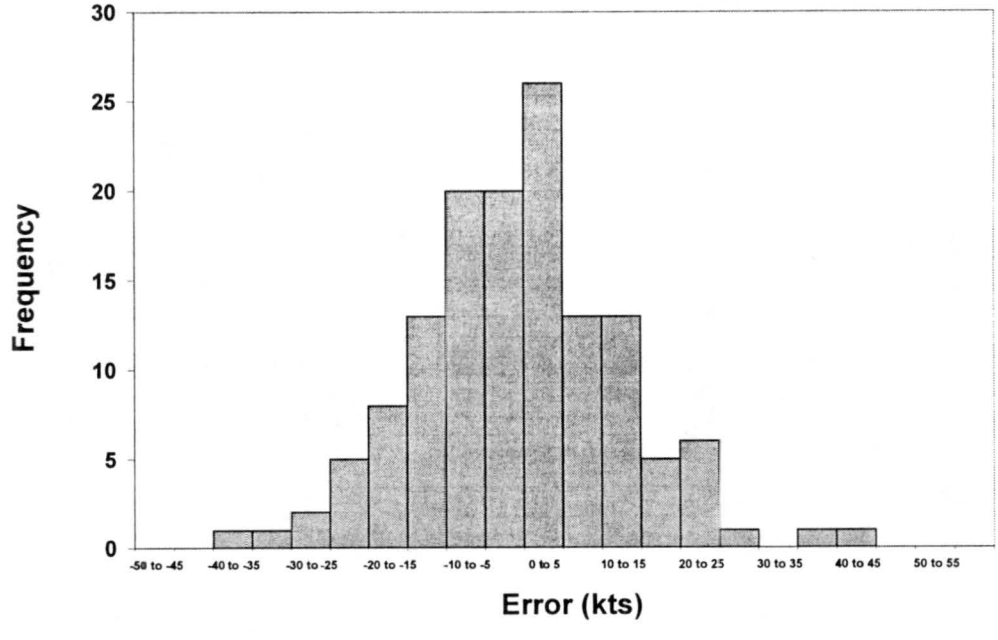
Frequency
30
25
20
15
10
5
0
-50 to -45
-40 to -35
-30 to -25
-20 to -15
-10 to -5
0 to 5
10 to 15
20 to 25
30 to 35
40 to 45
50 to 55
Error (kts)

b)

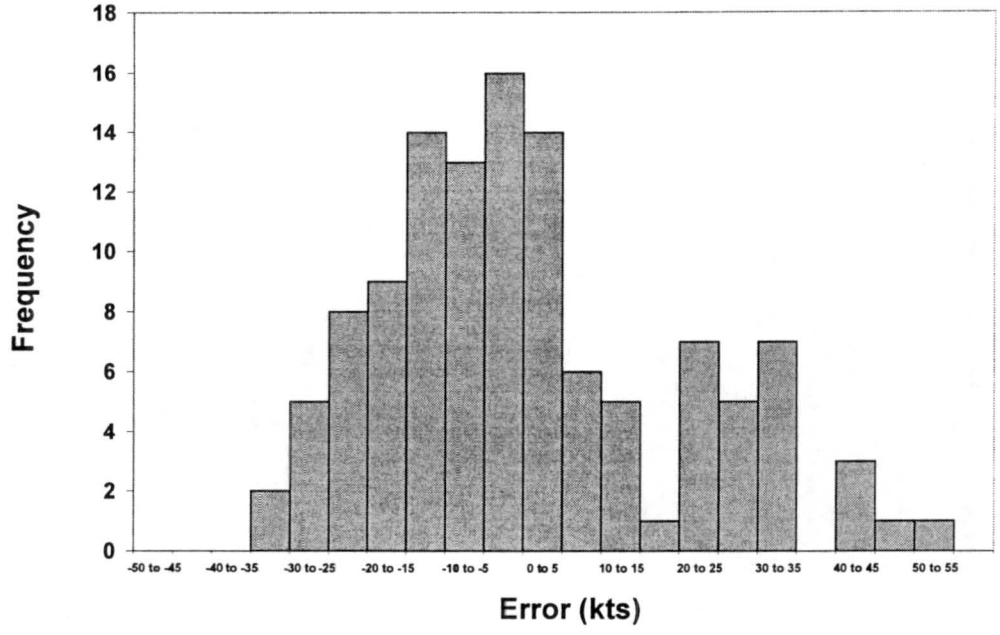

c)

Figure 4.13. Histogram of residuals (best track – AMSU predicted intensity) for 1999 and 2000 combined data in a) both basins combined, b) Atlantic basin only, and c) East Pacific basin only.

Chapter 5 - Objectively Estimating Tropical Cyclone Wind Radii

5.1 Axisymmetric Wind Radii Estimations

The basic assumptions underlying the objective estimation of tropical cyclone wind radii by the AMSU are the same as those for estimating intensity. Again, due to the AMSU's coarse resolution, this study develops a statistical procedure utilizing AMSU-derived parameters to develop an algorithm to approximate the azimuthally averaged (hereafter referred to as AA) radii of 34, 50, and 64 kt winds. These three specific wind magnitudes are chosen because they are given operationally by the National Hurricane Center. The 34 and 64 kt winds are the thresholds for tropical storms and hurricanes, respectively, and the 50 kt winds are roughly the greatest force sustainable by most ships. The azimuthally averaged information derived from this study subsequently is used with a Rankine vortex model to make asymmetric estimations of the 34, 50, and 64 kt wind radii. In Section 5.1 of this chapter, the development of the azimuthally averaged wind radii estimative algorithms with AMSU data and their performance on the developmental and independent data sets is discussed. In Section 5.2, the method of using the azimuthally averaged data in a Rankine vortex model is detailed followed by the results.

5.1.1 Data

The same 11 AMSU-derived and two non-AMSU-derived parameters described in Section 4.1.1 make up the independent data set (predictors) for the AA 34, 50, and 64 kt wind radii estimations. The validation data come from forecast advisories issued every six hours by the NHC beginning when a tropical cyclone is classified as a tropical depression and continuing until the storm dies out. The advisories give information on a TC's center location, maximum sustained wind speeds, gust speeds, and central pressure. They also include the height of 12 foot seas and the radii of 34, 50, and 64 kt winds (when applicable) in the northeast (NE), northwest (NW), southeast (SE), and southwest (SW) quadrants of the TC as well as six-hourly forecasts of the maximum winds and the wind radii. Text descriptions of watches and warnings also may be part of an advisory if a TC is threatening land. Information in the advisories is derived from all available surface data and aircraft reconnaissance data; VIS and IR imagery also sometimes are used to estimate the outer wind circulation of TCs. As with the best track data, it is noted that the wind radii validation data are not always *in situ* measurements, but unlike the BT data, there is no post-season analysis of the wind radii measurements. This suggests large error may be inherent in the validation data set, but it is the only option available for development of the objective algorithms. The NHC reports the wind radii in nautical miles (nm) in the NE, NW, SE, and SW quadrants of the TC. The average of the four quadrants is calculated and used as the dependent data for the azimuthally averaged 34, 50, and 64 kt wind radii approximations, denoted as AVE34, AVE50, and AVE64, respectively. The advisories used are those closest in time to the AMSU swath but not differing by more than three hours.

The same base data set from the 1999 tropical season is used for the wind radii estimations as for the intensity estimations (Section 4.1.1). However, since the 125-case

data set is comprised of all tropical disturbances including depressions, storms, and hurricanes, the data sets for each of the 34, 50, and 64 kt wind radii contain subsequently fewer cases. Moreover, cases without corresponding NHC advisories are not considered. This occurs occasionally when a TC is near 34, 50, or 64 kts so that, operationally, it is defined as being below the threshold and is not given associated wind radii; then, during the post-season BT analysis, the intensity is upgraded slightly, but there is no concurrent operational estimates of wind radii. Overall, there are only 90 cases with winds 34 kts or greater, 75 with winds 50 kts or greater, and 51 with winds 64 kts or greater from the 1999 data. The same statistical methods are run on all three data sets.

Data from the 2000 tropical season are used for cross-validation. Again cases without simultaneous best track data are deleted, but those in which the TC is within 100 km of land are retained for validation purposes since these cases will be estimated in real time. Of the 138 cases from the 2000 tropical season, the wind radii data sets consist of 94 cases with winds 34 kts or greater, 61 cases with winds 50 kts or greater, and 44 cases with winds 64 kts or greater.

5.1.2 Methods

The dual statistical method of correlating each predictor with the predictand first, followed by a backward stepwise regression using all significant variables, is used to derive all three wind radii algorithms, as it was for the intensity estimations (Section 4.1.2). However, an additional step is used; to make the algorithms for the average 34, 50, and 64 kt wind radii consistent, it is desirable to use the same set of predictors for all three. Accordingly, any predictor kept by at least one of the backward stepwise regressions was retained and subsequently used in a final linear (non-stepwise) regression. This latter non-stepwise regression is the one from which the algorithms are

established. Again, significance levels of five percent are used for the correlation and the backward stepwise regression, and the MAE is the main measurement of error. Since there are no other studies with which to compare results, the RMSE of the azimuthally averaged wind radii is not reported.

5.1.3 Results and Error Analysis

Of the original 13 parameters, eight are significantly correlated with the azimuthally averaged 34 kt wind radii, seven with the 50 kt wind radii, and eight with the 64 kt wind radii (Table 5.1). The set of predictors are nearly consistent for all three, only differing due to the p-value of R015 being slightly too high (0.057) to be retained for the 50 kt wind radii. The wind radii predictors kept by the correlation are nearly the same as those significantly correlated with the best track intensity (Section 4.1.3). The only difference is that storm latitude (STORMLAT) replaces the height of the maximum temperature perturbation (ZMAX) as a potential predictor, so that the wind radii set includes STORMLAT, DP, VMX0, VMX3, TMAX, R015 (not for 50 kt), R315, and CLW. Of these eight, the predictors kept by at least one of the three stepwise regressions, used in the final, linear (non-stepwise) regression, are STORMLAT, DP, VMX0, VMX3, and CLW.

According to the linear regression for the AA 34 kt wind radii, the five aforementioned variables explain 76.4 percent of the variation in the 1999 wind radii observations from the NHC advisories (Figure 5.1a). For the 50 and 64 kt wind radii, 69.3 percent (Figure 5.1b) and 77.5 percent (Figure 5.1c) of the variation is explained, respectively. The normalized coefficients (Table 5.2) reveal that no predictor is markedly better than the others at predicting the 34 kt wind radii. Rather, all are useful, with the AMSU-derived intensities at the surface (VMX0) and at a height of 3 km (VMX3) slightly more so. On the other hand, for the 50 kt wind radii, the relative weights of DP and

VMX0 are nearly double those of VMX3 and CLW. However, despite its lower normalized coefficient, the lower p-value of CLW suggests statistically that there may be more confidence in its ability to explain variations in AVE50, whereas the p-value of VMX0 implies it is not as informative. The normalized coefficient and p-value both suggest STORMLAT is of least utility. Finally, for the 64 kt wind radii, VMX0 stands out as the most beneficial predictor, followed closely by DP and VMX3. Again, the storm latitude is of little value, as is the cloud liquid water. In summary, DP, VMX0, and VMX3 are all likely valuable in explaining the variation in all three AA wind radii. Each of these three becomes correspondingly more influential in predicting the radii of stronger winds, signifying the importance of the pressure gradient and the strong wind speeds for detecting hurricane-force winds. On the other hand, STORMLAT is only valuable for estimating gale force wind radii. There is a strong relationship between the increasing radius of AA 34 kt winds with increasing latitude (Figure 5.4a); this likely occurs because the Coriolis force increases with distance from the equator, and the balance of this with pressure gradient and centrifugal forces causes the TC to expand. The relationship with STORMLAT is not as obvious for 50 and 64 kt wind radii (figures not shown), possibly because of the smaller data sets, which explains why this variable is more useful for 34 kt wind radii estimations. Finally, the relative unimportance of CLW in estimating AVE64 likely is due to its inferiority compared to DP, VMX0, and VMX3.

A set of AMSU-derived equations for estimating the azimuthally averaged 34, 50, and 64 kt wind radii can be written similar to Equation 4.8 using the coefficients in Table 5.2.

$$\begin{aligned} AVE34 = {} & 8.638 + (2.227*STORMLAT) + (2.204*DP) + \\ & (-1.988*VMX0) + (1.801*VMX3) + (50.391*CLW) \end{aligned} \qquad [5.1]$$

$$AVE50 = 21.665 + (-0.018*STORMLAT) + (4.553*DP) + (-2.279*VMX0) + (1.301*VMX3) + (41.110*CLW) \quad [5.2]$$

$$AVE64 = 33.589 + (-0.132*STORMLAT) + (4.065*DP) + (-3.238*VMX0) + (2.501*VMX3) + (2.830*CLW) \quad [5.3]$$

These algorithms are tested against the azimuthally averaged wind radii from the 1999 NHC advisories. For the 34, 50, and 64 kt wind radii, the MAE are 16 nm, 17 nm, and 8 nm, respectively. Based on the average radii of the three winds speeds, calculated from AA NHC data, these MAE correspond to errors of 14.4 percent, 24.6 percent, and 17.8 percent, respectively. All three residual (NHC reported radii – AMSU calculated radii) versus AMSU calculated AA wind radii plots demonstrate very nearly balanced scatter about the zero line (Figures 5.2a – 5.2c). The lack of a pattern or tendency presumably validates the AMSU-derived prognostic equations for operational use.

As with the intensity estimation, it is physically reasonable to examine the residuals against the validation data from the NHC advisories. Recall, that, because of the way the residual is defined, negative (positive) residuals correspond to over (under) estimations. Paralleling the tendencies with the AMSU-derived intensity calculations, there is a propensity for over (under) estimation of smaller (larger) radii for all three wind speeds (Figures 5.3a – 5.4a). Specifically, for the 34 kt wind radii estimation, any radii less than approximately 100 nm is generally inflated and vice versa. For the 50 and 64 kt estimations, the divisions between over and under approximation are roughly 70 and 40 nm, respectively.

These error tendencies likely can be attributed to the same reasons as those mentioned for the over and under estimates of AMSU-derived TC intensity. In general, the wind radii errors result from the propensity of the predictors to have a wide range of values. For example, the minimum values of all five variables occur for 34 kt wind radii ranging from 25 to over 125 nm, and moderate values occur for radii from 50 to over 225 nm (Figures 5.4a-e). Similar patterns exist for the 50 and 64 kt wind radii (figures not shown). As with the intensity estimates, the coarse AMSU resolution also likely contributes to the under estimations as does the azimuthal averaging technique used in deriving the AMSU parameters. Finally, it is possible that the lack of good wind radii validation data suggests larger errors from the AMSU-derived estimates than actually exist, reiterating that dependent data from aircraft reconnaissance only is desired

The residuals for the azimuthally averaged 34 kt wind radii are roughly evenly distributed (Figure 5.5a), with 46 (44) of the 90 cases over (under) predicted. Furthermore, the approximate bell-shaped curve reveals the majority of error lies within 15 nm. Only 14 cases (15.6 percent) are miscalculated by 35 nm or more, half of which are over estimated, half of which are under estimated. Unlike the AMSU-estimated intensity, however, the errors in the Atlantic basin are not considerably better than those in the East Pacific basin (Figures 5.5b,c) for the 1999 data. In the Atlantic, the data is skewed to the left slightly with 34 (26) of 60 cases over (under) predicted; only 12 (18) of 30 cases are over (under) predicted in the East Pacific, and correspondingly, the data is skewed rightward. Additionally, a slightly higher percentage of Atlantic cases (38.3 percent) compared to East Pacific cases (33.3 percent) are in error by more than 15 nm.

In contrast, fewer azimuthally averaged 50 kt wind radii are over approximated (34 cases) than under predicted (41 cases) by the AMSU (Figure 5.6a). Accordingly, only 17 cases are in excess error by at least 15 nm compared to 21 cases that are under

estimated by an equal magnitude; the large number of cases (8) under estimated by 15 to 20 nm is the primary cause of this. The subtle skewness to the left, however, highlights the larger magnitudes of the over approximated cases; there are six cases with residuals between –35 and –55 nm as opposed to only three cases with residuals from 35 to 50 nm. Looking specifically at the Atlantic and East Pacific basins (Figures 5.6b,c), the error distributions are vastly different. The former is much more spread out, with residuals ranging from –55 to 50 nm, while the configuration of the latter is much more compact, ranging from –15 to 30 nm. The residual pattern for the Atlantic is roughly bell-shaped, despite a couple low frequency bins; however, all nine cases in error by more than 35 nm occur in this basin. On the other hand, with only three of 22 cases over predicted, all of which are in error by less than 15 nm, the histogram of the East Pacific cases shows the residuals do not vary greatly.

At 25 and 26, an approximately equal number of AA 64 kt wind radii cases are over predicted as under predicted, although the maximum magnitudes of the former are larger (Figure 5.7a). As with the 50 kt residuals, the largest errors occur in the Atlantic basin, although 36.4 percent of the cases are in error by plus or minus 5 nm (Figure 5.7b). Again, the distribution of residuals in the East Pacific is very compact, with the majority of cases (55.6 percent) within 5 nm of error (Figure 5.7c).

To briefly summarize, the residuals in the Atlantic are less precise than those in the East Pacific for all wind radii for the 1999 data. The former generally are over and under estimated, sometimes by large magnitudes, while the latter more commonly are under approximated by the AMSU. The underlying physical mechanisms causing errors in the two basins are difficult to ascertain, and in fact, the distributions change by year as discussed below.

The cross validation test of the AMSU-derived 34, 50, and 64 kt wind radii on the 2000 data shows the MAE of the 34 and 64 kt wind radii greatly increased to 25 and 12 nm. However, the MAE of the 50 kt wind radii decreased slightly to 16 nm. Based on the average AA 34, 50, and 64 kt wind radii, these correspond to errors of 27.2, 32.7, and 42.9 percent, respectively. The errors most likely stem from the small data set from which the algorithms are developed and errors within the NHC operational advisories. Inaccuracies also could be due to the fewer intense hurricane cases during the 2000 tropical season.

Unlike the developmental 1999 data set, the distributions of residuals against the NHC AA 34, 50, and 64 kt wind radii do not show as strong of a tendency for over (under) estimation of small (large) wind radii, especially for the 50 and 64 kt wind radii (Figures 5.8a-c). In comparison to the 1999 data, the AMSU-derived wind radii generally are over approximating more cases for the 2000 data for all wind speeds. Specifically, 59 (35) cases are over (under) approximated for the AA 34 kt wind radii, as are 41 (20) cases for the AA 50 kt wind radii, and 32 (12) cases for the AA 64 kt wind radii (Figures 5.9a, 5.10a, 5.11a). For the 34 kt winds, the magnitude of errors nearly double for the 2000 data, ranging from approximately 75 nm over estimated to 120 nm under estimated. The AMSU under estimates a smaller percentage (22.4 percent) of Atlantic cases in 2000 compared to 1999 (43.3 percent) (Figures 5.5b, 5.9b), while the East Pacific distributions are roughly the same with a slightly lower percentage of cases under estimated in 2000 (Figures 5.5c, 5.9c). For the 50 kt wind radii, the magnitude of errors is nearly constant from the 1999 to 2000 data sets (Figures 5.6a, 5.10a). However, the over and under estimations by basin vary greatly; for example, in the East Pacific, 3 of 22 cases (13.6 percent) are over predicted in 1999 whereas 13 of 23 cases (56.5 percent) are over predicted in 2000 (Figures 5.10b,c). For the AA 64kt wind radii, the

residuals shift from being evenly distributed in 1999 to a majority (72.7 percent) of cases being over estimated in 2000 (Figure 5.7a, 5.11a). This is largely due to the great increase in the number of over estimated cases in the Atlantic (90.0 percent) (Figures 5.11b,c).

Despite the chaotic shift in error distributions from 1999 to 2000, for each case in the 2000 cross-validation data set, AVE34 is greater than AVE50, which is greater than AVE64 indicating the AMSU-derived algorithms are consistent; this provides additional confidence for their use in an operational setting.

5.1.4 1999 and 2000 Combined Data Set

As with the intensity estimations, the 1999 and 2000 data sets are combined (hereafter referred to as 9900) to refine the 34, 50, and 64 kt wind radii estimations for tropical cyclones. After removing the cases within 100 km of land from the 2000 data set (to eliminate land effects during algorithm development, as discussed in Section 4.1.1), the resultant 9900 data set consists of 176 cases with winds 34 kts or greater, 133 cases with winds 50 kts or greater, and 91 cases with winds 64 kts or greater. The statistical methods used on the 1999-only data, summarized in Section 5.1.2, are the same as those used on the 9900 data. In brief, they consist of an initial correlation with the predictand, a subsequent backward stepwise regression, and a final linear regression using every parameter kept by at least one of the stepwise regressions. The same predictands, AVE34, AVE50, AVE64, are used as well, and all significance levels are set at five percent.

The data in Table 5.3 reveal that, of the 11 AMSU-derived and two non-AMSU-derived parameters, nine are correlated significantly with AVE34, eight with AVE50, and seven with AVE64. The significant variables are nearly the same as those for the 1999-only data (Table 5.1) with the exception of STRMSP being retained for the azimuthally

averaged 34 kt wind radii estimation and STORMLAT not being retained for the AA 64 kt wind radii. Six parameters are kept by at least one of the backward stepwise regressions, including STRMSP, DP, VMX0, VMX3, TMAX, and CLW; this differs from the 1999-only data in that STORMLAT is replaced by STRMSP and TMAX.

The final, linear regressions for AVE34, AVE50, and AVE64 show that the six variables mentioned above explain 67.4 percent, 64.8 percent, and 66.5 percent of the variation in the 9900 NHC wind radii, respectively (Figure 5.12a-c). Despite the lower R^2 values compared to 1999-only data, the normalized coefficients are somewhat more consistent, suggesting that VMX0 and VMX3 likely are most useful in estimating all three predictands, followed closely by DP. The higher normalized coefficient of TMAX for 50 and 64 kt wind radii estimations is expected since stronger TCs have warmer temperature anomalies aloft. Finally, as with the 1999 data alone, the low normalized coefficient of CLW for AVE64 likely is due to its insignificance compared to the other parameters. Using the data in Table 5.4, a refined set of estimative algorithms for azimuthally averaged 34, 50, and 64 kt wind radii are established.

$$\begin{aligned} AVE34 = {} & 45.019 + (0.943*STRMSP) + (3.195*DP) + \\ & (-1.789*VMX0) + (1.984*VMX3) + (3.313*TMAX) + \\ & (22.395*CLW) \end{aligned} \qquad [5.4]$$

$$\begin{aligned} AVE50 = {} & 16.369 + (0.254*STRMSP) + (1.752*DP) + \\ & (-1.916*VMX0) + (1.584*VMX3) + (7.526*TMAX) + \\ & (18.998*CLW) \end{aligned} \qquad [5.5]$$

$$AVE64 = 23.095 + (-0.336*STRMSP) + (1.815*DP) + (-1.835*VMX0) + (1.595*VMX3) + (3.593*TMAX) + (1.263*CLW) \quad [5.6]$$

When [5.4] – [5.6] are tested on the 9900 data set, the MAE are 19 nm, 16 nm, and 9 nm for AVE34, AVE50, and AVE64, respectively, corresponding to errors of 18.6 percent, 26.2 percent, and 23.7 percent. The even scatter and lack of tendency in the plots of the residuals against the AMSU-calculated radii suggest the algorithms from the 9900 data are legitimate (Figure 5.13a-c).

Examining the residuals plotted against the NHC validation data, the trend of over (under) estimating smaller (larger) wind radii again is apparent (Figure 5.14a-c). In fact, the divisions between over and under calculations are nearly exactly the same as for the 1999-only data at 100 nm for AVE34, 70 nm for AVE50, and 40 for AVE64. The reasons for the error in the estimates probably is the same as that explained in Section 5.1.3 for the 1999 data alone; every parameter has magnitudes that correspond to a wide range of radii and the azimuthal averaging technique perhaps over-smoothes detail. As always, the error statistics are somewhat questionable due to lack of good validation data, and they will continue to be until a larger data set of aircraft reconnaissance data becomes available.

The residuals for the azimuthally averaged 34 kt wind radii from the 9900 data mimic those from 1999 alone (Figures 5.5, 5.15). Slightly more cases are over estimated than under for both basins combined and the Atlantic basin with the opposite being true for the East Pacific basin. In general, the distribution is bell-shaped with only three outliers, which are under approximated by 70 to 115 nm. The distribution consistency from 1999 to 9900 holds for the AA 50 and 64 kt wind radii as well. Just

over 50 percent of the data is under approximated for AVE50 (54.5 percent) (Figure 5.16a) and AVE64 (52.7 percent) (Figure 5.17a). Examining the basins individually, the majority of cases for AVE50 are over (under) estimated for the Atlantic (East Pacific) (Figure 5.16b,c); the same is true for AVE64 (Figure 5.17b,c). As with the AA wind radii estimations from the 1999 data alone, the distributions are wider in the Atlantic with larger magnitudes of error, and more compact in the East Pacific, with most cases in error by 15 nm or less. As mentioned previously, the large difference in distributions between both basins may be remedied with separate algorithms.

5.2 Asymmetric Wind Radii Estimations

As described in Section 5.1.1, the National Hurricane Center issues 6-hourly forecast advisories for tropical cyclones in the Atlantic and East Pacific basins. Included in the advisories are estimates of the 34, 50, and 64 kt wind radii in the NE, NW, SE, and SW quadrants of the TC. Utilizing a Rankine vortex model, the azimuthally averaged AMSU-derived 34, 50, and 64 kt wind radii (Section 5.1), and an estimate of TC maximum sustained winds, the goal is to make an approximation of the 34, 50, and 64 kt wind radii (when applicable) in the four quadrants mentioned. It should be noted that the predictors from the 1999 data only are used for the AMSU-estimated azimuthally averaged radii as opposed to the refined 9900 predictors; the latter are not used because they have not been cross validated against the independent 2001 tropical season.

5.2.1 Data

Unlike the TC intensity and azimuthally averaged wind radii estimates, no algorithm is created to approximate the asymmetric wind radii; rather, an analytical model is used in conjunction with other information (Section 5.2.2). Therefore, the data

from the 2000 tropical season is not needed for cross-validation, so all AMSU passes from the 1999 and 2000 tropical seasons (again, referred to as 9900) are combined and used. The validation data come from the same NHC operational forecast advisories as used for the AA wind radii estimation algorithms, only the data in the NE, NW, SE, and SW quadrants are used explicitly for comparison rather than being averaged.

As will be explained in the following section, there are three ways to use the AA AMSU-derived wind radii, and thus, three data sets are utilized. For cases in which there is only a 34 kt wind radii to assess, the data set is limited to those cases with best track intensities greater than or equal to 34 kts and less than 50 kts. The second data set includes only cases with BT intensities greater than or equal to 50 kts and less than 64 kts in order to estimate the 34 and 50 kt wind radii. Finally, for cases in which all three wind radii in the four quadrants are approximated, the third data set includes all cases with BT intensities greater than or equal to 64 kts. Although the best track data are not available in real time, this information is used in place of the operational TC maximum sustained wind estimates that will be used operationally. It is not known at this time what exactly will be used for the real-time TC intensity estimates; aircraft reconnaissance data will be used if available, otherwise it is likely that a combination of Dvorak, ODT, and AMSU estimates will be employed.

Once the three data sets are shortened based on available best track data, they are condensed further by removing any cases for which there is no corresponding NHC data for validation purposes. Again, this generally occurs for TCs just over the 34, 50, or 64 kt threshold, which may not have been classified as such until the post-season BT analysis, thus, they received no wind radii estimates operationally. The resultant three data sets consist of 37 cases for the 34 kt wind radii, 35 cases for 34 and 50 kt wind radii, and 91 cases for 34, 50, and 64 kt wind radii.

5.2.2 Methods

As Holland (1980) notes, a good way of using sparse observations to provide objective estimates of destructive wind extent is with an analytical model of hurricane wind profiles. Holland (1980) and Abraham *et al.* (1995) combined refer to five such models of which Abraham *et al.* (1995) report that the modified Rankine vortex (Depperman, 1947) and Holland's vortex offer the best representations. Because of its relative ease of use, the modified Rankine vortex is used in this study to analyze the 34, 50, and 64 kt asymmetric wind radii.

The Rankine vortex consists of two main areas of interest, one inside the radius of maximum winds (r_m) and one outside r_m. The inner region is assumed to be in solid-body rotation meaning the angular velocity is constant (Houze, 1993). Hence, inside r_m, the tangential wind, V, is directly proportional to the radial distance from the center of the tropical cyclone. It is expressed as,

$$V = V_m\left(\frac{r}{r_m}\right), \quad r < r_m \qquad [5.7]$$

where r is the radial distance from the center, and V_m is the maximum tangential velocity of the TC (i.e. the maximum sustained winds). The region outside r_m is characterized by potential vortex flow where the tangential velocity is inversely proportional to r. Depperman's modified Rankine vortex, with a negative exponential relation, causes the tangential wind speed to decrease exponentially with r outside of r_m. In this outer region, V is expressed as,

$$V = V_m\left(\frac{r}{r_m}\right)^{-x}, \quad r \geq r_m \qquad [5.8]$$

where x is a unitless, positive number determined empirically from AMSU data. According to Holland (1980), the value of x is less than unity and it usually lies between

0.4 and 0.6, although it can be lower or higher. Figure 5.18 is an example of Rankine tangential wind profile of a tropical cyclone with maximum sustained winds of 100 kts, a maximum wind radius of 40 nm, and x set to 0.5.

The modified Rankine vortex model can be applied to a polar coordinate system to determine a tropical cyclone's wind radii in the NE, NW, SE, and SW quadrants,

$$V(r,\theta) = (V_m - a)\left(\frac{r}{r_m}\right)^{-x} + a\cos\theta \qquad [5.9]$$

where a is the maximum asymmetry parameter of a moving storm (Equation 4.4) (Schwerdt *et al.*, 1979). In real time, the estimated parameters available are the maximum wind speed (V_m), the storm translational speed which is used to give a, and the AMSU-derived azimuthally averaged radii of 34, 50, and 64 kt winds, when applicable. In order to utilize the latter, Equation 5.9 is solved for r, to yield

$$r = r_m\left(\frac{V_m - a}{V - a\cos\theta}\right)^{1/x} \qquad [5.10]$$

and then azimuthally averaged to yield

$$\bar{r} = \frac{r_m}{2\pi}\int_0^{2\pi}\left(\frac{V_m - a}{V - a\cos\theta}\right)^{1/x} d\theta\,. \qquad [5.11]$$

Depending on which AMSU-derived azimuthally averaged radii is being used, the corresponding value of V is applied (i.e. if using the AMSU-derived AA 34 kt wind radii, V is 34 kts). Therefore, the only unknown variables in Equation 5.11 are r_m and x. Since it is difficult to integrate [5.11] and solve for x by hand, Equation 5.11 is written as a summation. Letting

$$F = \left(\frac{V_m - a}{V - a\cos\theta}\right), \qquad [5.12]$$

then [5.11] is written as

$$\bar{r} = r_m \frac{1}{n} \sum_{i=1}^{n} F_n^{1/x}, \qquad [5.13]$$

where F is calculated by incrementing θ by two degrees from zero to 358 degrees, thus the summation is calculated over 180 points.

For cases in which the intensity is greater than or equal to 50 kts but less than 64 kts, AMSU-derived estimates of the 34 and 50 kt wind radii are available. Thus, [5.13] is used to write two equations which are solved for r_m and equated to find x.

$$\frac{\overline{r_{34}}}{\sum_{i=1}^{180} F_{180,34}^{1/x}} = \frac{\overline{r_{50}}}{\sum_{i=1}^{180} F_{180,50}^{1/x}} \qquad [5.14]$$

Nevertheless, even using a summation, it still is not easy to manipulate [5.14] to give an expression for x. Therefore [5.14] is set to zero, and x is varied by 0.01 until the expression equals zero or the value closest to zero. Upon calculation of x, it subsequently is used to solve for r_m so that all variables in [5.11] are known.

For cases in which the maximum sustained winds are greater than or equal to 64 kts, the three AMSU estimates of azimuthally averaged 34, 50, and 64 kt wind radii provide too much information. As a result, three estimates of r_m and x are derived as described above using all three possible pairs of data (i.e. the azimuthally averaged 34 and 50 kt wind radii, 50 and 64 kt wind radii, and 34 and 64 kt wind radii), which are then averaged to give one set of values.

The difficult cases are those in which the maximum sustained winds are less than 50 kts. With only an AMSU-derived estimate of the azimuthally averaged 34 kt wind radius, not enough information is available to solve for r_m and x. For these cases, a value of r_m is assumed via data from the Extended Best Track (EBT) file; the EBT is a

comprehensive data set of all Atlantic storms since 1988, which includes information on TC size, including r_m.

In addition to r_m, the EBT also has the estimates of winds in the NE, NW, SE, and SW quadrants, which are averaged to give an azimuthal mean. For every case from 1999 and 2000 in the EBT with maximum wind speeds between 34 and 50 kts, a ratio of r_m to the azimuthally averaged radius is calculated. The average of all ratios is calculated where the maximum winds minus the asymmetry parameter are 1) less than 34 kts, and 2) greater than or equal to 34 kts; the corresponding ratios are 1.04 and 0.87, respectively. The reason for calculating separate ratios for these two situations, and the cause of the former being larger, are discussed in the next paragraph. For each case in the 34 kt asymmetric wind data set, the AMSU-derived azimuthally averaged 34 kt wind radius is multiplied by the appropriate ratio to give a value of r_m. Again, due to the difficulty of finding an expression for x, with a value of r_m, x is calculated by setting [5.13] equal to zero and, again, varying x until the equation equals zero or the closest value to zero.

In all three data sets, there are cases to which it is difficult to fit [5.11]. In general, the problematic cases are those with maximum sustained winds close to the 34, 50, and 64 kt thresholds. When accounting for the tropical cyclone's motion, these cases may have quadrants without any radii to be estimated at all. For example, if a TC is moving northwest, the maximum winds are assumed to be 90 degrees to the right, in the northeast, due to the storm motion and the minimum winds are 90 degrees to the left, in the southwest. For a tropical storm with winds of 35 kts moving at 5 kts, the asymmetry parameter will add approximately 4 kts in the NE, and subtract 4 kts in the SW; thus in the latter quadrant, there is no 34 kt wind radii to estimate, rather there is only a small arc to the right of the storm center with 34 kt winds for which a radius can

be estimated. Although these cases were included in the development of the AMSU algorithms to estimate AA wind radii, they only make up a small number of cases such that they do not greatly influence the estimative parameters. Accordingly, Equations 5.4 – 5.6 tend to over estimate the azimuthally averaged radii for these cases. When an azimuthally averaged radius is used to find the r_m for only a few azimuths, r_m is larger than the AA radius. Consequently, if the AA radius is largely over estimated, r_m is unrealistically large; this leads to largely over estimated radii in all quadrants, and it does not give zero wind radii in some quadrants as it should. This is a problem even for the 34 kt wind cases, which use the factors of 1.04 and 0.87 to approximate r_m because the AA 34 kt radius is too large.

To remedy this problem for the cases where r_m and x are actually calculated from two AMSU estimates of azimuthally averaged wind radii (i.e. cases with maximum sustained winds greater than or equal to 50 kts), r_m is constrained to not get too large. A separate restriction is established for cases with intensities greater than or equal to 50 kts but less than 64 kts and one for cases with intensities greater than or equal to 64 kts. The constraints are derived from the EBT file for all cases in which r_m is greater than the azimuthally averaged radius from NHC data; a ratio similar to that described above is calculated from the average r_m and the average AA radius. For the 50 kt wind estimates, the ratio is 1.87, and for the 64 kt wind estimates, it is 1.85. In other words, for all cases in which the calculated value of r_m is greater than 1.87 (1.85) times the AMSU-derived azimuthally averaged 50 (64) kt radius, r_m is constrained to equal 1.85 (1.87) times the radius.

Because the r_m is specified for the cases in which there is only a 34 kt wind radius, the problem is remedied differently. Cases where the storm motion causes $V_m - a$ to be close to or less than 34 kts lead to very small values of x, on the order of

approximately 0.02. This leads to a shallow exponential decline of the tangential wind profile, which in turn causes unrealistically large estimates of radii. To resolve this problem, the average x value is computed for all cases for which this is not an issue. The resultant value of 0.56 is the replacement x value, allowing for a steeper decline of the wind profile and more practical radii estimates.

The ensuing mean values of x and r_m and their standard deviations are given in Table 5.5. Three sets of values are calculated for each of the three aforementioned data sets. The average x value increases for the two data sets with stronger winds (X 50 and X 64) indicating a steeper decline of the modified Rankine wind profile outside of r_m to resolve the smaller radii of stronger winds. However, the mean value of x is smaller for data with winds greater than or equal to 64 kts compared to data with winds between 50 kts and 64 kts. Recall that for cases with winds greater than 64 kts, three pairs of data are averaged to calculate x and r_m lowering the mean values of these two parameters. Furthermore, the high mean value of x for cases with winds between 50 and 64 kts likely is less accurate due this data set having the fewest number of cases.

Once the final values of r_m and x are established for all three data sets, Equation 5.10 is used to estimate the wind radii in the NE, NW, SE, and SW quadrants of the storm based on the value of theta. Theta is determined by considering the motion of the tropical cyclone which is given in degrees based on the meteorological coordination system where north is zero degrees, east in 90 degrees, south is 180 degrees, and west is 270 degrees. The estimates of storm motion come from NHC operational estimates calculated from TC center fixes over time.

A coordinate transform is necessary to convert the meteorological estimate of storm motion to the polar coordinate system used with the modified Rankine vortex model. This is established by assuming that the maximum winds are 90 degrees to the

right of TC motion, and the asymmetry parameter should be greatest at the position of the maximum winds so that θ equals zero. The ensuing coordinate transformation equation is,

$$\theta = (\alpha_s + 90) - \alpha \qquad [5.15]$$

where α_s is the direction of storm motion in degrees, and α is the degree equivalent of the NE, SE, SW, and NW quadrants (i.e. 45, 135, 225 and 315 degrees, respectively). With the calculated θ for each quadrant, [5.10] is solved for r based on the values of V_m, V, a, x, and r_m, where V corresponds to the value of the radii being estimated (i.e. V equals 34 when estimating the 34 kt wind radii). For selected cases (i.e. Hurricanes Lenny and Dennis and Tropical Storm Carlotta), α was calculated at every 15 degrees to give a more thorough profile of wind asymmetry. Finally, if the radius in any quadrant is less than the r_m for that case, then it is outside the area being modeled by the modified Rankine vortex (Figure 5.17); thus the radius is set to zero.

5.2.3 Results and Error Analysis

In most cases, the estimates of the wind radii in the NE, NW, SE, and SW quadrants using objective AMSU-derived azimuthally averaged wind radii in the modified Rankine vortex model are consistent with the NHC data. For example, for Hurricane Lenny, the 64 kt asymmetric wind estimates in the four major quadrants are very close to the NHC estimates (Figure 5.19); the minimum radii of the 50 kt winds also compare well as do the maximum of the 34 kt wind radii. As expected with a TC moving nearly easterly at 70 degrees, the larger wind radii are found in the SE quadrant and the smaller are in the NW. The calculated maximum radii are approximately 144 nm, 73 nm, and 48 nm for the 34, 50, and 64 kt winds, respectively, occurring at around 165

degrees; the minimum are 107 nm, 58 nm, and 41 nm existing at approximately 345 degrees.

Another example of Hurricane Dennis portrays how the methods can capture the asymmetry (Figure 5.20). The storm motion is nearly northwesterly at 300 degrees, thus the largest radii are in the NE, the smallest in the SW as depicted with the Rankine vortex model. While the minimum calculated radii of the 34 kt winds compare well with those reported by the NHC, the larger radii, in the SE, NE, and NW, are not as large as those reported. The estimates of the 50 kt radii do not seem to be as accurate; not only are the maximum radii under estimated compared to the NHC, but the calculated estimates do give a radius in the SW quadrant while the NHC does not. The disagreement seems suspect, however, considering the maximum sustained winds of the TC are 65 kts, and the asymmetry parameter is just under 5 kts. Assuming the general rule of being able to add and subtract the asymmetric contribution 90 degrees to the right and left, respectively, gives the maximum winds of 65 kts in the NE and winds of approximately 55 kts in the SW. Thus, it seems unlikely that there is no 50 kt wind to estimate a radius of in the SW quadrant. On the other hand, the comparison of the 64 kt wind radii are very similar, showing only a small wedge of radii with this magnitude of winds in the NE quadrant. Furthermore, the extent of the winds to nearly 40 nm compare well with NHC.

These two examples likely compare relatively well with the NHC because the estimates of the azimuthally averaged 34, 50, and 64 kt wind radii by the AMSU are similar to the NHC's. For Hurricane Dennis, the AMSU (NHC) estimates are 93 (94), 41 (40), and 31 (10) nm for the 34, 50, and 64 kt winds respectively. The latter estimate of 31 nm by the AMSU is an example of the aforementioned overestimate that often occurs when the difference between the maximum winds and the asymmetry parameter is close

to the 64 kt threshold. However, recall that when 34, 50, and 64 kt azimuthally averaged radii are available, r_m and x are calculated for all three pairs of data and then averaged. Thus, it is likely that the very close estimates of the 34 and 50 kt wind radii to the NHC provided good r_m and x values which carry over to the averaged values providing a good profile of the 64 kt asymmetric winds. Similarly, the comparisons for Hurricane Lenny are 116 (118), 71 (79), and 40 (42) for the 34, 50, and 64 kt wind azimuthally averaged radii, again leading to good asymmetric comparisons.

An example of Tropical Storm Carlotta suggests that the asymmetric calculations may be superior to the NHC estimates in some cases (Figure 5.21). For this case, TS Carlotta had maximum sustained winds of 50 kts and an asymmetry parameter of 6.84 kts with motion approximately to the NW at 295 degrees. Thus, it is assumed that the maximum winds are approximately in the NE quadrant, and, as earlier indicated, there likely are many azimuths with no 50 kt radius to estimate, most obviously in the SW quadrant. Nonetheless, the NHC estimates the largest 34 kt radius in the NW quadrant, and it gives a solid ring of 50 kt wind radii estimates of 50 nm. In contrast, the estimates calculated with the Rankine model and AMSU data put the largest radii in the NE quadrant, where it also reveals only a sliver of 50 kt winds around 15 to 30 degrees. Considering the TC intensity and motion, these calculated estimates seem more reasonable.

In addition to looking at the specific examples cited above, the mean absolute errors and biases compared to the NHC data are calculated at all major quadrants for all three data sets (Table 5.6). In some cases, such as the 64 kt data set, the comparison with NHC is encouraging. On the other hand, the 34 and 50 kt data sets contain significant differences and the biases in some quadrants are large. The validity of these statistics is debatable, however, due to the lack of good validation data. In fact, in some

cases, the NHC reports wind radii based solely on climatology as may be the case in TS Carlotta (Figure 5.21). Therefore, it is preferable to have validation data exclusively from aircraft reconnaissance to determine the soundness of using AMSU data in the modified Rankine vortex model to estimate the asymmetric wind radii. DeMaria *et al.* (2001) plan to evaluate these methods against aircraft reconnaissance data from the 2001 tropical season.

Table 5.1. Correlations and probabilities (that the correlation is zero) of 34, 50, and 64 kt wind radii with potential predictors from 1999 data.

Independent Variable	34kt Correlation	34 kt Probability	50 kt Correlation	50 kt Probability	64kt Correlation	64 kt Probability
CLW	0.723	0.000	0.722	0.000	0.663	0.000
DP	0.764	0.000	0.436	0.000	0.823	0.000
R015	0.479	0.000	0.325	0.057	0.557	0.000
R315	0.557	0.000	0.414	0.003	0.567	0.000
RMX0	-0.040	1.000	-0.197	1.000	-0.148	1.000
RMX3	-0.073	1.000	-0.224	0.692	-0.231	1.000
SS	0.013	1.000	0.068	1.000	0.010	1.000
TMAX	0.788	0.000	0.761	0.000	0.737	0.000
ZMAX	0.139	1.000	0.102	1.000	0.103	1.000
VMX0	0.716	0.000	0.681	0.000	0.778	0.000
VMX3	0.748	0.000	0.729	0.000	0.807	0.000
STORMLAT	0.613	0.000	0.436	0.001	0.451	0.012
STRMSP	0.296	0.061	0.190	1.000	-0.014	1.000

Table 5.2. Best variables for predicting 34, 50, and 64 kt wind radii and their corresponding coefficients and normalized coefficients from 1999 data.

Dependent Variable	Independent Variable	Coefficient	Normalized Coefficent	P-Value
AVE 34 n = 90 (r^2 = 76.4%)	Constant	8.638	0.000	0.578
	STORMLAT	2.227	0.367	0.000
	DP	2.204	0.348	0.133
	VMX0	-1.988	-0.621	0.071
	VMX3	1.801	0.539	0.100
	CLW	50.391	0.434	0.000
AVE 50 n = 75 (r^2 = 69.3%)	Constant	21.665	0.000	0.210
	STORMLAT	-0.018	-0.004	0.975
	DP	4.553	0.886	0.004
	VMX0	-2.279	-0.840	0.061
	VMX3	1.301	0.461	0.247
	CLW	41.110	0.406	0.000
AVE 64 n = 51 (r^2 = 77.5%)	Constant	33.589	0.000	0.002
	STORMLAT	-0.132	-0.043	0.709
	DP	4.065	1.385	0.000
	VMX0	-3.238	-2.196	0.000
	VMX3	2.501	1.651	0.002
	CLW	2.830	0.045	0.688

Table 5.3. Correlations and probabilities (that the correlation is zero) of 34, 50, and 64 kt wind radii with potential predictors from 1999 and 2000 combined data.

Independent Variable	34kt Correlation	34 kt Probability	50 kt Correlation	50 kt Probability	64kt Correlation	64 kt Probability
CLW	0.620	0.000	0.644	0.000	0.602	0.000
DP	0.739	0.000	0.711	0.000	0.752	0.000
R015	0.509	0.000	0.345	0.001	0.463	0.000
R315	0.555	0.000	0.416	0.000	0.475	0.000
RMX0	-0.008	1.000	-0.160	0.874	-0.150	1.000
RMX3	-0.121	1.000	-0.237	0.080	-0.208	0.625
SS	0.071	1.000	0.084	1.000	0.056	1.000
TMAX	0.757	0.000	0.765	0.000	0.730	0.000
ZMAX	0.081	1.000	0.092	1.000	0.194	0.844
VMX0	0.712	0.000	0.688	0.000	0.724	0.000
VMX3	0.746	0.000	0.722	0.000	0.756	0.000
STORMLAT	0.503	0.000	0.326	0.002	0.246	0.246
STRMSP	0.278	0.002	0.185	0.439	-0.096	1.000

Table 5.4. Best variables for predicting 34, 50, and 64 kt wind radii and their corresponding coefficients and normalized coefficients from 1999 and 2000 combined data.

Dependent Variable	Independent Variable	Coefficient	Normalized Coefficent	P-Value
AVE 34 n = 176 (r^2 = 67.4%)	Constant	45.019	0.000	0.000
	STRMSP	0.943	0.166	0.001
	DP	3.195	0.474	0.003
	VMX0	-1.789	-0.526	0.033
	VMX3	1.984	0.574	0.010
	TMAX	3.313	0.137	0.276
	CLW	22.395	0.194	0.004
AVE 50 n = 132 (r^2 = 64.8%)	Constant	16.369	0.000	0.042
	STRMSP	0.254	0.065	0.261
	DP	1.752	0.360	0.077
	VMX0	-1.916	-0.756	0.020
	VMX3	1.584	0.612	0.028
	TMAX	7.526	0.434	0.006
	CLW	18.998	0.208	0.011
AVE 64 n = 91 (r^2 = 66.5%)	Constant	23.095	0.000	0.000
	STRMSP	-0.336	-0.147	0.051
	DP	1.815	0.611	0.015
	VMX0	-1.835	-1.217	0.004
	VMX3	1.595	1.053	0.004
	TMAX	3.593	0.347	0.073
	CLW	1.263	0.021	0.845

Table 5.5. The mean and standard deviation values of x and the radius of maximum winds, r_m, from the modified Rankine vortex model for all tropical cyclones with maximum sustained winds 1) greater than or equal to 34 kts but less than 50 kts, 2) greater or equal to 50 kts but less than 64 kts, and 3) greater than or equal to 64 kts.

	X 34	**X 50**	**X 64**	**R_m 34**	**R_m 50**	**R_m 64**
Mean	0.531	0.931	0.745	72.035	63.372	39.495
Standard Deviation	0.269	0.157	0.146	23.530	26.287	20.952

Table 5.6. The mean absolute error and bias of the calculated versus NHC radii of 34, 50, and 64 kt winds in the northeast, southeast, southwest, and northwest quadrants of a tropical cyclone.

		34NE	34SE	34SW	34NW	50NE	50SE	50SW	50NW	64NE	64SE	64SW	64NW
34 kt Data Set n = 37	MAE	49	30	22	34								
	Bias	39.01	3.39	-0.74	22.37								
50 kt Data Set n = 35	MAE	31	29	32	26	28	35	34	32				
	Bias	-6.98	-3.56	4.14	2.36	8.86	21.92	24.34	26.40				
64 kt Data Set n = 91	MAE	32	28	27	24	21	21	17	18	17	16	17	16
	Bias	5.39	2.99	0.68	-2.05	-3.43	-0.42	4.43	1.41	10.11	13.35	14.84	12.33

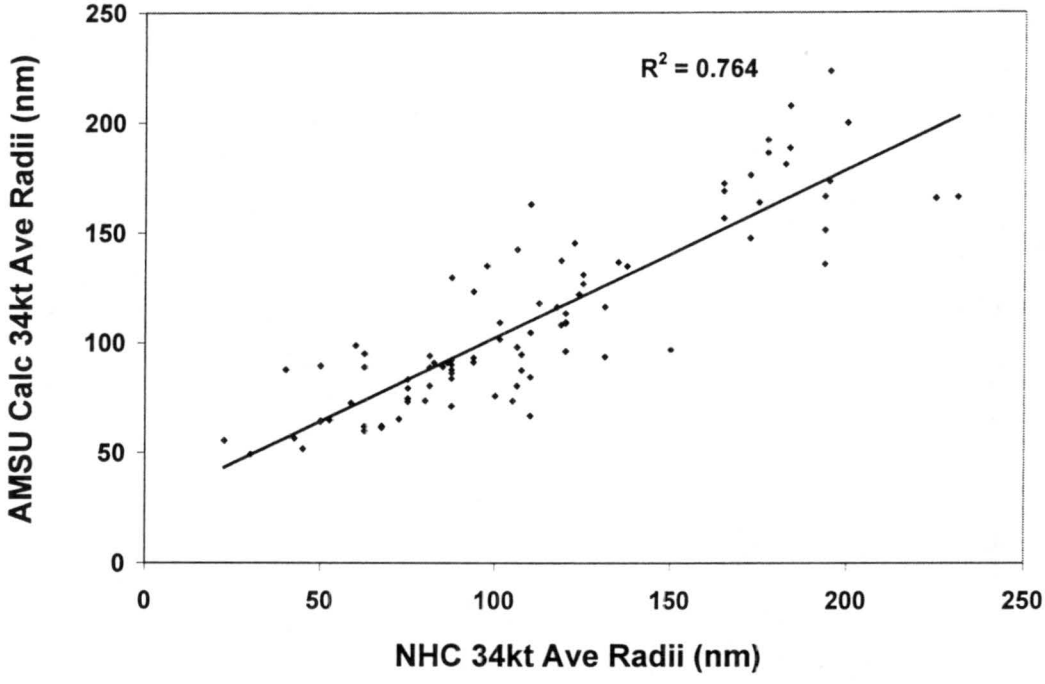
AMSU Calc 34kt Ave Radii (nm)
NHC 34kt Ave Radii (nm)
R^2 = 0.764
0
50
100
150
200
250

a)

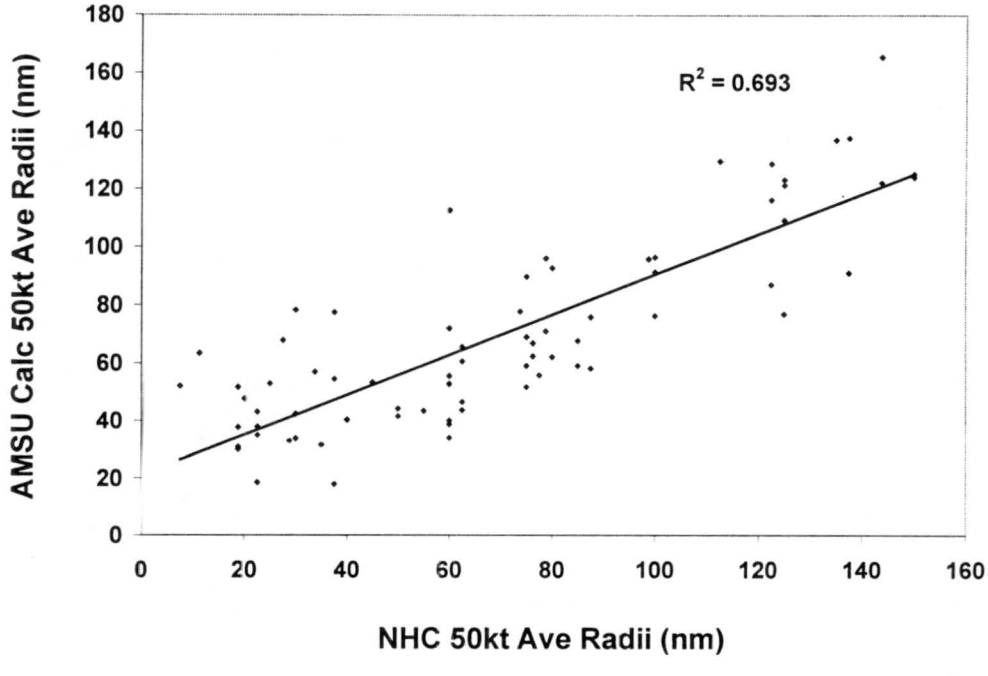
AMSU Calc 50kt Ave Radii (nm)
NHC 50kt Ave Radii (nm)
R^2 = 0.693
0
20
40
60
80
100
120
140
160
180

b)

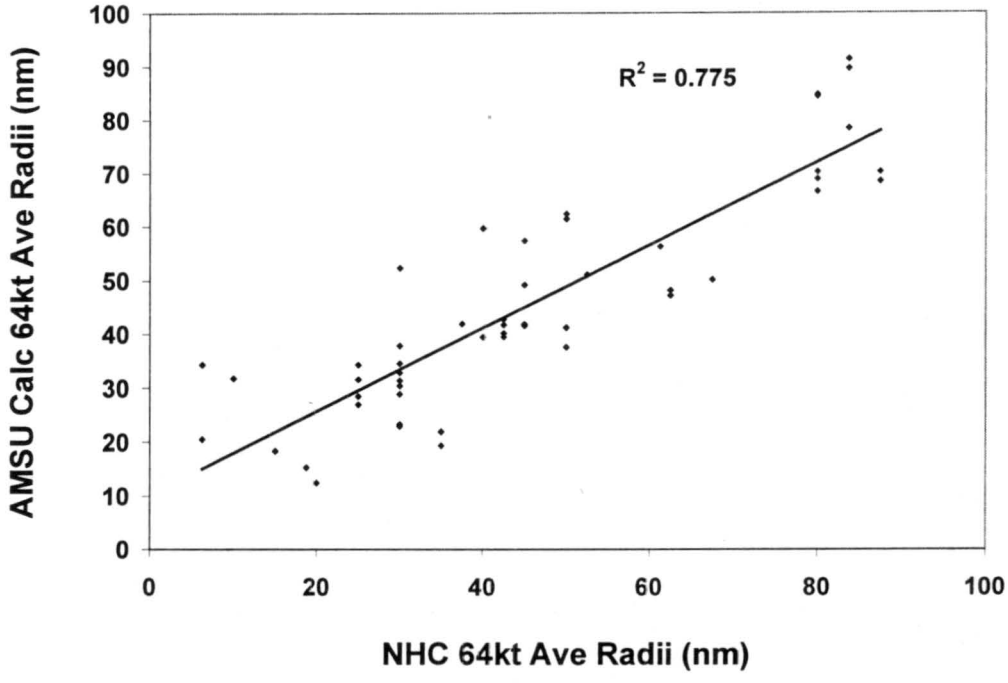

c)

Figure 5.1. Relationship between the AMSU-derived and NHC reports of azimuthally-averaged wind radii from 1999 data for a) 34 kt winds, b) 50 kt winds, and c) 64 kt winds.

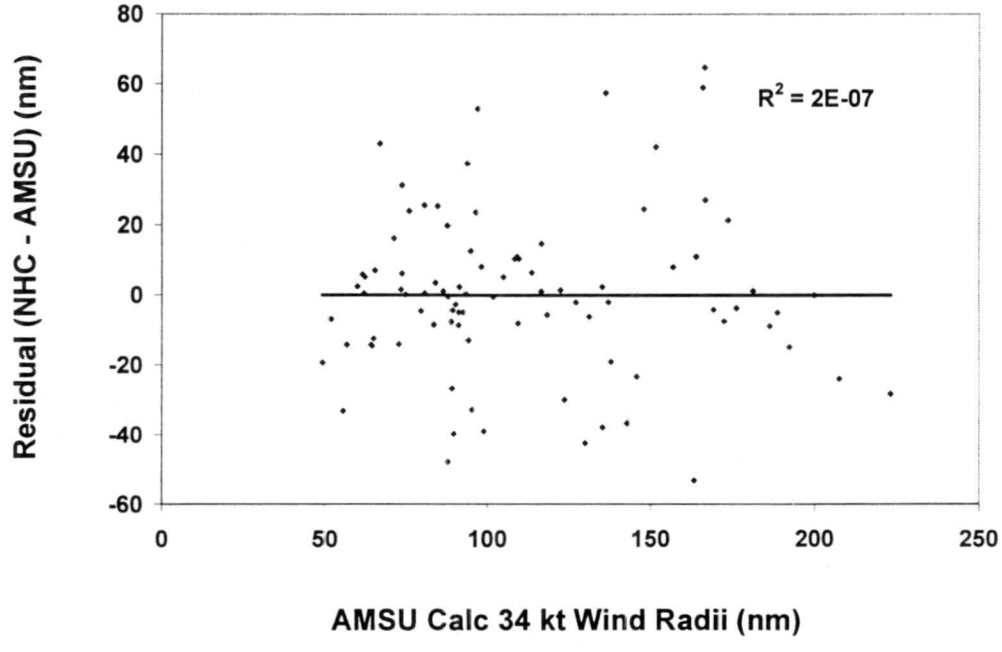

a)

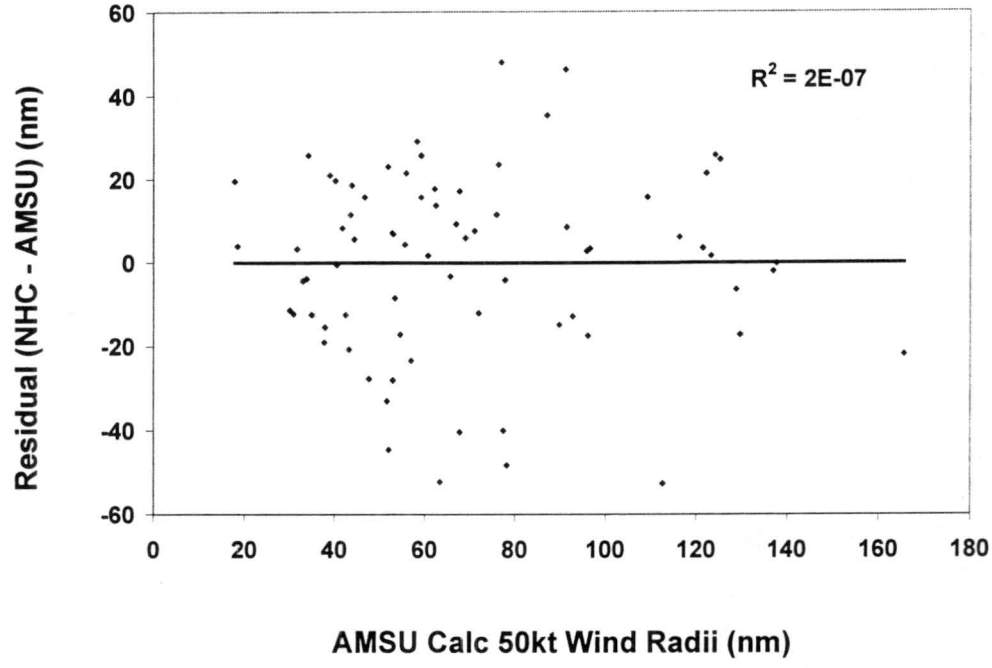

b)

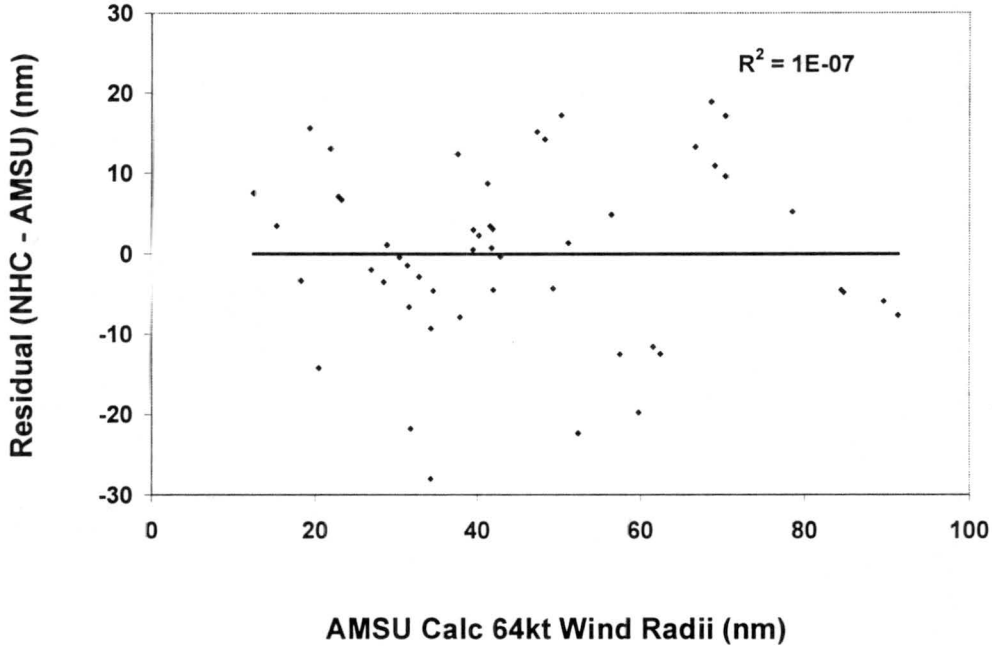

c)

Figure 5.2. Residual (NHC average radii – AMSU calculated average radii) plot versus AMSU calculated azimuthally-averaged wind radii from 1999 data for a) 34 kt winds, b) 50 kt winds, and c) 64 kt winds.

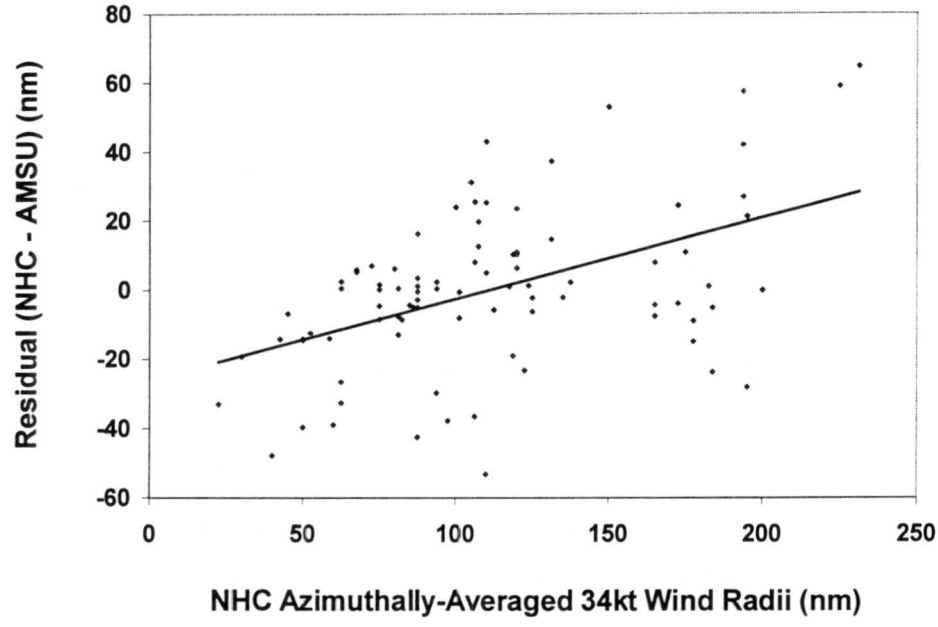
Residual (NHC - AMSU) (nm)
80
60
40
20
0
-20
-40
-60
0
50
100
150
200
250
NHC Azimuthally-Averaged 34kt Wind Radii (nm)

a)

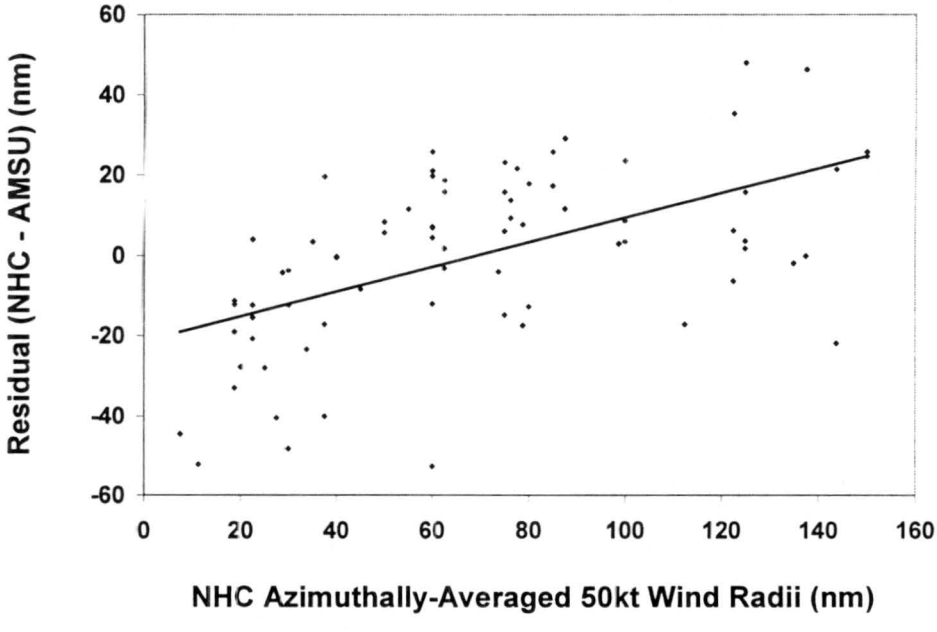
Residual (NHC - AMSU) (nm)
60
40
20
0
-20
-40
-60
0
20
40
60
80
100
120
140
160
NHC Azimuthally-Averaged 50kt Wind Radii (nm)

b)

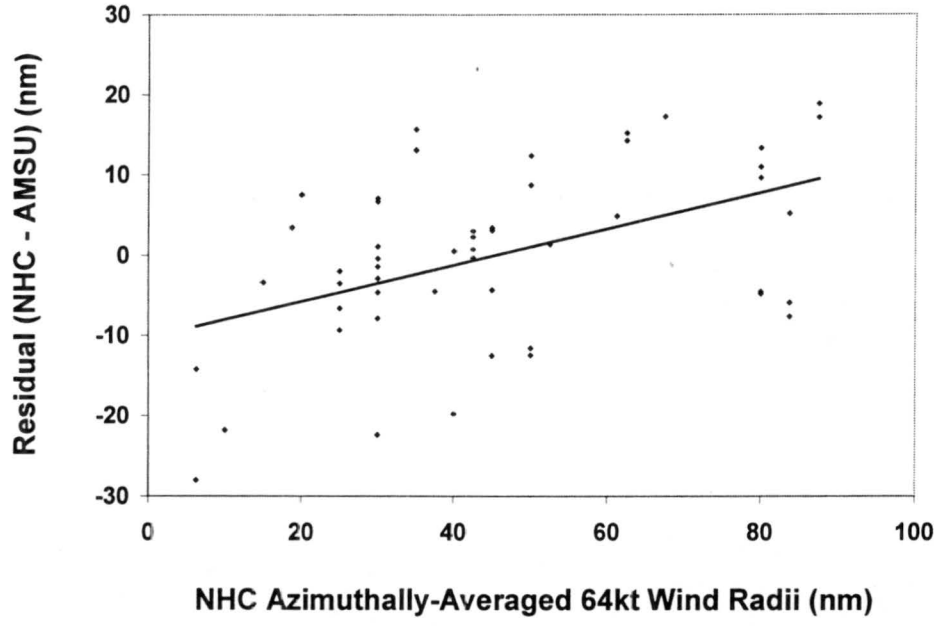

c)

Figure 5.3. Residual (NHC average radii – AMSU calculated average radii) plot versus NHC azimuthally-averaged wind radii from 1999 data for a) 34 kt winds, b) 50 kt winds, and c) 64 kt winds.

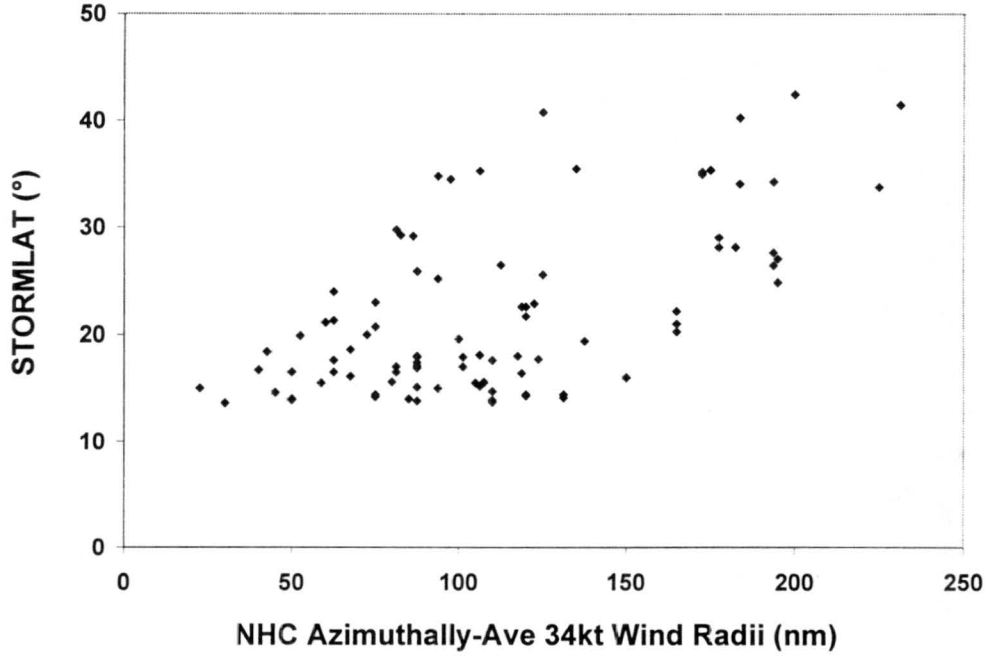

a)

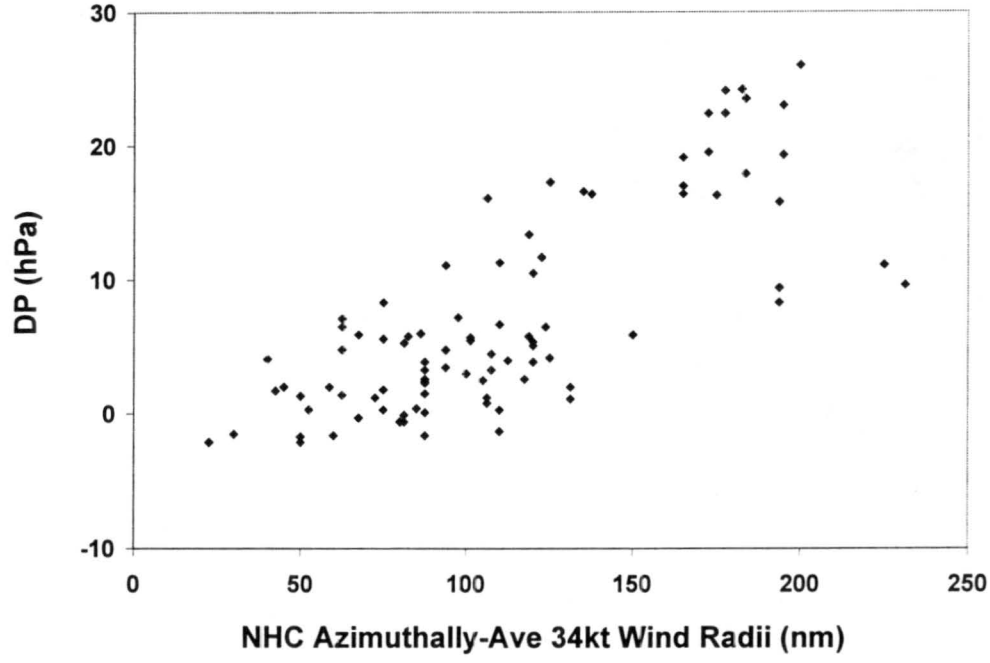
30
20
10
0
-10
DP (hPa)
0
50
100
150
200
250
NHC Azimuthally-Ave 34kt Wind Radii (nm)

b)

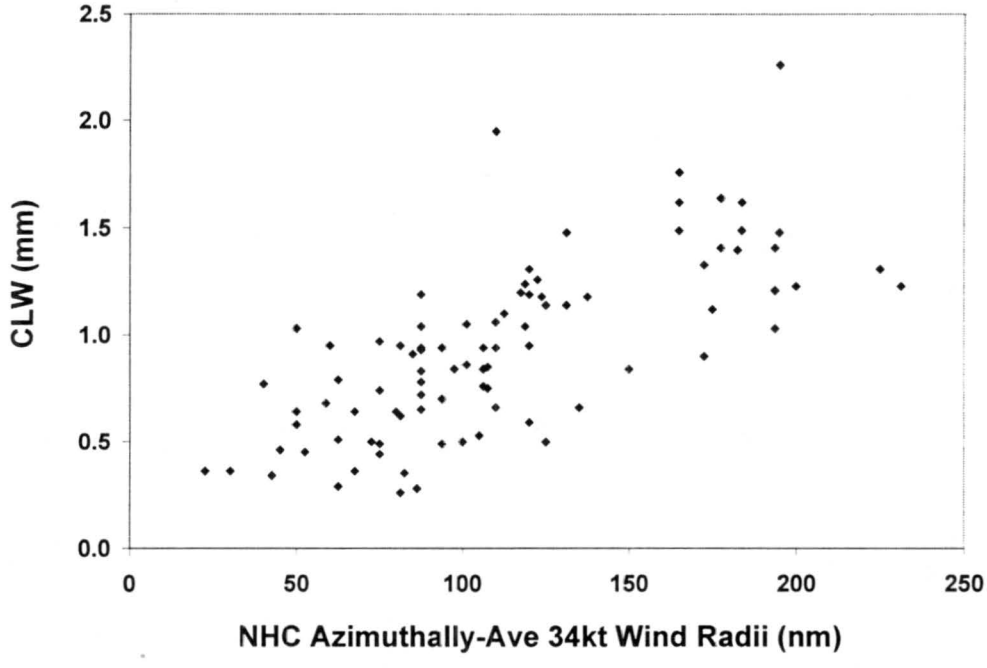
2.5
2.0
1.5
1.0
0.5
0.0
CLW (mm)
0
50
100
150
200
250
NHC Azimuthally-Ave 34kt Wind Radii (nm)

c)

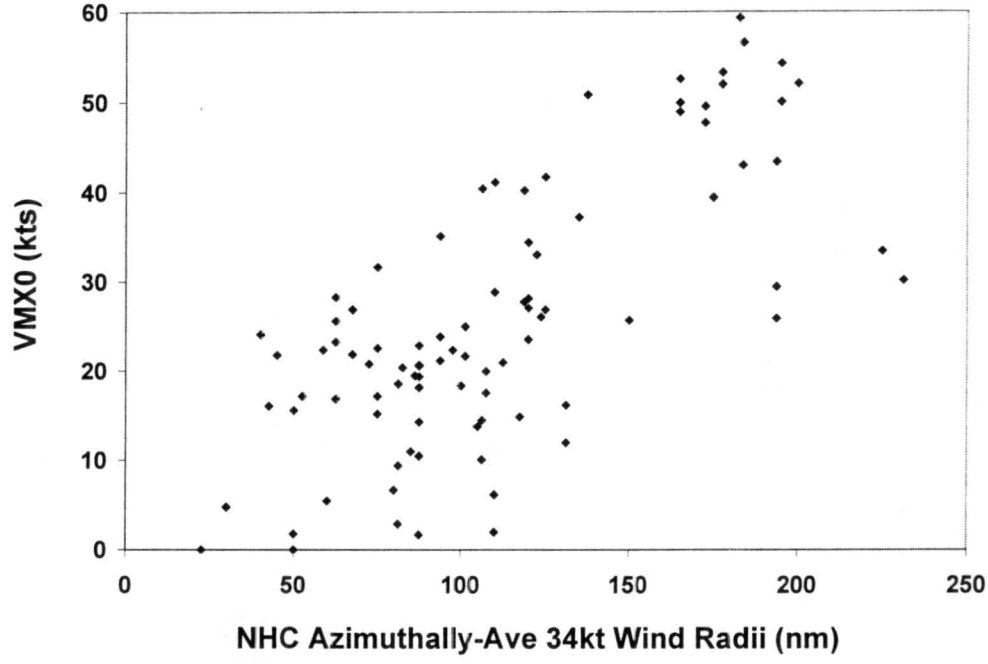

d)

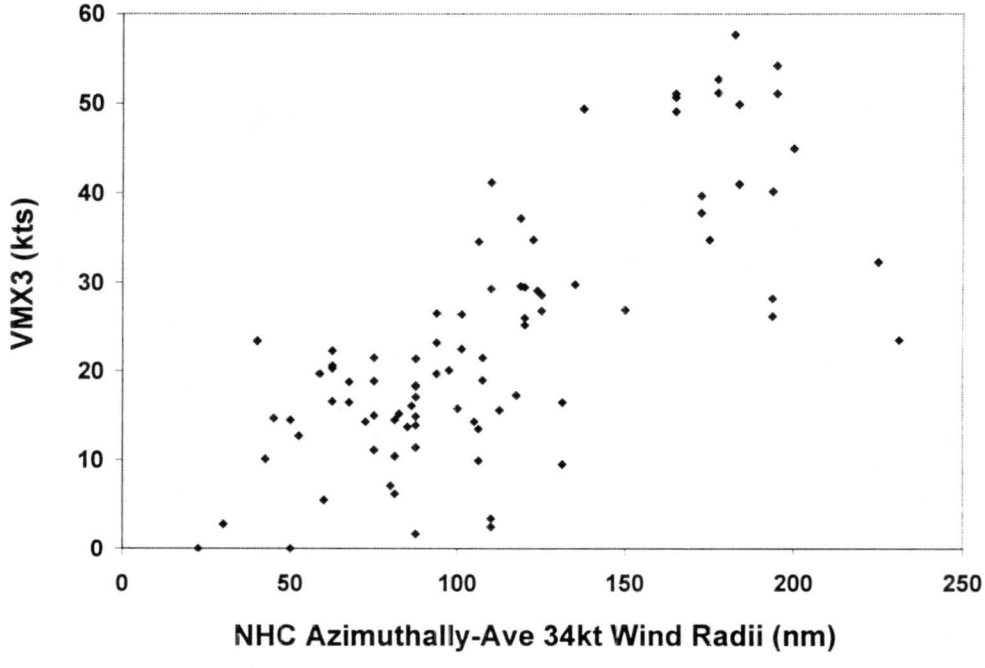

e)

Figure 5.4. Comparison of estimator values with NHC azimuthally-averaged 34 kt wind radii (AVE34) for all 125 cases from 1999 data for a) STORMLAT, b) DP, c) CLW, d) VMX0, and e) VMX3.

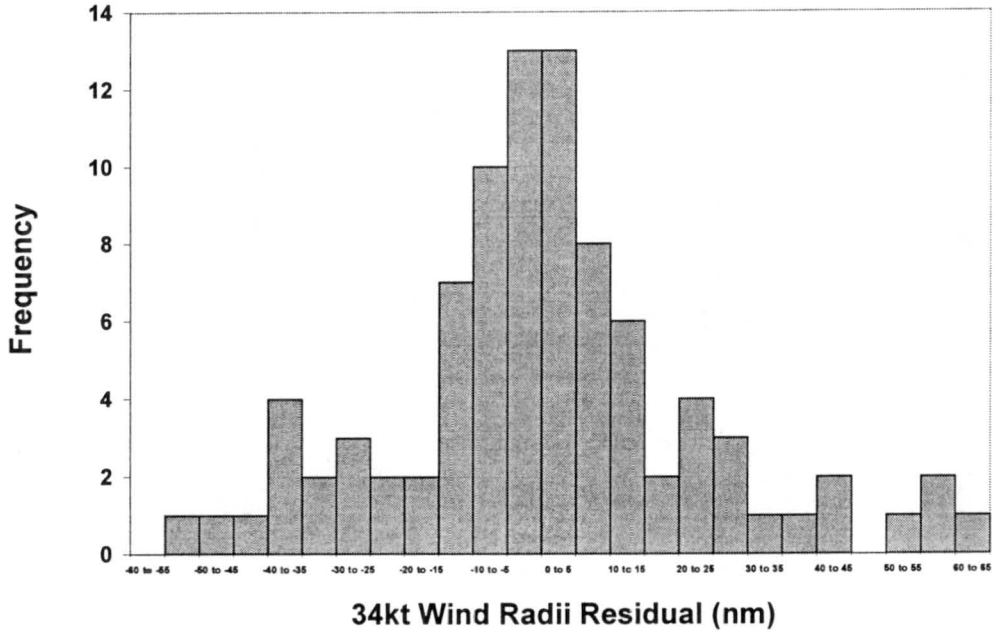
Frequency
14
12
10
8
6
4
2
0
-60 to -55
-50 to -45
-40 to -35
-30 to -25
-20 to -15
-10 to -5
0 to 5
10 to 15
20 to 25
30 to 35
40 to 45
50 to 55
60 to 65
34kt Wind Radii Residual (nm)

a)

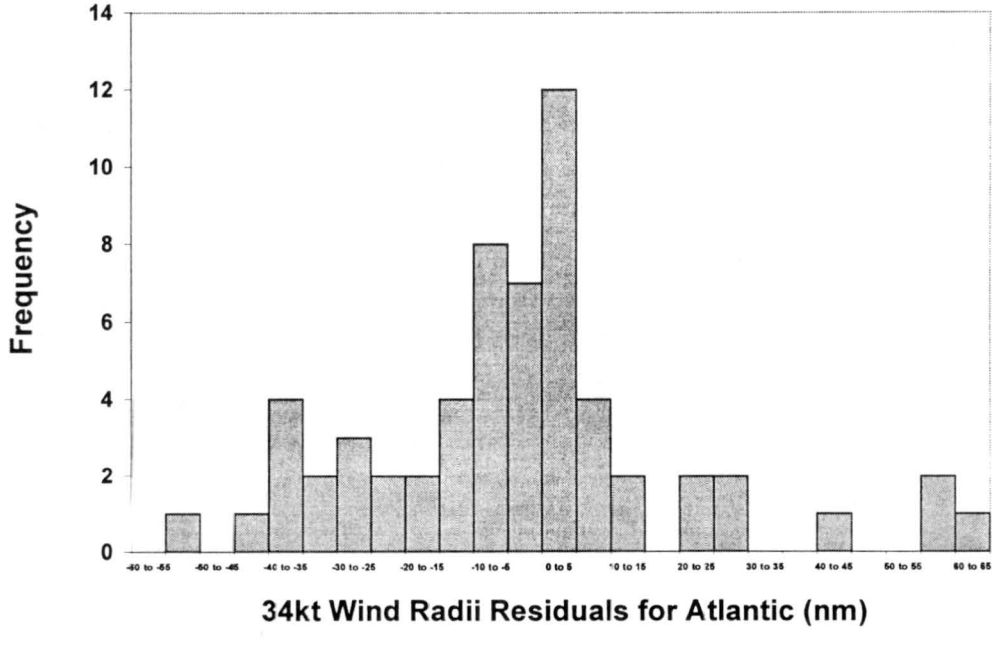
Frequency
14
12
10
8
6
4
2
0
-60 to -55
-50 to -45
-40 to -35
-30 to -25
-20 to -15
-10 to -5
0 to 5
10 to 15
20 to 25
30 to 35
40 to 45
50 to 55
60 to 65
34kt Wind Radii Residuals for Atlantic (nm)

b)

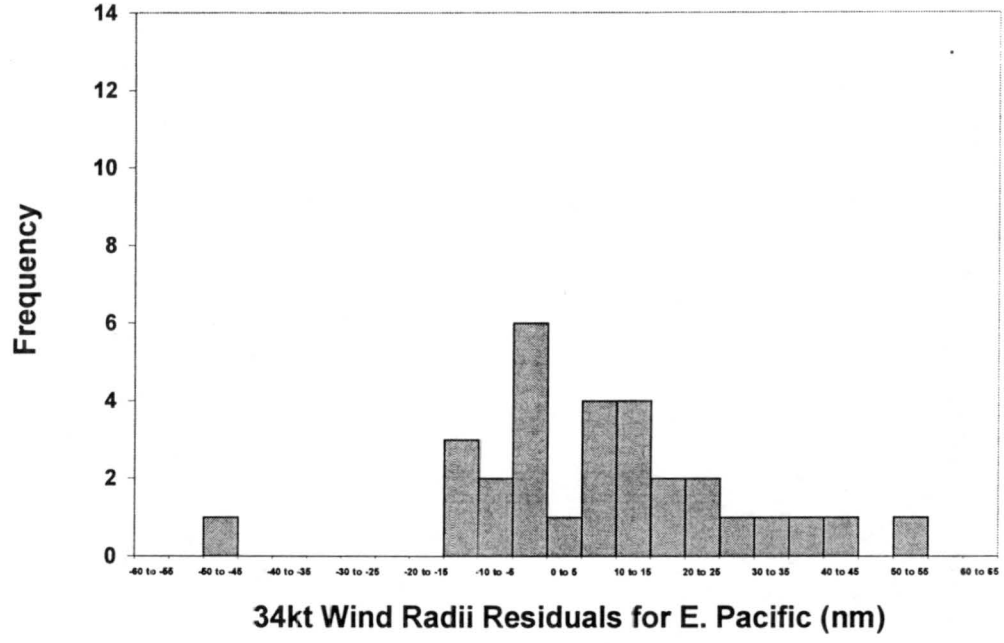

c)

Figure 5.5. Histogram of residuals (NHC average radii – AMSU calculated average wind radii) from 1999 data for 34 kt winds in the a) Atlantic and East Pacific basins combined, b) Atlantic basin only, and c) East Pacific basin only.

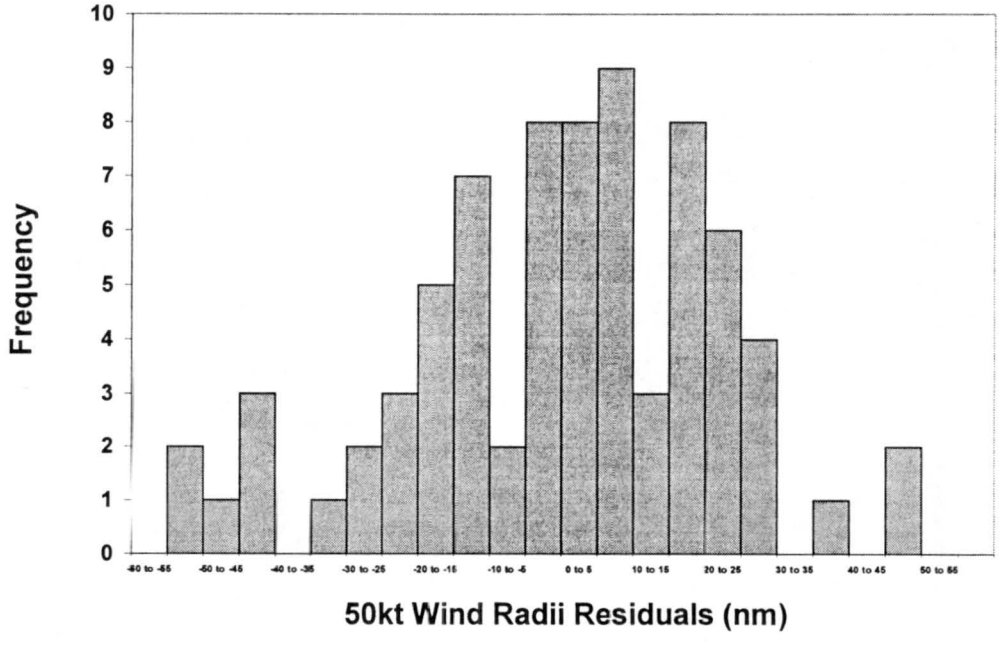

a)

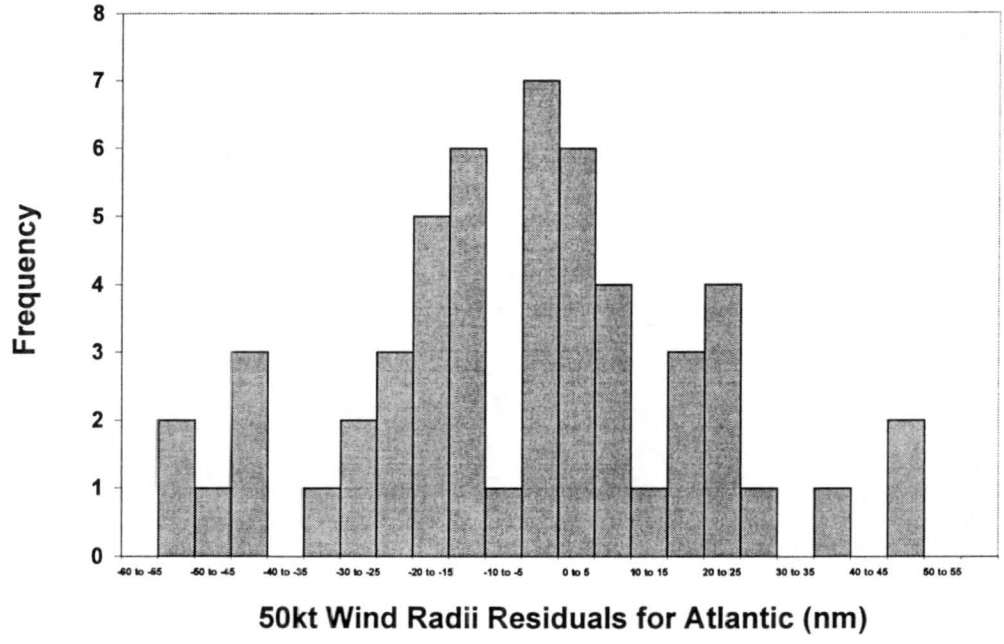

b)

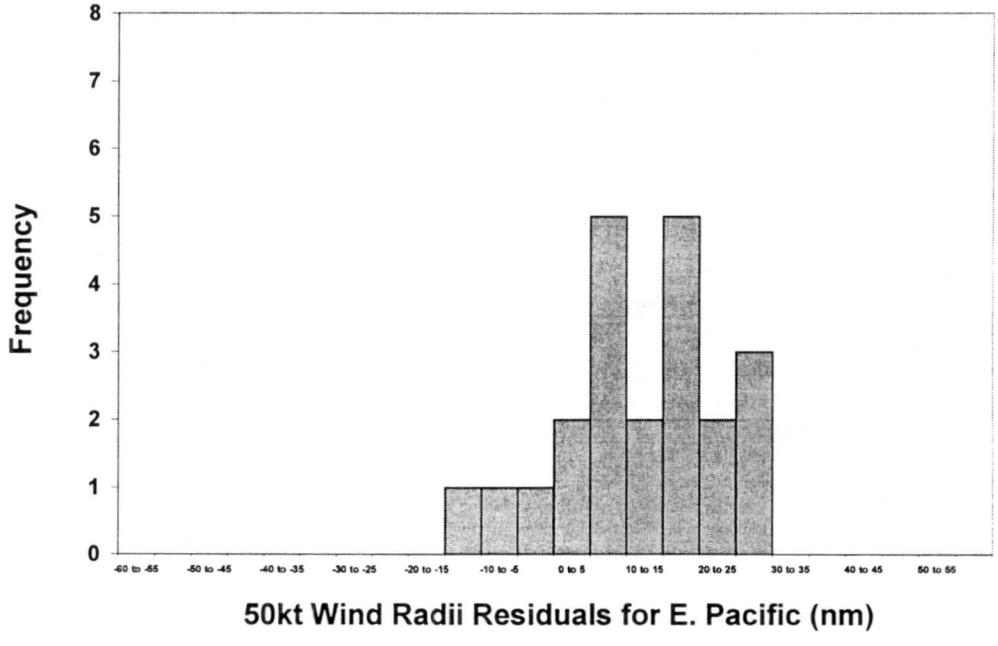

c)

Figure 5.6. Histogram of residuals (NHC average radii – AMSU calculated average wind radii) from 1999 data for 50 kt winds in the a) Atlantic and East Pacific basins combined, b) Atlantic basin only, and c) East Pacific basin only.

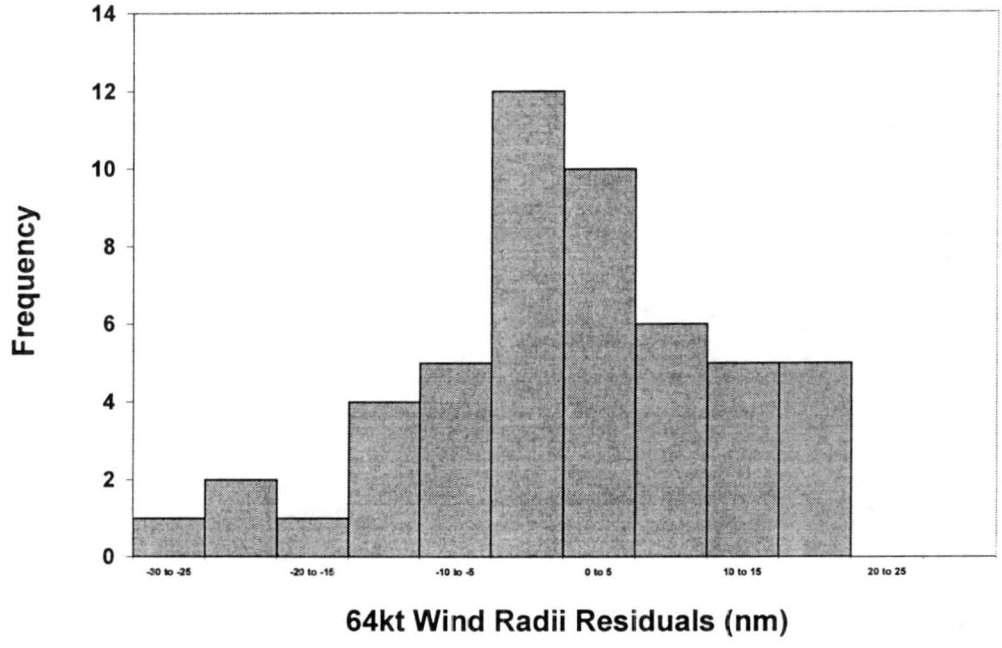
14
12
10
8
6
4
2
0
Frequency
-30 to -25
-20 to -15
-10 to -5
0 to 5
10 to 15
20 to 25
64kt Wind Radii Residuals (nm)

a)

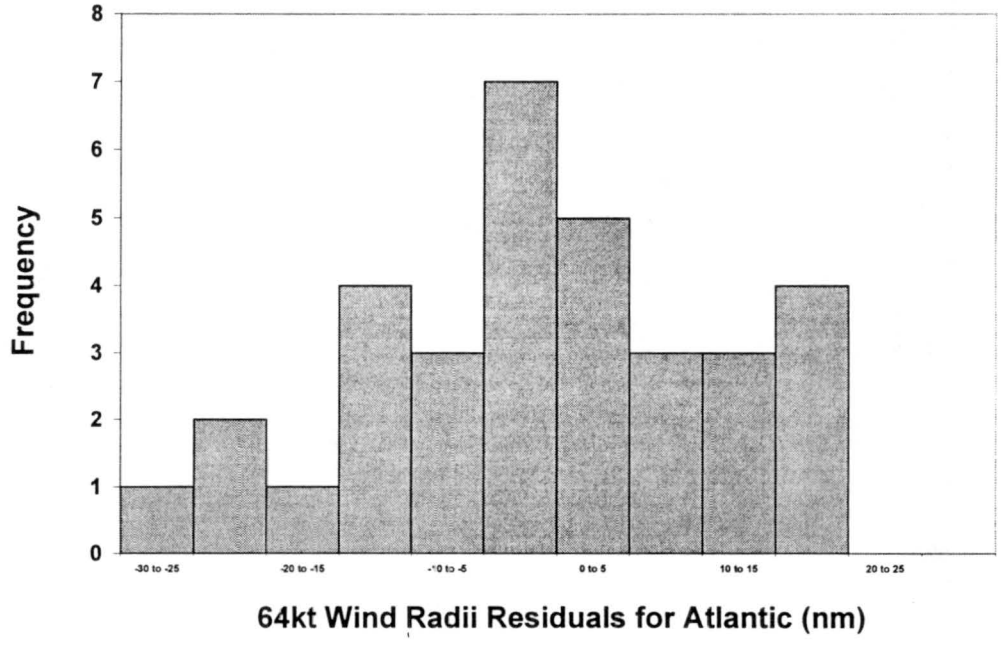
8
7
6
5
4
3
2
1
0
Frequency
-30 to -25
-20 to -15
-10 to -5
0 to 5
10 to 15
20 to 25
64kt Wind Radii Residuals for Atlantic (nm)

b)

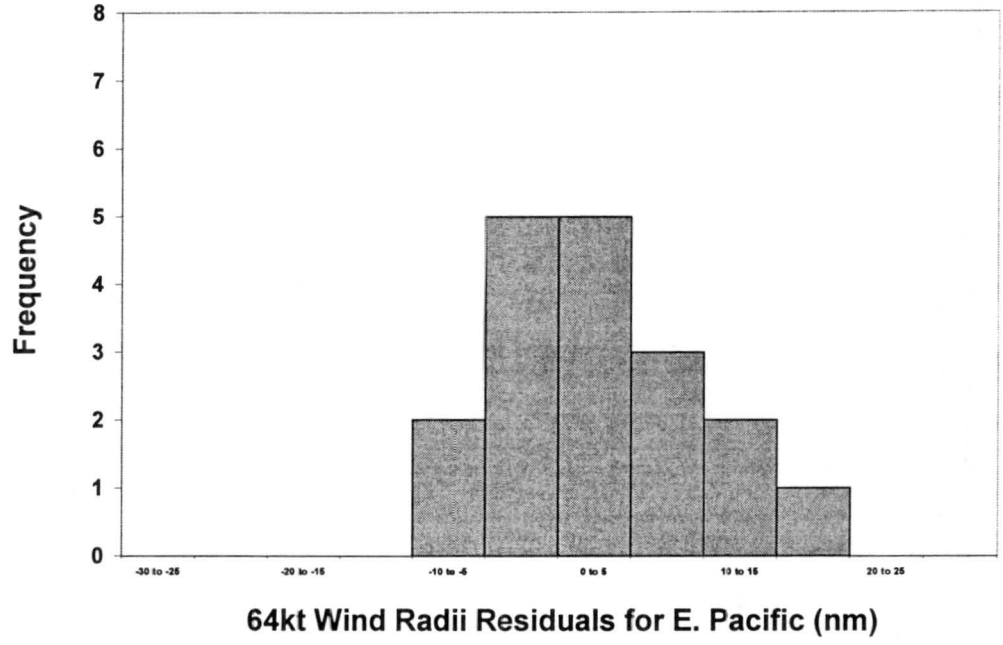

c)

Figure 5.7. Histogram of residuals (NHC average radii – AMSU calculated average wind radii) from 1999 data for 64 kt winds in the a) Atlantic and East Pacific basins combined, b) Atlantic basin only, and c) East Pacific basin only.

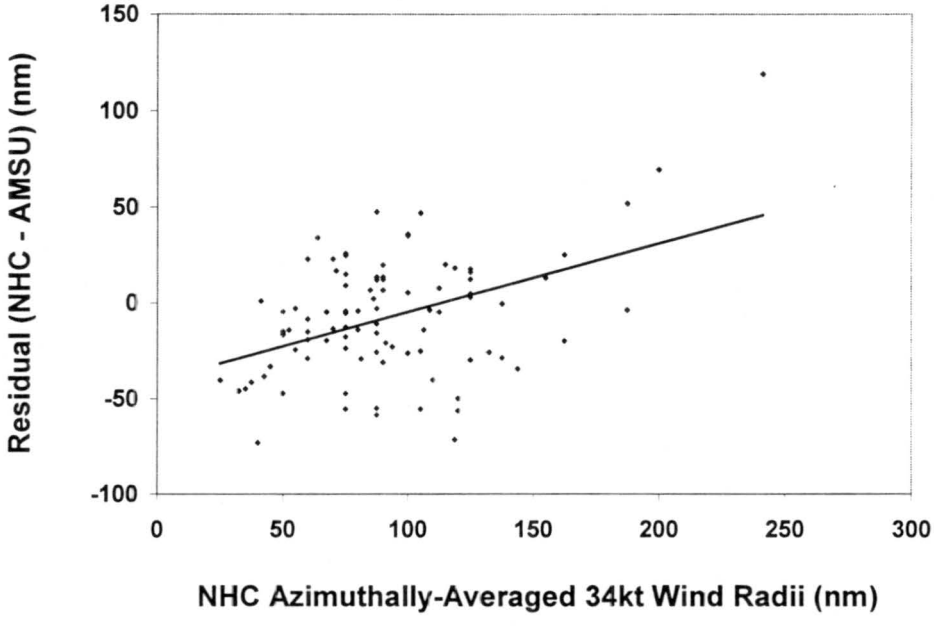

a)

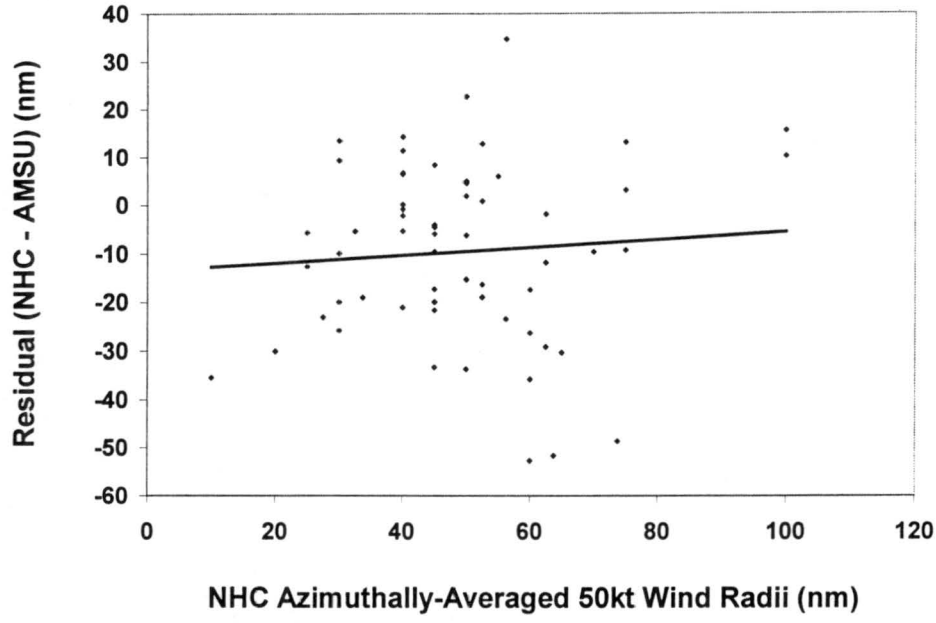

b)

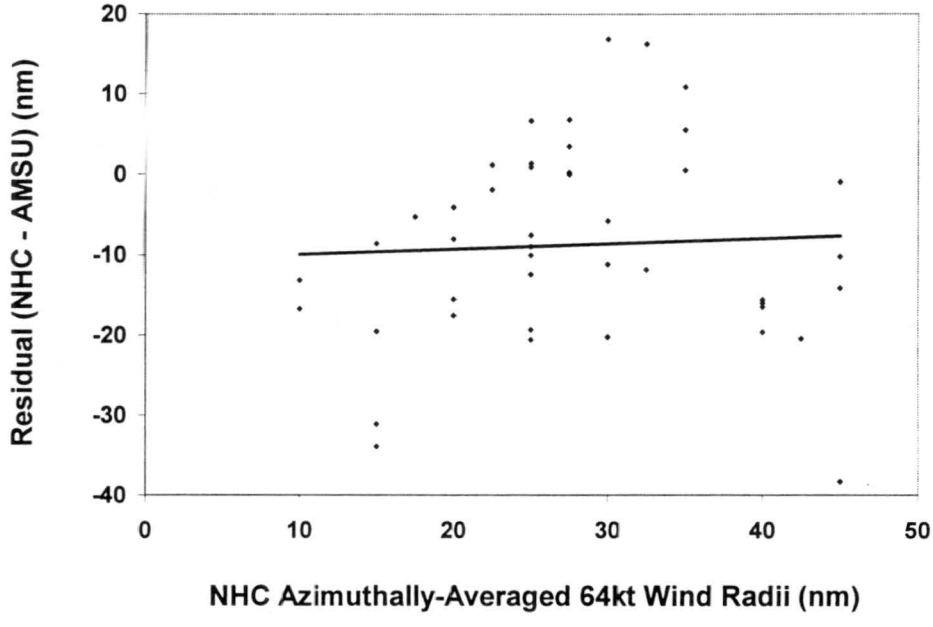

c)

Figure 5.8. Residual (NHC average radii – AMSU calculated average radii) plot versus NHC azimuthally-averaged wind radii from 2000 cross-validation data for a) 34 kt winds, b) 50 kt winds, and c) 64 kt winds.

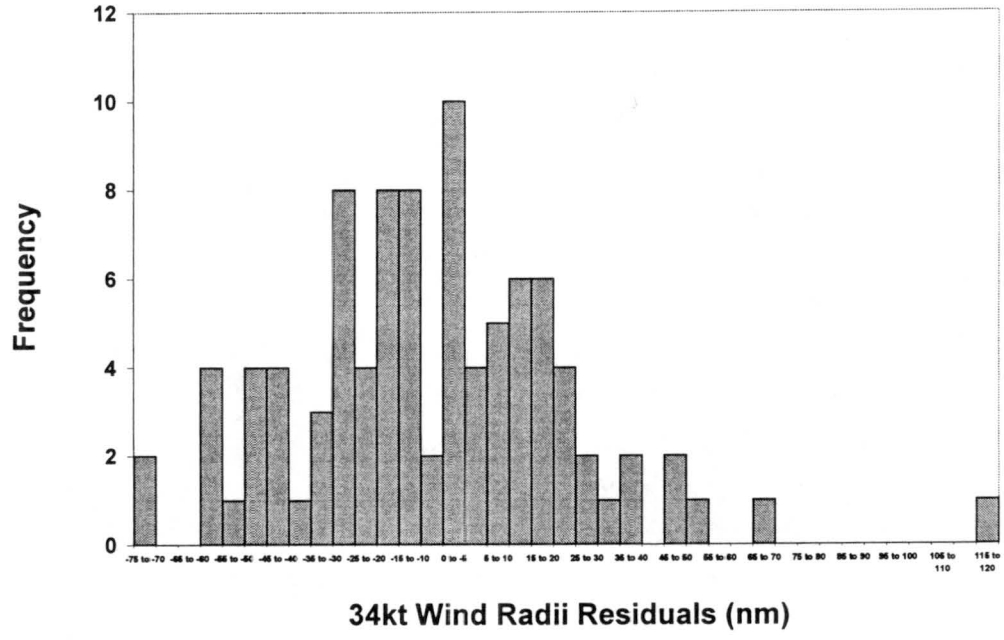
Frequency
12
10
8
6
4
2
0
-75 to -70
-66 to -60
-45 to -40
-36 to -30
-25 to -20
-15 to -10
0 to -5
5 to 10
15 to 20
25 to 30
35 to 40
45 to 50
55 to 60
65 to 70
75 to 90
95 to 100
105 to 110
115 to 120
34kt Wind Radii Residuals (nm)

a)

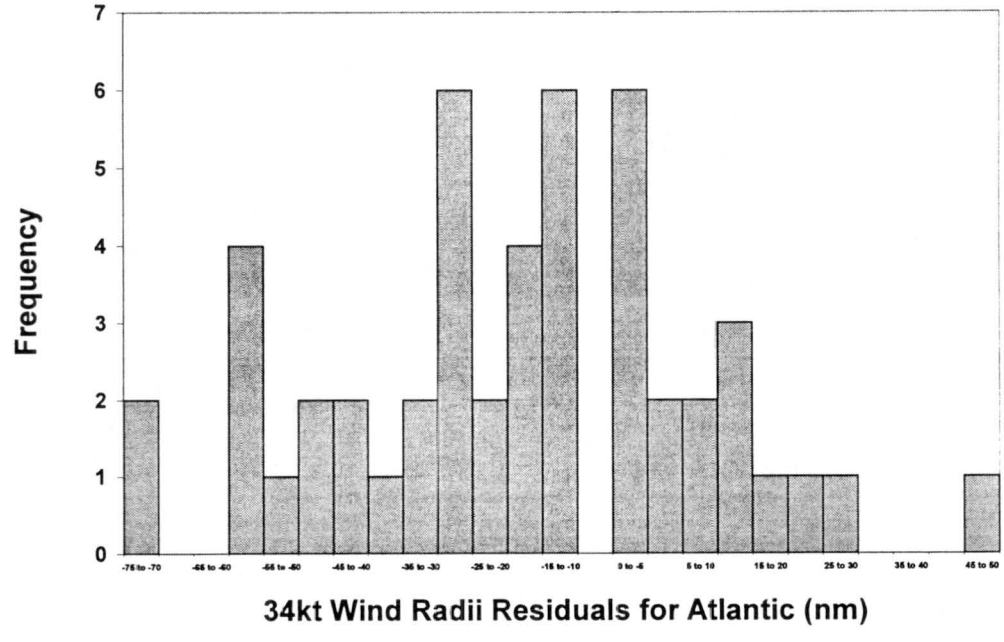
Frequency
7
6
5
4
3
2
1
0
-75 to -70
-45 to -40
-36 to -30
-25 to -20
-15 to -10
5 to 10
15 to 20
25 to 30
35 to 40
45 to 50
34kt Wind Radii Residuals for Atlantic (nm)

b)

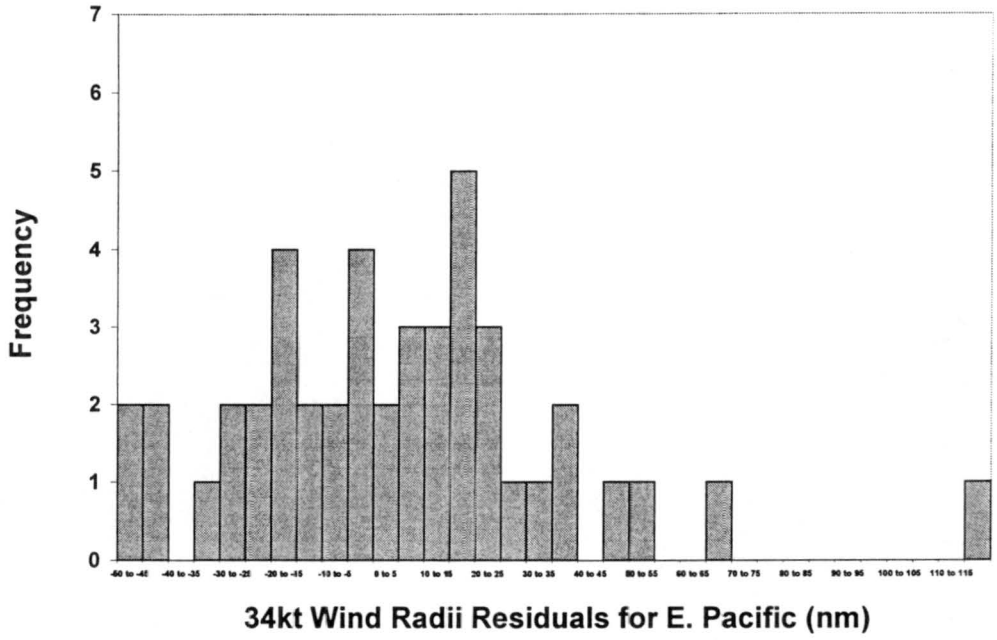

c)

Figure 5.9. Histogram of residuals (NHC average radii – AMSU calculated average wind radii) from 2000 cross-validation data for 34 kt winds in the a) Atlantic and East Pacific basins combined, b) Atlantic basin only, and c) East Pacific basin only.

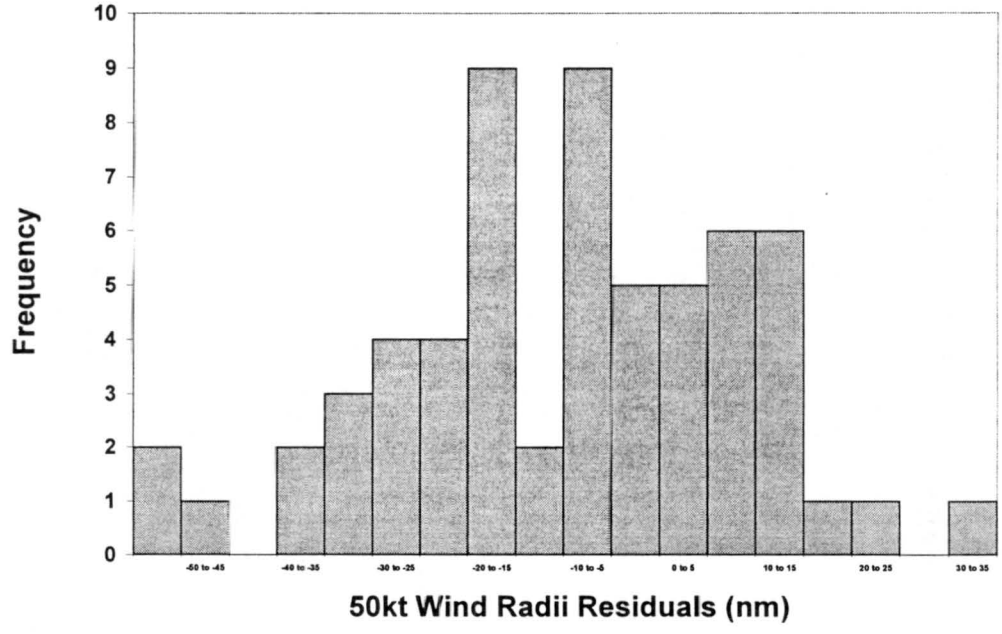

a)

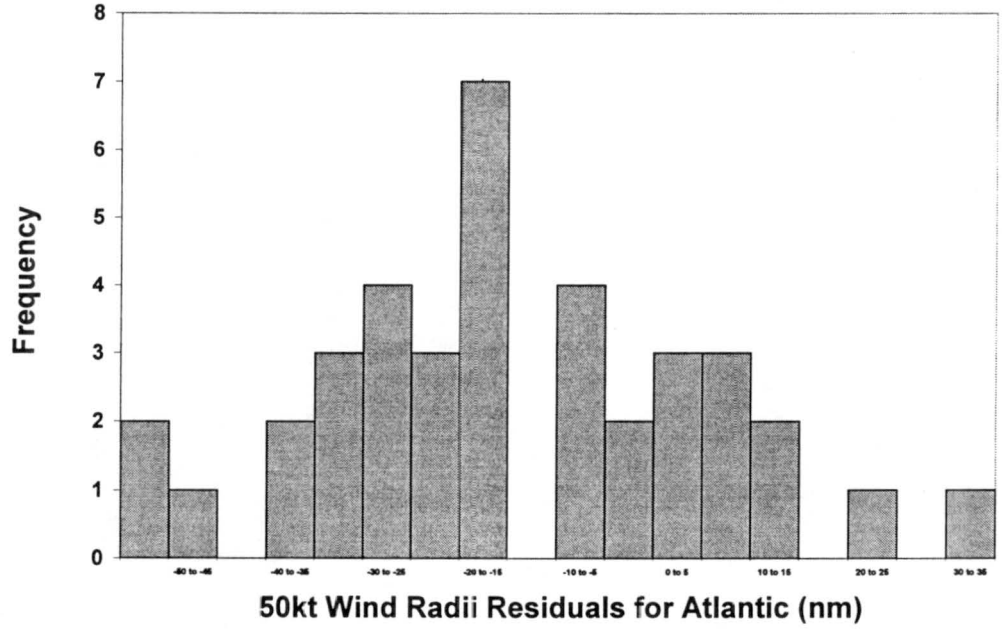

b)

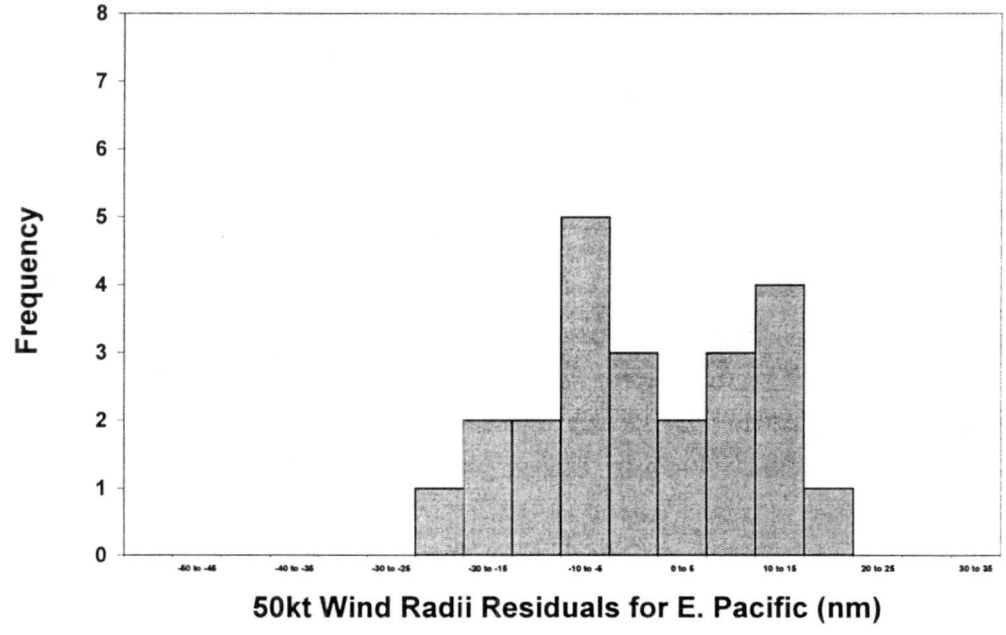

c)

Figure 5.10. Histogram of residuals (NHC average radii – AMSU calculated average wind radii) from 2000 cross-validation data for 50 kt winds in the a) Atlantic and East Pacific basins combined, b) Atlantic basin only, and c) East Pacific basin only.

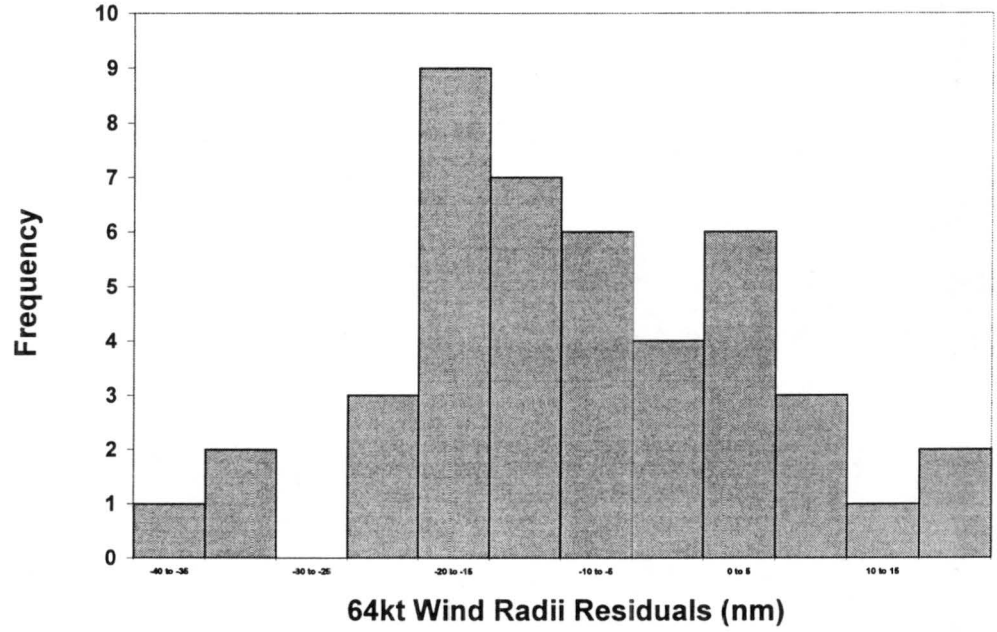
Frequency
10
9
8
7
6
5
4
3
2
1
0
-40 to -36
-30 to -25
-20 to -15
-10 to -6
0 to 5
10 to 15
64kt Wind Radii Residuals (nm)

a)

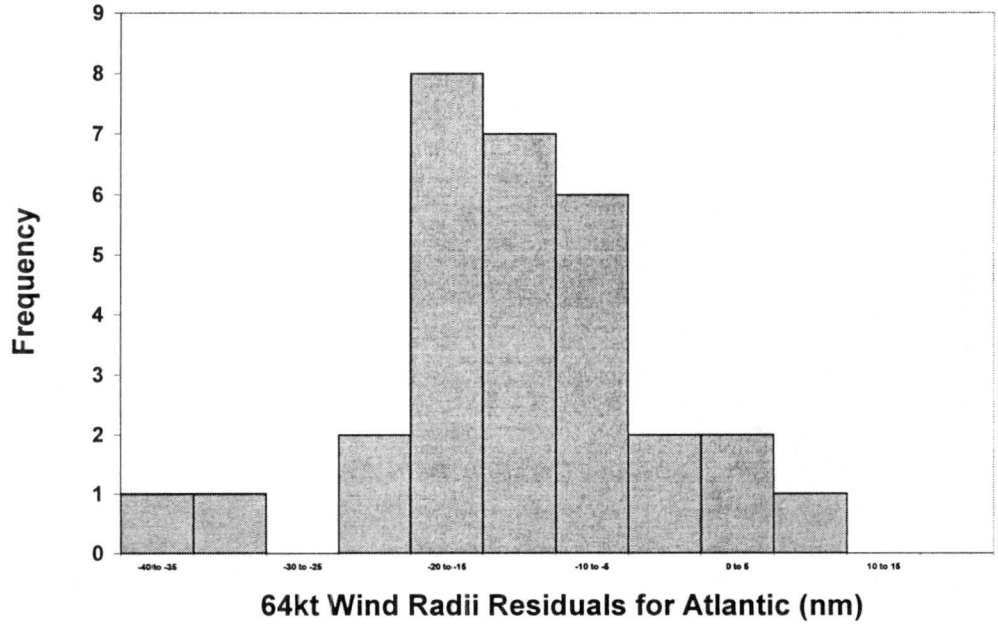
Frequency
9
8
7
6
5
4
3
2
1
0
-40to -35
-30 to -25
-20 to -15
-10 to -6
0 to 5
10 to 15
64kt Wind Radii Residuals for Atlantic (nm)

b)

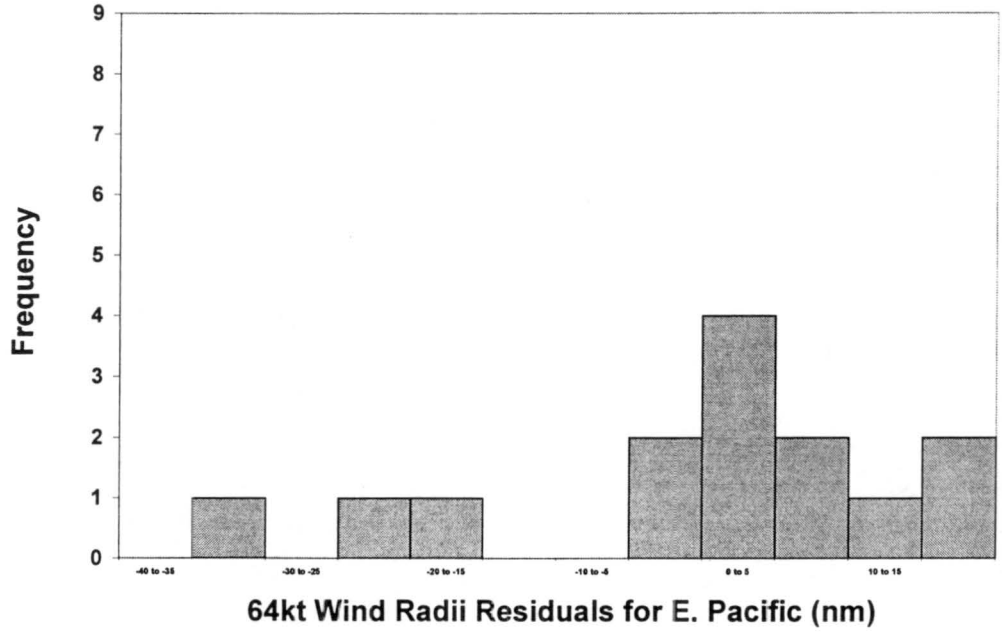

c)

Figure 5.11. Histogram of residuals (NHC average radii – AMSU calculated average wind radii) from 2000 cross-validation data for 64 kt winds in the a) Atlantic and East Pacific basins combined, b) Atlantic basin only, and c) East Pacific basin only.

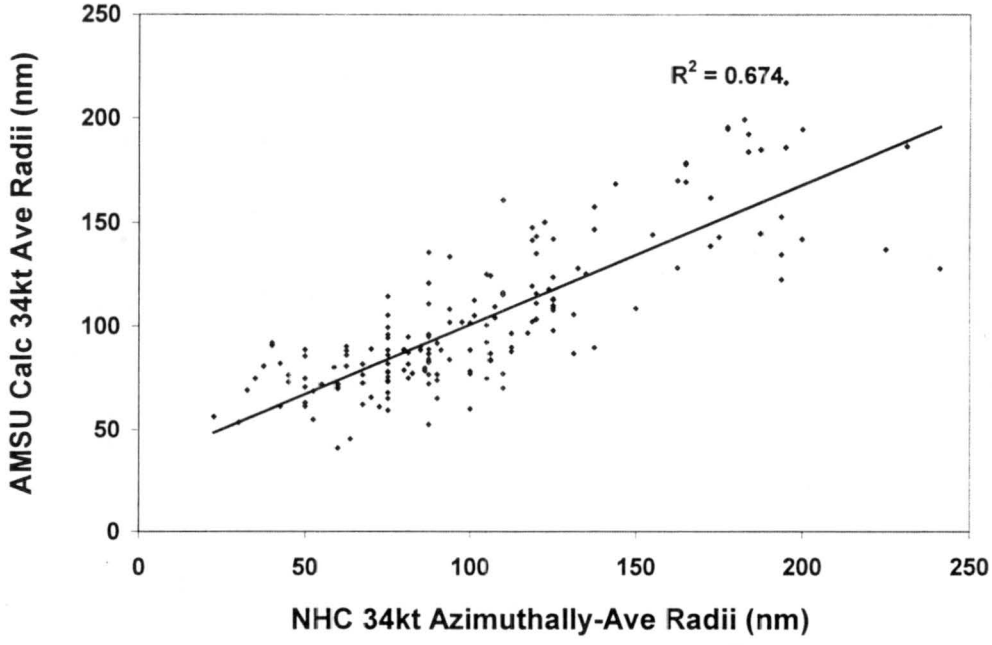

a)

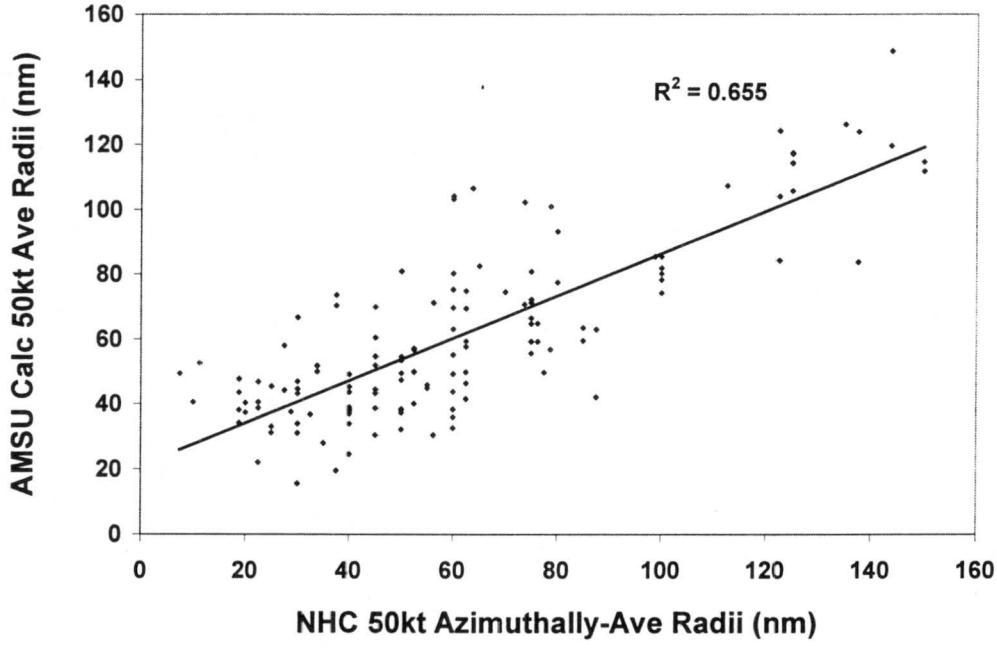

b)

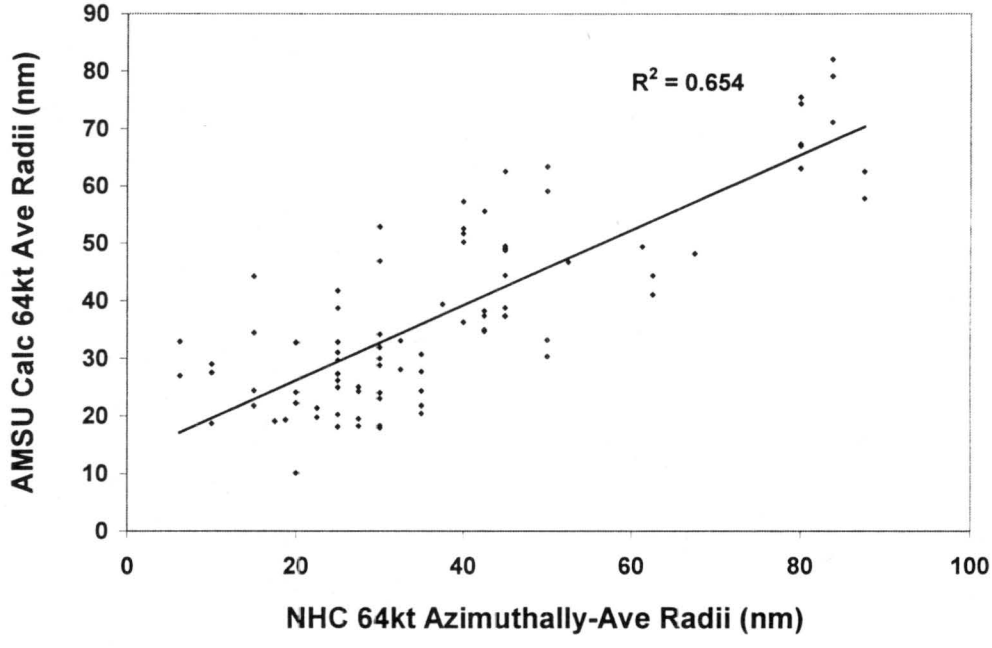

c)

Figure 5.12. Relationship between the AMSU-derived and NHC reports of azimuthally-averaged wind radii from 1999 and 2000 combined data for a) 34 kt winds, b) 50 kt winds, and c) 64 kt winds.

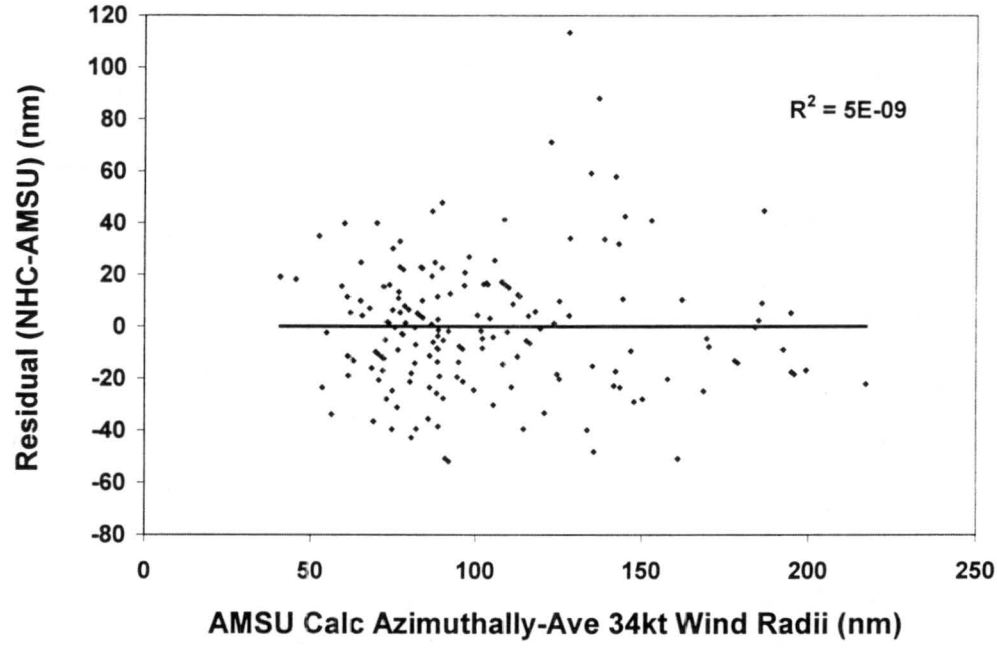
Residual (NHC-AMSU) (nm)
120
100
80
60
40
20
0
-20
-40
-60
-80
R^2 = 5E-09
0
50
100
150
200
250
AMSU Calc Azimuthally-Ave 34kt Wind Radii (nm)

a)

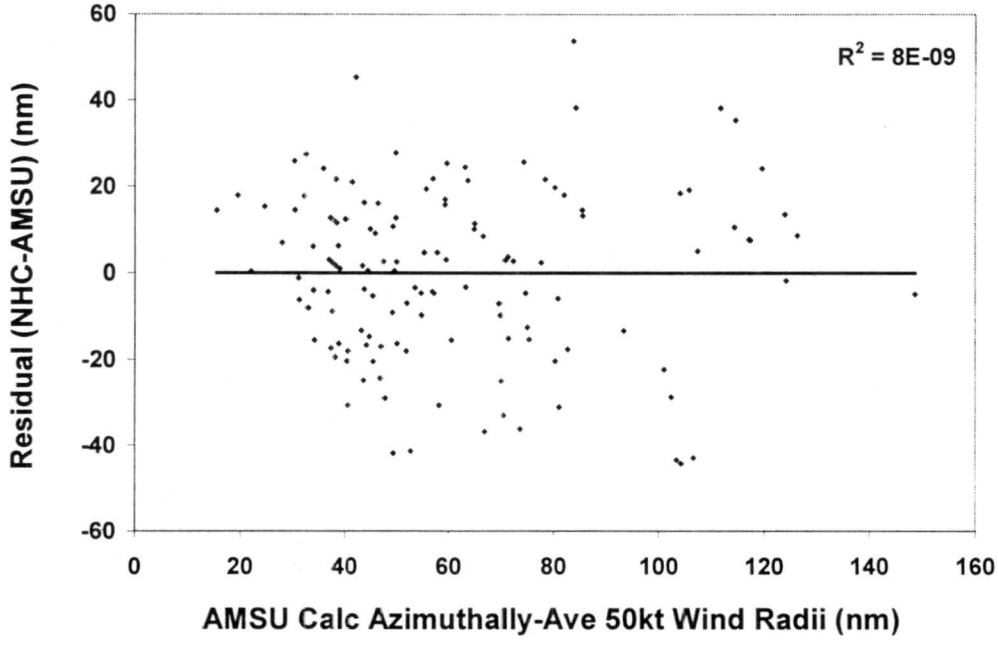
Residual (NHC-AMSU) (nm)
60
40
20
0
-20
-40
-60
R^2 = 8E-09
0
20
40
60
80
100
120
140
160
AMSU Calc Azimuthally-Ave 50kt Wind Radii (nm)

b)

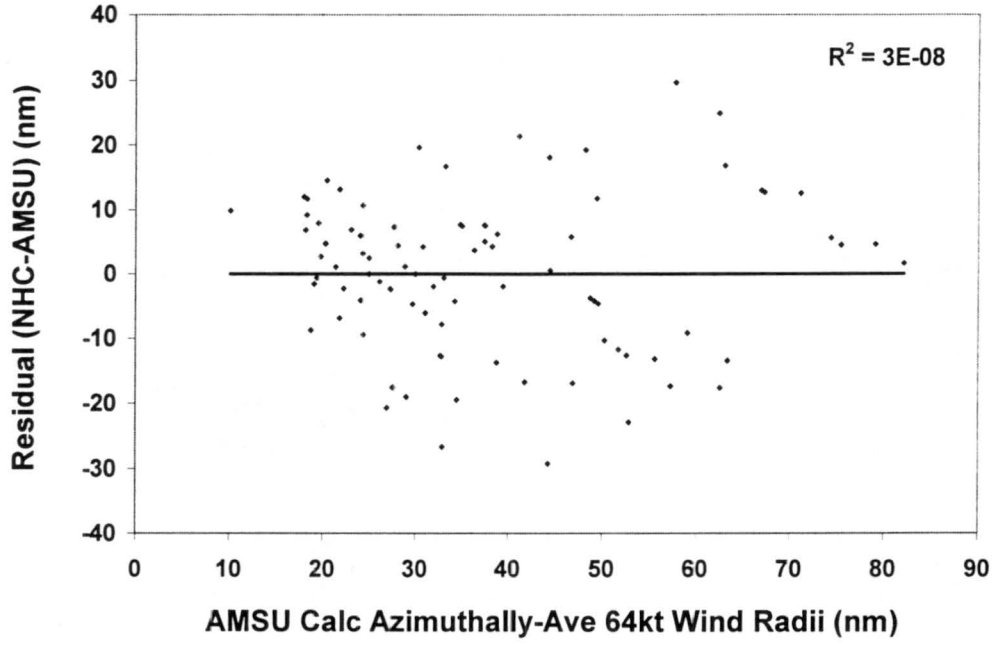

c)

Figure 5.13. Residual (NHC average radii – AMSU calculated average radii) plot versus AMSU calculated azimuthally-averaged wind radii from 1999 and 2000 combined data for a) 34 kt winds, b) 50 kt winds, and c) 64 kt winds.

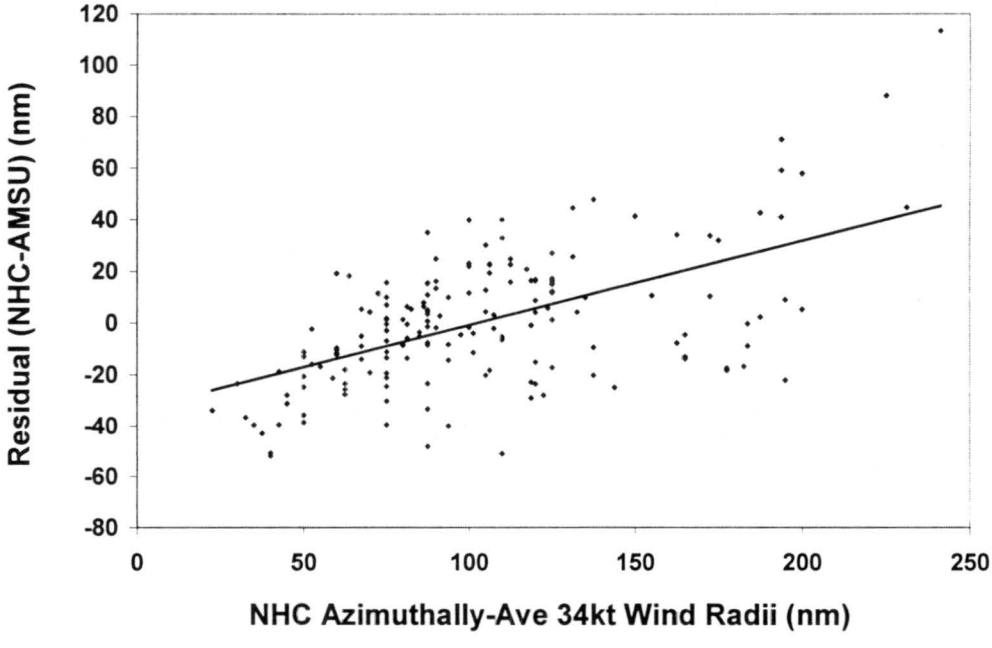

a)

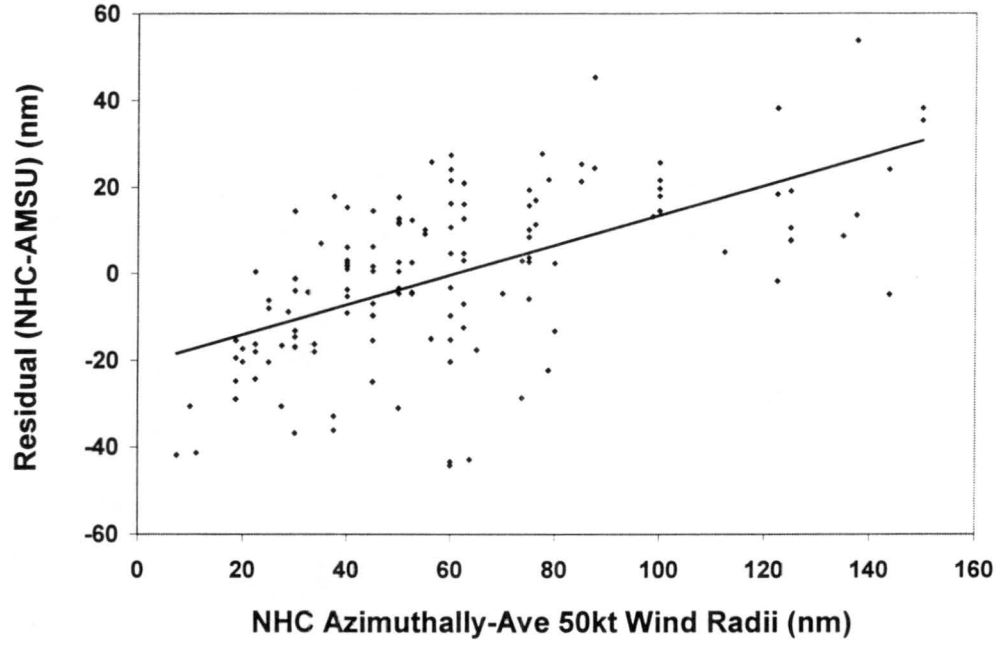

b)

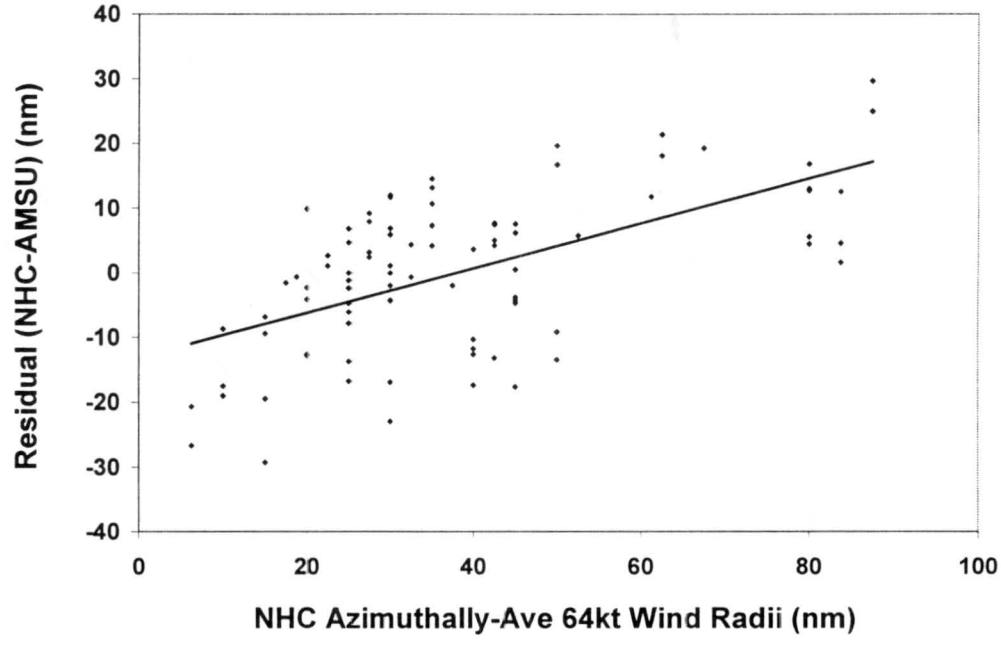

c)

Figure 5.14. Residual (NHC average radii – AMSU calculated average radii) plot versus NHC azimuthally-averaged wind radii from 1999 and 2000 combined data for a) 34 kt winds, b) 50 kt winds, and c) 64 kt winds.

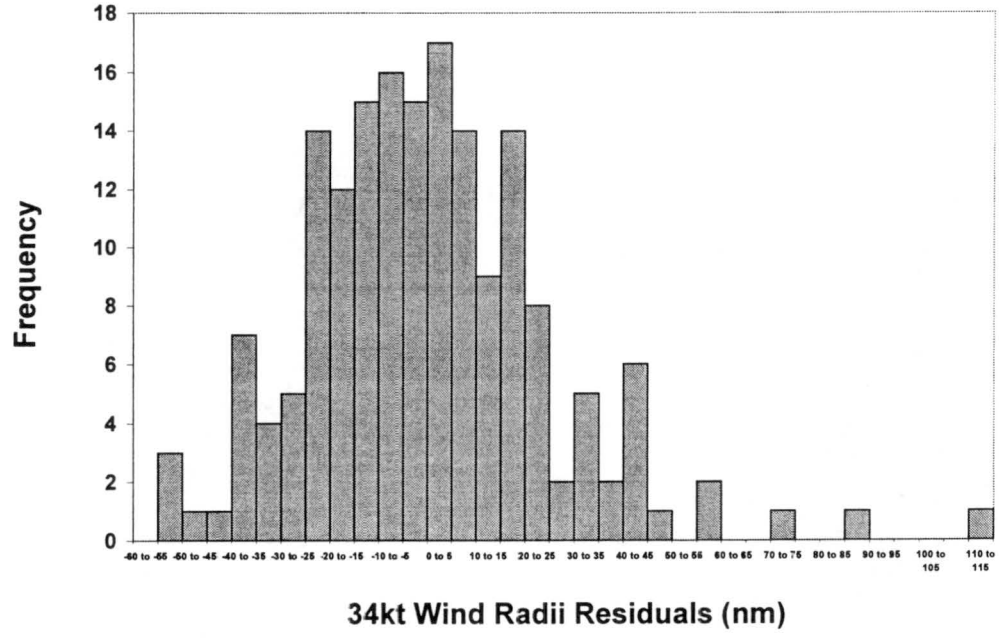
Frequency
18
16
14
12
10
8
6
4
2
0
-60 to -55
-50 to -45
-40 to -35
-30 to -25
-20 to -15
-10 to -5
0 to 5
10 to 15
20 to 25
30 to 35
40 to 45
50 to 55
60 to 65
70 to 75
80 to 85
90 to 95
100 to 105
110 to 115
34kt Wind Radii Residuals (nm)

a)

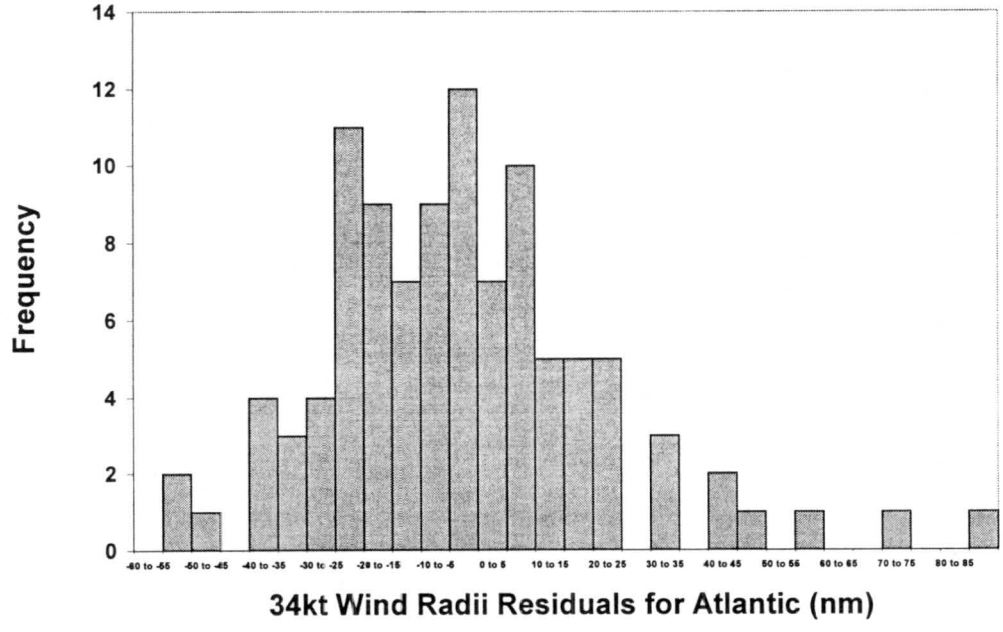
Frequency
14
12
10
8
6
4
2
0
-60 to -55
-50 to -45
-40 to -35
-30 to -25
-20 to -15
-10 to -5
0 to 5
10 to 15
20 to 25
30 to 35
40 to 45
50 to 55
60 to 65
70 to 75
80 to 85
34kt Wind Radii Residuals for Atlantic (nm)

b)

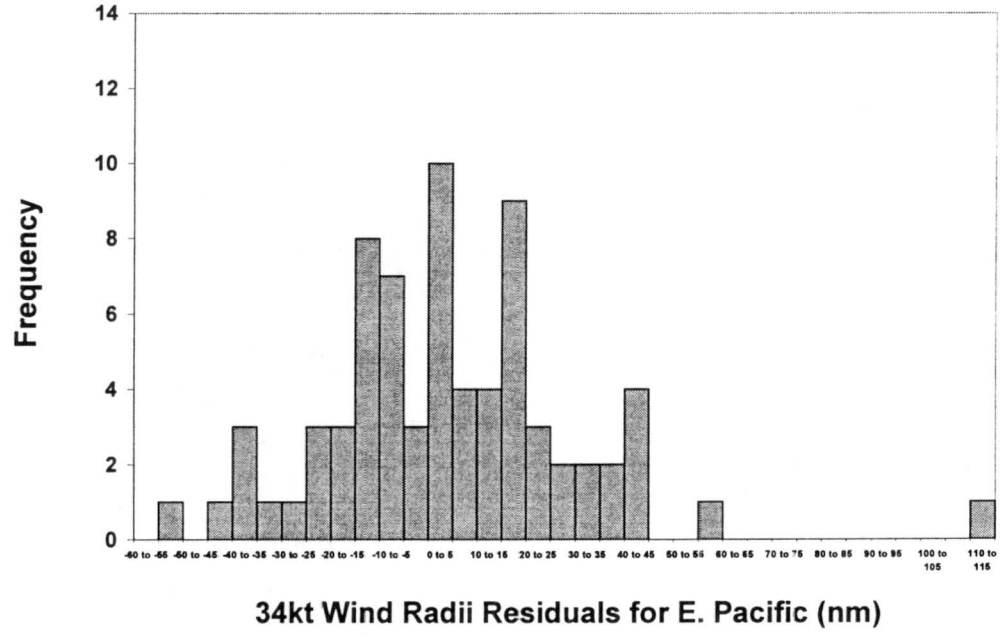

c)

Figure 5.15. Histogram of residuals (NHC average radii – AMSU calculated average wind radii) from 1999 and 2000 combined data for 34 kt winds in the a) Atlantic and East Pacific basins combined, b) Atlantic basin only, and c) East Pacific basin only.

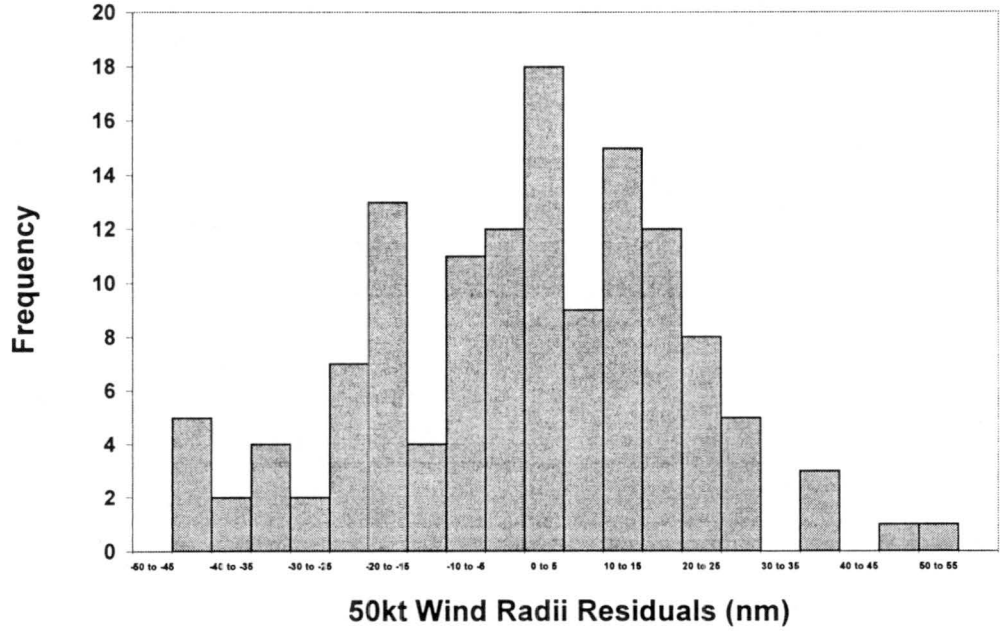

a)

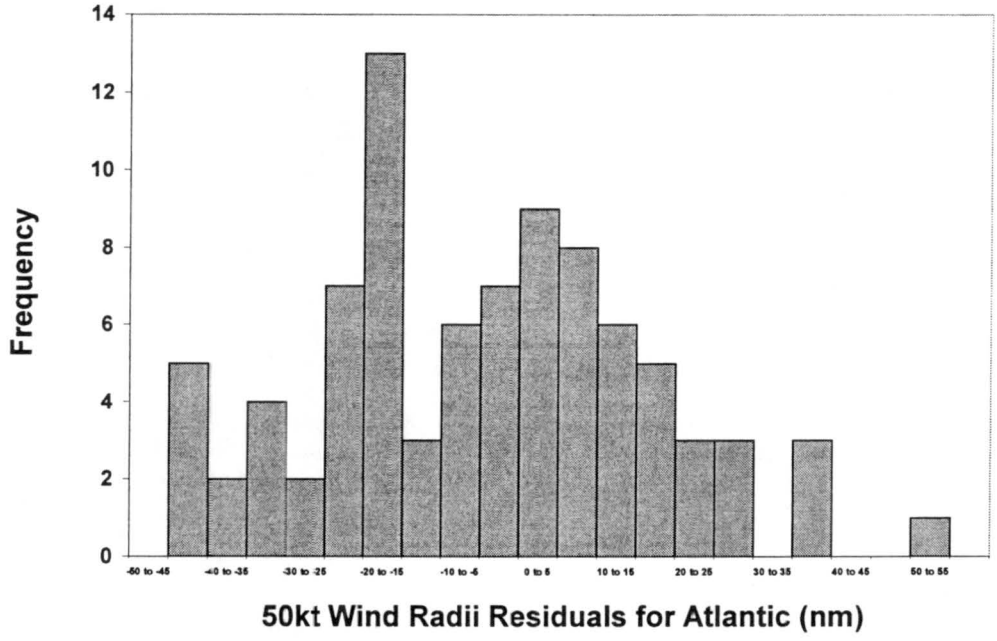

b)

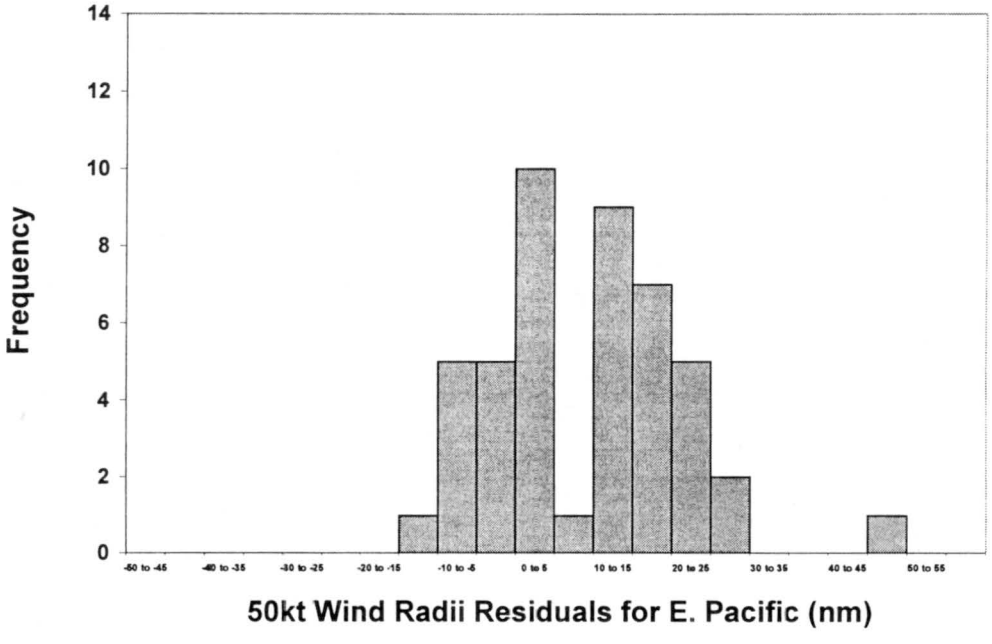

c)

Figure 5.16. Histogram of residuals (NHC average radii – AMSU calculated average wind radii) from 1999 and 2000 combined data for 50 kt winds in the a) Atlantic and East Pacific basins combined, b) Atlantic basin only, and c) East Pacific basin only.

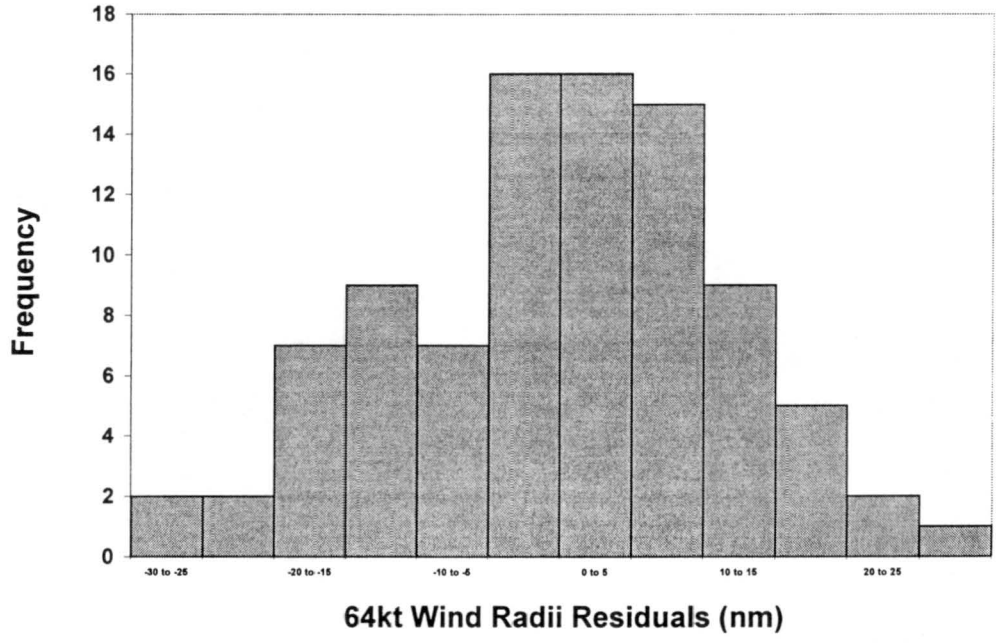
Frequency
18
16
14
12
10
8
6
4
2
0
-30 to -25
-20 to -15
-10 to -5
0 to 5
10 to 15
20 to 25
64kt Wind Radii Residuals (nm)

a)

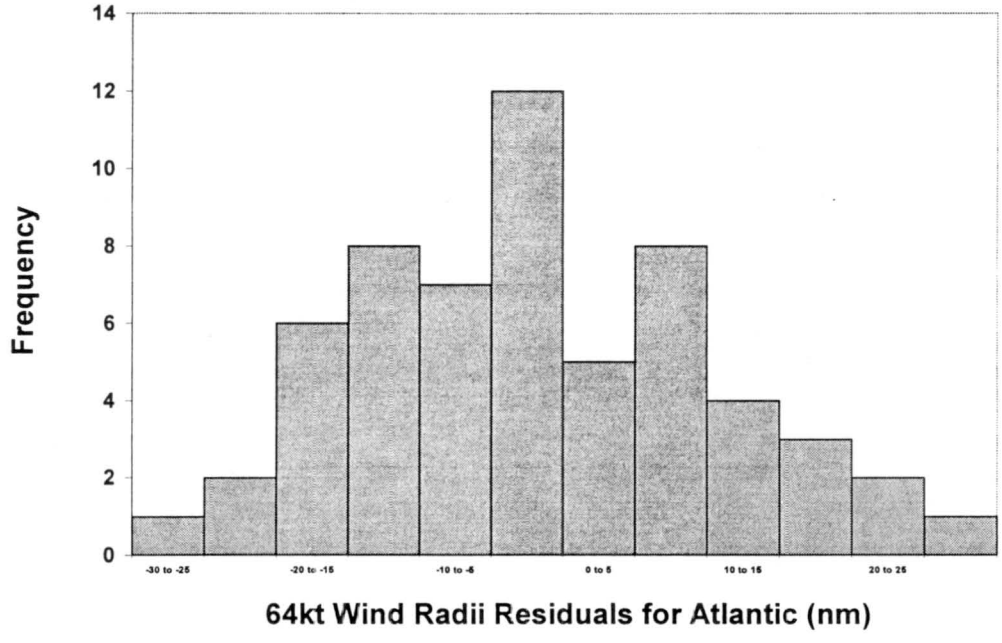
Frequency
14
12
10
8
6
4
2
0
-30 to -25
-20 to -15
-10 to -5
0 to 5
10 to 15
20 to 25
64kt Wind Radii Residuals for Atlantic (nm)

b)

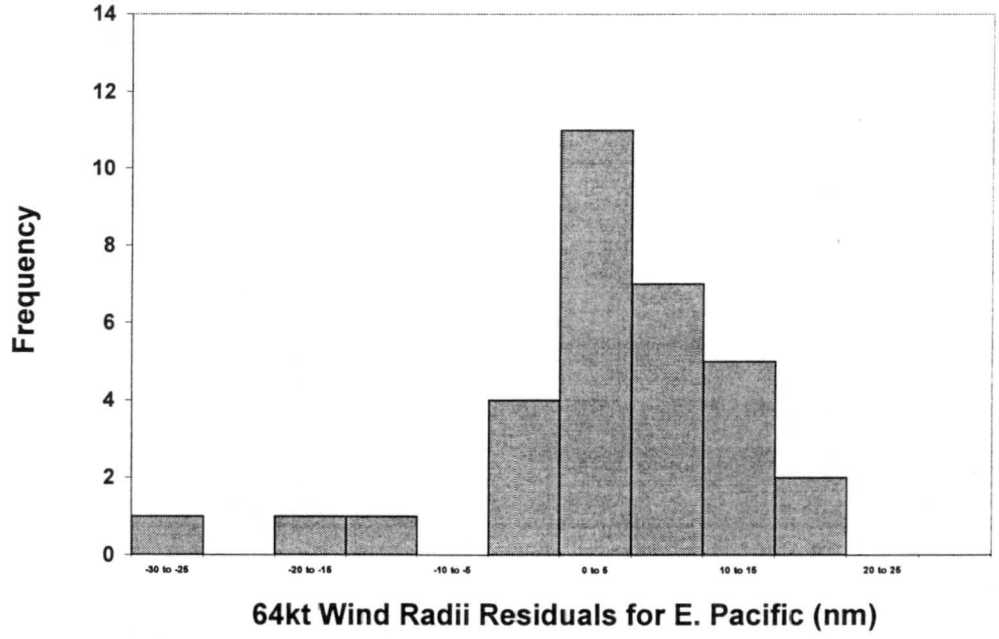

c)

Figure 5.17. Histogram of residuals (NHC average radii – AMSU calculated average wind radii) from 1999 and 2000 combined data for 64 kt winds in the a) Atlantic and East Pacific basins combined, b) Atlantic basin only, and c) East Pacific basin only.

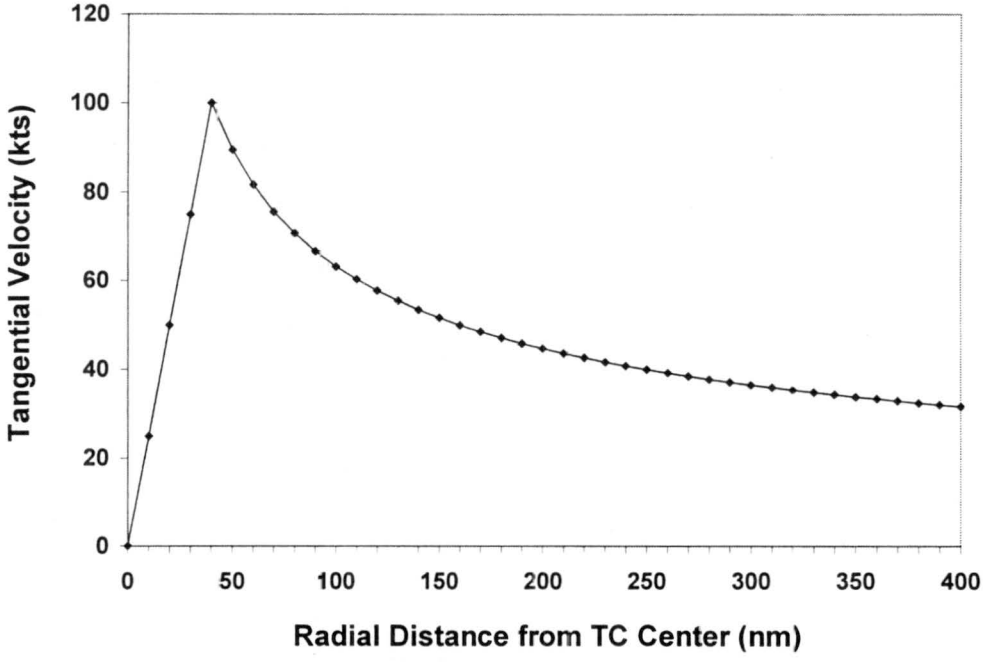

Figure 5.18. Example of tangential wind profile of a hurricane based on the modified Rankine vortex model (Depperman, 1947) with a maximum wind radius of 40 nm.

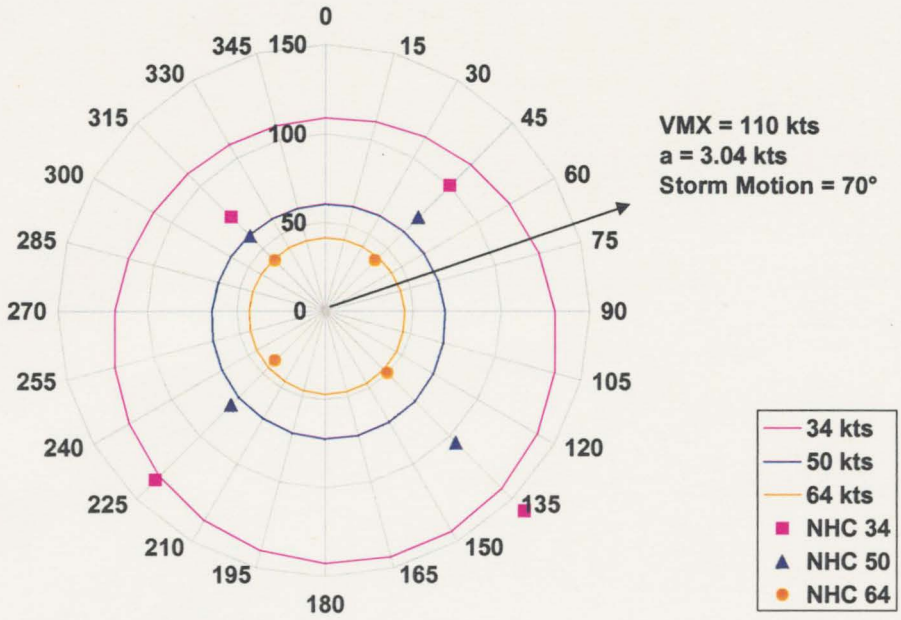

Figure 5.19. Calculated asymmetric radii of 34, 50, and 64 kt winds for Hurricane Lenny.

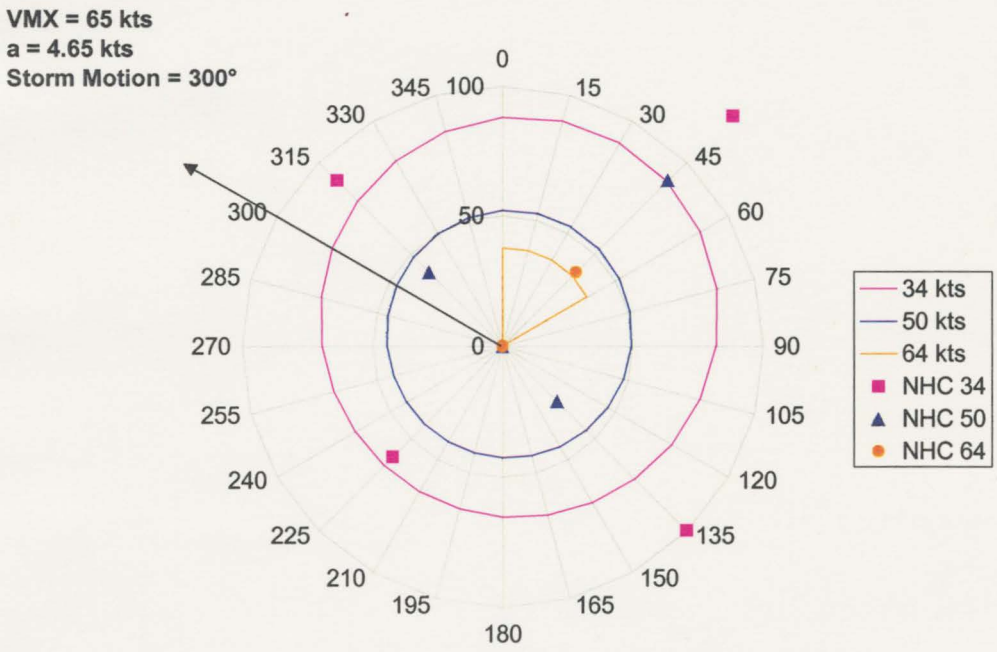

Figure 5.20. Calculated asymmetric radii of 34, 50, and 64 kt winds for Hurricane Dennis.

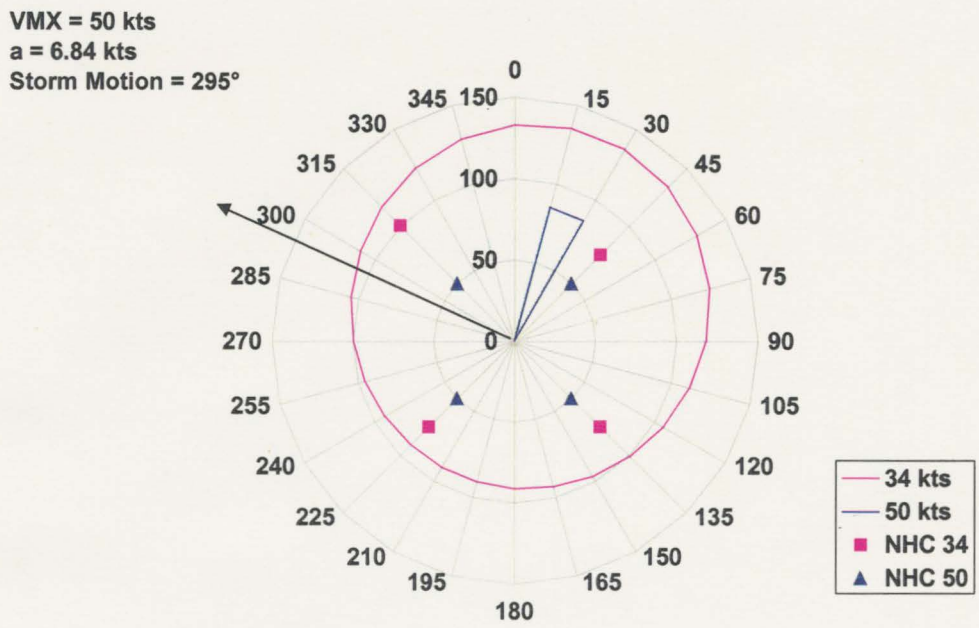

Figure 5.21. Calculated asymmetric radii of 34 and 50 kt winds for Tropical Storm Carlotta.

Chapter 6 - Conclusions and Future Work

6.1 Conclusions

With a booming population along coastal regions and the possibility of increased tropical activity in the Atlantic basin, accurately estimating tropical cyclone winds is essential. With the recent launch of the first Advanced Microwave Sounding Unit in May 1998, followed by a second in September 2000, there now exists remote sensing data with good enough resolution to estimate tropical cyclone maximum sustained winds and the extent of the 34, 50, and 64 kt wind radii.

Using the AMSU data from the 1999 and 2000 tropical seasons, algorithms for objectively predicting TC intensity and the azimuthally averaged radii of 34, 50, and 64 kt winds were developed. Subsequently, Depperman's (1947) modified Rankine vortex model was used with the AMSU-derived estimates of azimuthally averaged wind radii to estimate the wind radii asymmetrically, specifically in the NE, SE, SW, and NW quadrants of tropical cyclones.

The results of this study suggest the objective AMSU technique for predicting TC intensity is comparable to the objective Dvorak technique with the significant advantage of being able to estimate the maximum winds of tropical depressions and weak tropical storms. The AMSU data also were used to predict the wind radii within reasonable error

on a more regular basis than alternate methods currently being utilized. Furthermore, the methods may be superior to estimates provided by the National Hurricane Center in some cases.

Despite the reasonable results of this work, there are some factors that may limit the conclusions drawn in this study. The major shortcoming is the lack of a long data set; two years of observations are not enough to draw solid conclusions between the AMSU parameters and the tropical cyclone characteristics discussed here. Nonetheless, data gathered from the second AMSU and another to be launched in the near future will provide enhanced spatial and temporal coverage of tropical cyclones, allowing for the possibility of improved relationships. Of even greater potential is the proposed launch of the Advanced Technology Microwave Sounder (ATMS), a follow on to the AMSU. The ATMS is part of the National Polar-orbiting Operational Environmental Satellite System (NPOESS). Its improvements will likely be beneficial in aiding TC research in the future.

6.2 Future Work

While some prospects of future work were mentioned in the main text, they are reiterated here along with other prospective ideas.

As alluded to previously, validation of the intensity algorithm derived from the combined 1999/2000 data will be done when the National Hurricane Center releases their post-season best track analysis of the 2001 tropical season. The refined azimuthally averaged wind radii algorithms also will be cross-validated after the final tropical cyclone of the 2001 season, when all NHC forecast advisories are available.

Based upon preliminary results of this work (Demuth *et al.*, 2000), the AMSU estimative algorithms were chosen as a high priority for transition from research to operations by the USWRP. Thus, upon final validation from the 2001 season, the AMSU

intensity and azimuthally averaged wind algorithms and asymmetric wind radii estimation technique will be incorporated into the National Hurricane Center's operational system by the 2002 tropical season.

Although these two objectives definitely are scheduled to transpire, there are several other possibilities for more work to be done with the AMSU. As mentioned in Section 4.1.3, the azimuthal-averaging technique used in deriving most of the AMSU predictors does not account for a tropical cyclone's specific features. Work is already being done to examine each predictor's entire grid of points over a TC, as opposed to the single, averaged value currently used as representation of the storms. The multiple data points may highlight features and spatial variations, allowing for better visualizations of TCs and possibly improved estimations of intensity and wind radii. Furthermore, development of separate, basin-dependent algorithms for the Atlantic and East Pacific is likely a good idea based on the reported variability in the results for each. In fact, it is possible that intensity and wind algorithms could be developed for all seven tropical basins worldwide. Perhaps with more years of data, and especially now with the second AMSU in operation, there may be a sufficient number of AMSU cases with corresponding aircraft reconnaissance data to make up the dependent data set; thus, the algorithms for the Atlantic basin could be developed based entirely upon *in situ* data.

Future work should also include direct comparisons between Objective Dvorak Technique and AMSU estimates of TC intensity. Some work has already been done using operational ODT estimates received from the Tropical Analysis and Forecasting Branch (TAFB), but there currently are too few cases for comparison. The Cooperative Institute for Research in the Atmosphere recently received the ODT software so that a larger data set of estimates may be generated using archived IR imagery for times concurrent with AMSU passes. Additionally, comparison of the asymmetric wind radii

should be done against QuikSCAT scatterometers in basins without reconnaissance data, especially for the 34 kt wind radii which generally are less associated with areas of deep convection which affect scatterometer estimates.

Finally, it would be useful to see how the AMSU estimates of intensity and winds perform on specific cases, including highly sheared storms, rapidly intensifying or weakening storms, and storms with central dense overcasts. If there are certain conditions for which the AMSU techniques are consistently under or over predicting, adjustments, such as those used by Dvorak, could be utilized in the quest for improved TC intensity and wind structure estimates.

References

Abraham, K.R., U.C. Mohanty, and S.K. Dash, 1995: Simulation of cyclones using synthetic data. Proceedings of the Indian academy of sciences: Earth and planetary sciences, **104**, 635-666.

Barnes, S., 1964: A Technique for Maximizing Details in Numerical Weather Map Analysis. *Journal of Applied Meteorology*, **3**, 396-409.

Brueske K.F. and C.S. Velden, 2001: Satellite-based tropical cyclone intensity estimation using the NOAA-KLM series Advanced Microwave Sounding Unit (AMSU). *Monthly Weather Review*, in press.

DeMaria, M., 2000a: Personal communication re: AMSU wind retrievals.

DeMaria, M., 2000b: Personal communication re: response functions.

DeMaria, M., J.L. Demuth, and J.A. Knaff, 2001: Validation of an advanced microwave sounder unit (AMSU) tropical cyclone intensity and size estimation algorithm. *11th Conference on Satellite Meteorology and Oceanography*, Madison, WI, page numbers unknown at the time of this writing.

DeMaria, M., J.A. Knaff, S.Q. Kidder, and M.D. Goldberg, 2000: Tropical Cyclone Wind Retrievals Using AMSU-A Data from NOAA-15. *10th Conference on Satellite Meteorology and Oceanography*, Long Beach, CA, 149-152.

Demuth, J.L., M. DeMaria, J.A. Knaff, and T.H. Vonder Haar, 2000: An objective method for estimating tropical cyclone intensity and structure from NOAA-15 AMSU data. *24th Conference on Hurricanes and Tropical Meteorology*, Fort Lauderdale, FL, 484-485.

Depperman, C.E., 1947: Notes on the origin and structure of Philippine typhoons. *Bulletin of the American Meteorological Society*, **28**, 399-404.

Dvorak, V.F., 1975: Tropical cyclone intensity analysis and forecasting from satellite imagery. *Monthly Weather Review*, **103**, 420-430

----, 1984: Tropical cyclone intensity analysis using satellite data. NOAA Technical Report NESDIS 11, 47 pp.

Elsberry, R., 2001: Personal communication, July 17.

Goldberg, M.D., 1999: Generation of retrieval products from AMSU-A: Methodology and validation. *10th Int. ATOVS Study Conference*, Boulder, CO, 219-229.

Goldenberg, S.B., C.W. Landsea, A.M. Mestas-Nunez, W.M. Gray, 2001: The recent increase in Atlantic hurricane activity: Causes and implications. *Science*, **293**, 474-479.

Gray, W.M., C.W. Landsea, P.W. Mielke, Jr., and K.J. Berry, cited 2000: Summary of 2000 Atlantic tropical cyclone activity and verification of authors' seasonal activity forecast. [Available on-line from http://typhoon.atmos.colostate.edu/forecasts/2000/nov2000/index.html].

Gray, W.M., C.W. Landsea, P.W. Mielke, Jr., K.J. Berry, and E. Blake, cited 2001: Updated Early August Forecast of Atlantic Seasonal Hurricane Activity and US Landfall Strike Probabilities for 2001. [Available on-line from http://typhoon.atmos.colostate.edu/forecasts/2001/aug2001/].

Hebert, P.J., J.D. Jarrell and M. Mayfield, 1993: The deadliest, costliest, and most intense United States hurricanes of this century (and other frequently requested hurricane facts). NOAA Technical Memorandum NWS NHC-31, February 1993, National Hurricane Center, Coral Gables, FL.

Holland, G., 1980: An analytical model of the wind and pressure profiles in hurricanes. *Monthly Weather Review*, **108**, 1212-1218.

Houze, Jr., R.A, 1993: Cloud Dynamics. Academic Press, 573 pp.

Kidder, S.Q., M. D. Goldberg, R. M. Zehr, M. DeMaria, J. F. W. Purdom, C. S. Velden, N. C. Grody, and S. J. Kusselson, 2000: Satellite analysis of tropical cyclones using the Advanced Microwave Sounding Unit (AMSU). *Bulletin of the American Meteorological Society*, **81**, 1241-1259.

Kidder, S.Q., W.M. Gray, T.H. Vonder Haar, 1980: Tropical cyclone outer surface winds derived from satellite microwave sounder data. *Monthly Weather Review*, **108**, 144-152.

Kidder, S.Q., J.A. Knaff, and S.J. Kusselson, 2001: Using AMSU data to forecast precipitation from landfalling hurricanes. *Symposium on Precipitation Extremes: Predictions, Impacts, and Responses*, Albuquerque, NM, 344-347.

Kidder, S.Q., and T.H. Vonder Haar, 1995: Satellite Meteorology: An Introduction. Academic Press, 466 pp.

Knaff, J.A., R.M. Zehr, M.D. Goldberg, and S.Q. Kidder, 2000: An example of temperature structure differences in two cyclone systems derived from the Advanced Microwave Sounding Unit. *Weather and Forecasting*, **15**, 476-483.

Landsea, C., cited 2001: FAQ: Hurricanes, Typhoons, and Tropical Cyclones. [Available on-line from http://www.aoml.noaa.gov/hrd/tcfaq/tcfaqHED.html].

Linstid, B., 2000: An algorithm for the correction of corrupted AMSU temperature data in tropical cyclones. Masters Thesis, Colorado State University, Department of Mathematics, 24 pp.

National Hurricane Center, cited 2001: Average Cumulative Profile Throughout the Hurricane Season [Available on-line from http://www.nhc.noaa.gov/pastprofile.html].

Pielke Jr, R.A. and C.W. Landsea, 1998: Normalized Hurricane Damages in the United States: 1925-95. *Weather and Forecasting*, **13**, 621-631.

Schwerdt, R., F. Ho, and R. Watkins, 1979: Meteorological Criteria for Standard Project Hurricane and Probable Maximum Hurricane Wind Fields, Gulf and East Coasts of the United States.NOAA/NWS, 317pp.

Spencer, R.W. and W.D. Braswell, 2001: Atlantic tropical cyclone monitoring with AMSU-A: Estimation of maximum sustained wind speeds. *Monthly Weather Review*, **129**, 1518-1532.

Tropical Storm Risk, cited 2001: Season Tropical Cyclone Forecasts. [Available on-line from http://tropicalstormrisk.com].

Ulaby, F.T., R.K. Moore, and A.K. Fung, 1986: Microwave remote sensing: active and passive, Volume III: From Theory to Application. Addison-Wesley Publishing, 1097 pp.

Velden, C.S., 1989: Observational analyses of North Atlantic tropical cyclones from NOAA polar-orbiting satellite microwave data. *Journal of Applied Meteorology*, **28**, 59-70.

Velden, C.S., B.M. Goodman, and R.T. Merrill, 1991: Western North Pacific tropical cyclone intensity estimation from NOAA polar-orbiting satellite microwave data. *Monthly Weather Review*, **119**, 159-168.

Velden, C.S., T.L. Olander, and R.M. Zehr, 1998: Development of an objective scheme to estimate tropical cyclone intensity from digital geostationary satellite infrared imagery. *Weather and Forecasting*, **13,** 172-186.

Wilks, Daniel S., 1995: Statistical Methods in the Atmospheric Sciences. Academic Press, 467pp.

World Meteorological Organization Technical Document, 1993: Global Guide to Tropical Cyclone Forecasting. WMO-No.560, (TCP-31), World Meteorological Organization, Geneva.